FLAT PATTERN DEVELOPMENT FOR BENT AND DEEP DRAWN SHEET METAL COMPONENTS

by

ANAND SATYADEV

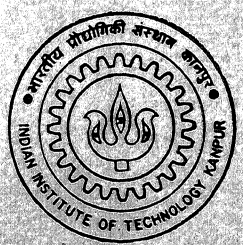

DEPARTMENT OF MECHANICAL ENGINEERING

INDIAN INSTITUTE OF TECHNOLOGY KANPUR

MARCH, 1995

FLAT PATTERN DEVELOPMENT FOR BENT AND DEEP DRAWN SHEET METAL COMPONENTS

A thesis
Submitted in the Partial Fulfillment
of the Requirement for the Degree
of

MASTER OF TECHNOLOGY

by

ANAND SATYADEV

to the

DEPARTMENT OF MECHANICAL ENGINEERING
INDIAN INSTITUTE OF TECHNOLOGY
KANPUR.

MARCH 1995

CERTIFICATE

It is certified that the work contained in the thesis entitled "**FLAT PATTERN DEVELOPMENT FOR BENT AND DEEP DRAWN SHEET METAL COMPONENTS**", by Anand Satyadev, has been carried out under my supervision and this work has not been submitted elsewhere for a degree.

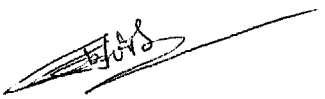

Dr. V. K. Jain,
Dept. Of Mechanical Engg.,
I. I. T. Kanpur.

ABSTRACT

Bending and axisymmetric deep drawing of sheet metal components are analyzed in this work to develop a method to find the flat pattern development for these components. For bending, the analysis is done on the basis of a 2D stress and strain field assuming the plane strain condition and neglecting the end effects. The radius of unstretched fiber in the bend zone is calculated considering the thinning of the sheet.

For deep drawing, a 2D stress field (plane stress field) is assumed to exist with a 3D strain field in the flange as well as in the curved segments of the sheet. The process is broken into a number of stages and for each stage, the stresses and strains are calculated using the values for the preceding stage. Subsequently, the reduction in flange diameter during that stage is evaluated. At the end, the initial flat pattern size is modified by comparing the part obtained and the part desired.

Prototype systems are developed for bending and deep drawing of sheet metal components and they are applied to a number of example cases. Results obtained were found to be satisfactory.

ACKNOWLEDGEMENTS

I express my deep and sincere gratitude to my thesis supervisor Dr. V. K. Jain for his constant encouragement, expert guidance and useful criticism during the course of this work. Their keen involvement at every step of this work have been invaluable.

I also acknowledge the help I received from Jagirdar and Venkat Reddy and for having many enlightening discussions on various aspects of this work.

Special thanks to friends like Gujral, Bansal, KP, Kale, Rao, Neelesh, Kher and the luckier ones who could manage to leave early, for making my stay at IIT very pleasant and memorable one.

Anand Satyadev

CONTENTS

CHAPTER 5 CONCLUSIONS AND SCOPE FOR FUTURE WORK

LIST OF FIGURES

LIST OF TABLES

NOMENCLATURE

$a_1, a_2, .., a_5$	Areas of various segments of cup
BA	Bend allowance
$d\varepsilon_\phi, d\varepsilon_\theta, d\varepsilon_t$	Incremental strains in meridian, circumferential and thickness directions
$d\sigma_\phi$	Incremental stress in meridinal direction
D_c	Diameter of the cup
D_i	Diameter of flat pattern
e_t	Thickness strain
e_{r_i}	Strain in radial direction at innermost fiber
e_{r_o}	Strain in radial direction at outermost fiber
h	Instantaneous height of the cup
H_{max}	Height of deep drawn cup
k	Strength coefficient for material
l_1, l_2, l_3	Lengths of various segments of the cup
L	Bend allowance
L_o	Length of unstretched fiber
L_{r_i}	Length of innermost fiber
L_{r_o}	Length of outermost fiber
n	Strain hardening exponent
r	Radius
r_d	Profile radius of die
r_f	Flange radius of deep drawn cup
r_i	Inner radius of bend zone
r_m	Radius of mid fiber
r_n	Radius of neutral fiber
r_o	Outer radius of bend zone
r_p	Profile radius of punch
r_u	Radius of unstretched fiber
R_f	Instantaneous radius of flange
R_i	Initial radius of blank
R_o	Radius at die entry
R_p	Radius of punch
t	Thickness of bend zone
t_f	Instantaneous thickness of flange
t_i	Initial thickness of the sheet

t_o	Thickness at die entry
ε	Clearance between die and punch
$\bar{\varepsilon}$	Effective or equivalent strain
$\varepsilon_1, \varepsilon_2, \varepsilon_3$	Strains in principal directions
ε_r	Strain in radial direction
$\varepsilon_\phi, \varepsilon_\theta, \varepsilon_t$	Strains in meridinal, circumferential and thickness directions
ϕ	Angle of wrap over die/punch corner
μ	Coefficient of friction
$\bar{\sigma}$	Effective or equivalent stress
$\sigma_1, \sigma_2, \sigma_3$	Stresses in principal direction
σ_o	Initial yield stress
σ_r	Stress in radial direction
$\sigma_\phi, \sigma_\theta, \sigma_t$	Stresses in meridinal, circumferential and thickness directions
θ	Included angle of bend.
τ_1, τ_2	Surface stresses in meridinal direction

CHAPTER 1

INTRODUCTION AND LITERATURE SURVEY

1.1 INTRODUCTION

Sheet metal components have innumerable applications in today's world. These are extensively used in aerospace and electronic industries where high precision is an essential requirement. These products can be simple components requiring simple fabrication process steps or complex components requiring many complex steps to fabricate them. Bending and deep drawing are the two of the most commonly used sheet metal forming processes. In this work, these two processes are analyzed to find the flat pattern development required for them.

Flat pattern for any sheet metal component is basically a piece of sheet from which the product can be obtained after performing certain pressworking operations (in the present context, forming operations). It is the minimum size of the blank which can be formed into the final product. Some authors have also defined a flat pattern as "the shape obtained by unfolding or unrolling of the surfaces of a bent component onto a plane" (Nee and Chong, 1992). This definition of flat pattern is specific to bent components and not for deep drawn components. In general, flat pattern for a sheet metal component can be defined as the shape and size of the sheet obtained by undeforming the final component into a plane.

Accuracy of the final product depends mainly on the accuracy of flat pattern in terms of size and shape. The accuracy of the flat pattern development becomes more important if the component is going to be used as a part of an assembly or a subassembly. Any inaccuracy of the component will lead to a misfit and subsequently, a failure of the complete assembly or

subassembly (Prasad and Somasundaram, 1993). So, knowing an accurate flat pattern is essential for manufacturing a dimensionally accurate component.

Another advantage of finding an accurate flat pattern is that it reduces the *trimming allowance* to a minimum level. In an ideal case, no trimming should be needed at all. The raw material cost, i.e., the sheet cost, for a sheet metal component is usually a significant part of the total cost of the component because the sheet is already partially processed, heat treated etc. So, any saving in the material cost affects the profitability of the product. In addition to the saving in the raw material cost by reducing the trimming allowance, the raw material cost can also be reduced by making a proper nesting of the flat patterns on the sheet to ensure maximum utilization of the sheet. For this, the knowledge of dimensions of the flat pattern helps in minimizing the wastage of the sheet. Other than the saving in the direct material cost, the cost of tooling for trimming operation can be eliminated, and the cost of handling and recycling the scrap generated can be reduced by using an accurately sized flat pattern. By eliminating the operation of trimming completely, the total time required to manufacture any component can also be reduced. This will also lead to a more productive operation.

For designing a cutting die for blanking operation, size of the flat pattern needed should be accurately known. This is essential to avoid expensive *"hit-and-trial"* method for designing a cutting die. The knowledge of an accurate flat pattern becomes very useful at this point in saving time as well as the money.

Flat pattern development helps in achieving a higher degree of automation in sheet metal forming centers. The flat pattern, along with the features in the final product, is used as an input to the process planning system for sheet metal components. The flat pattern development system can be used, along with other automatic systems (viz. automatic feature recognition

system, automated process planning system and automatic machine code generation system), so that CNC machines based fully automated computer integrated manufacturing system (CIMS) for sheet metal components can be obtained.

Presently, *"trial and error"* and *"thumb rules"* methods are used for finding the flat pattern. Such methods are inaccurate and unreliable. These methods are mainly experience based and generally, they are not supported by complete theoretical analysis. This kind of situation can be satisfactory for a few-product-large-batch size production systems but not for a multi-product-small-batch size system. In today's continuously changing world, where the products become obsolete very fast, these experience based techniques are not very useful. Methods have been proposed for finding the flat pattern development [Toh and Kobayashi (1985), Iseki and Murota (1986)] for sheet metal components using the finite element techniques. These methods use a detailed analysis of the system. These methods, being finite element based, are very time consuming and require skilled personnel to work with. So, these methods are not popular in industries. A need is therefore felt to develop a system for flat pattern development, such that it is fast, accurate and reliable and does not require any special expertise to work with. Before presenting such a method, a brief review of the literature available on the related topics is given in the following section.

Some of the terms related to the bend geometry are defined below, before the literature review is taken up (Fig. 1.1) :

Neutral Fiber : It is the fiber in the bend zone at which the stresses are zero.

Unstretched Fiber : It is the fiber in the bend zone at which the strains are zero. So, the length of this fiber will be equal to that of the original sheet

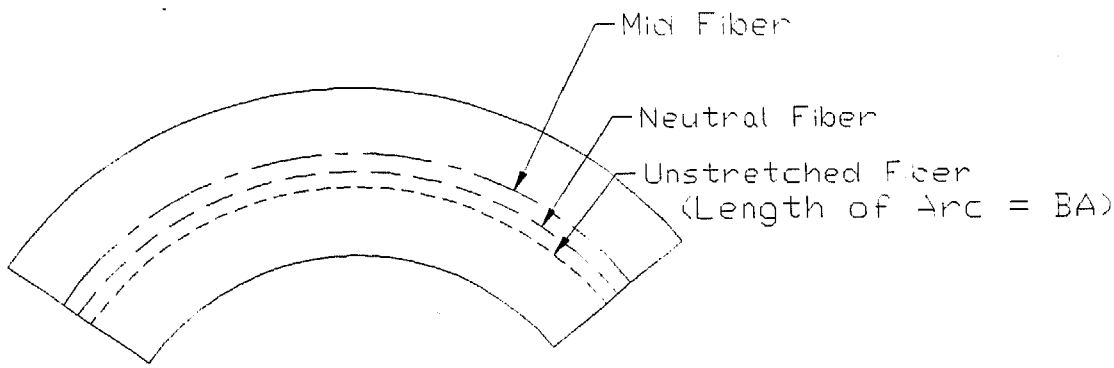

Fig. 1.1 Bending terminology

segment being bent.

Mid Fiber : It is the fiber which is exactly mid-way between the two free surfaces of the sheet.

Bend Allowance (BA) : It is the length of the original sheet which is bent to form the final product. It is equal to the length of the unstretched fiber in the bend zone.

1.2 LITERATURE REVIEW

A number of research papers, both on bending and deep drawing operation are reviewed in this work. First we consider the work reviewed on flat pattern development of bent components.

Nnaji et. al. (1991), have proposed a flattening process using the neutral fiber. They have considered the neutral fiber and unstretched fiber to be the same. The analysis is further simplified by assuming that the thickness of the sheet remains constant during bending. So, the bend allowance essentially becomes the length of the mid fiber of the sheet in the bend zone. This paper does not give the details of the flat pattern development procedure, but, gives a general methodology for transforming the bend plane and the plane next to it into the reference plane. The same procedure is repeated, one by one, for all the bend planes present in a component to obtain the complete flat pattern.

Nee et. al.(1992), have worked on a PC based system for flat pattern development of Heating, Ventilating and Air-conditioning (HVAC) ductings. They have considered a number of transition elements (a segment of the duct having different cross-sections at the two ends) for finding the flat pattern. They have neglected the effect of thickness of the sheet and treated the duct as a three dimensional surface for flat pattern

development. For finding a flat pattern, the duct surface is sliced into fine triangular or rectangular strips. The width of each strip is found using geometry. The flat pattern is obtained by arranging all such strips, one after the other, in one plane. Since, the sheet is treated as a surface, the thinning of the sheet, material hardening etc. don't come into picture.

Prasad and Somasundaram (1993), have developed a mathematical model for finding out the bend allowance for a bend plane. Their objective is to find the location of the unstretched fiber using which its length can be found. Since, the strain for this fiber is zero, its length is taken to be the same as the original length of the sheet. They have treated the neutral fiber and unstretched fiber to be different. They have assumed a plane strain field in the bend zone. The effects of anisotropy, variation in thickness during bending and end effects are neglected. The detailed analysis of stress and strain variation in the bend zone during the bending operation is also reported. The incremental strain values, during an incremental bend, are integrated to calculate the total strain during the bending. The changed thickness is calculated using these strains and the same procedure is repeated with the new thickness till the change in thickness between two consecutive iterations is less than a prespecified limit. Using this method, the flat pattern for any bend component can be found by applying this process to each bend plane separately.

Sachs (1966), has found the bend allowance for two cases. In case I, the thinning effect is neglected and is case II, thinning effect is considered. In the first case, the bend allowance (BA) is taken as equal to the length of the mid fiber of the sheet in the bend zone. So,

$$BA = A\ (R + T / 2) \qquad (1.1)$$

where A, R and T are angle of bend, radius of bend and

thickness of the sheet respectively. Some experiments were also conducted and following relationship was established

$$BA = A\ (R + 0.45\ T) \qquad (1.2)$$

This relationship is found to be in a better agreement, as compared to eq. (1.1), with the experimental results. This also shows that the unstretched fiber moves by a distance equal to 0.05T (from 0.50T (eq. (1.1)) to 0.45T (eq. (1.2)) from the inner surface of the bend) towards the center of the bend.

After discussing the research work related to the flat pattern development for bending operations, the available literature on flat pattern development for deep drawing operations is also presented. There is not much literature available on the flat pattern development for an axisymmetric deep drawn cup. Some researchers [Chen and Sowerby (1991), Karima (1985), Iseki and Murota (1986), Toh and Kobayashi (1985)] have reported the procedural details for flat pattern development for non-axisymmetric cases, like, square cups and some other cross sectioned cups. These are discussed below.

Chen and Sowerby (1991), have proposed a method to find the flat pattern for a square cup. In this work, the stress equations are solved using the *method of characteristics.* The stress field is assumed to be of plane stress type, i.e., stress in the thickness direction (σ_t) is zero. It uses the concept established by Szczepinski (1966) that the slope of the velocity characteristic is the same as that of the stress characteristics. Using the stress boundary conditions at the periphery of the sheet, the inward moving set of stress characteristics is generated. This set of characteristics gives the slope of the stress characteristics at the die cavity. Now, using the velocity boundary condition at the die cavity and the slope already found, another set of characteristics is drawn, but, this time moving outwards. This set of characteristics gives the velocity

omponents at the periphery of the sheet. Using this velocity ield at the periphery, the movement of the outer boundary of the heet during an incremental time interval is calculated giving the ew position of the boundary. The same procedure is repeated for he next time interval. Fig. 1.2 shows these two sets of haracteristics at different stages during the drawing operation. n this method, the accuracy of the result depends on the fineness of the net of characteristics, as well as, on the incremental time interval. The optimum blank size is obtained iteratively by modifying the blank size after every iteration. The modification to the blank size is done using the fact that the time taken for all the particles at the periphery of the initial blank, to come to the periphery of the final product, should be the same. Computational time can be significantly reduced if an approximate solution is used as an initial blank.

Karima (1988), has used a ***modified slip line field*** based approach to find the flat pattern for a deep drawn square cup. In this work, the velocity field in the flange area is found using the slip line field. Using the velocity field thus obtained, the movement of an element of the sheet is traced backward for an incremental backward movement of the punch. After finding the new locations of all the elements, the slip line field is modified accordingly and the same procedure is repeated till the entire punch movement is traced back. This method does not account for the effect of friction as well as that of strain hardening of the material. In the simplified form, even the thickness variation during the bending is neglected. The flat pattern obtained by this method may not be very accurate, but, they can be used as a starting solution for other methods like method of plane characteristic or finite element method.

Iseki and Murota (1986), have solved the problem of finding the flat pattern for a number of non-axisymmetrically shaped deep drawn cups. The ***finite element method*** is used to tackle this problem. The basic assumption made in this work is

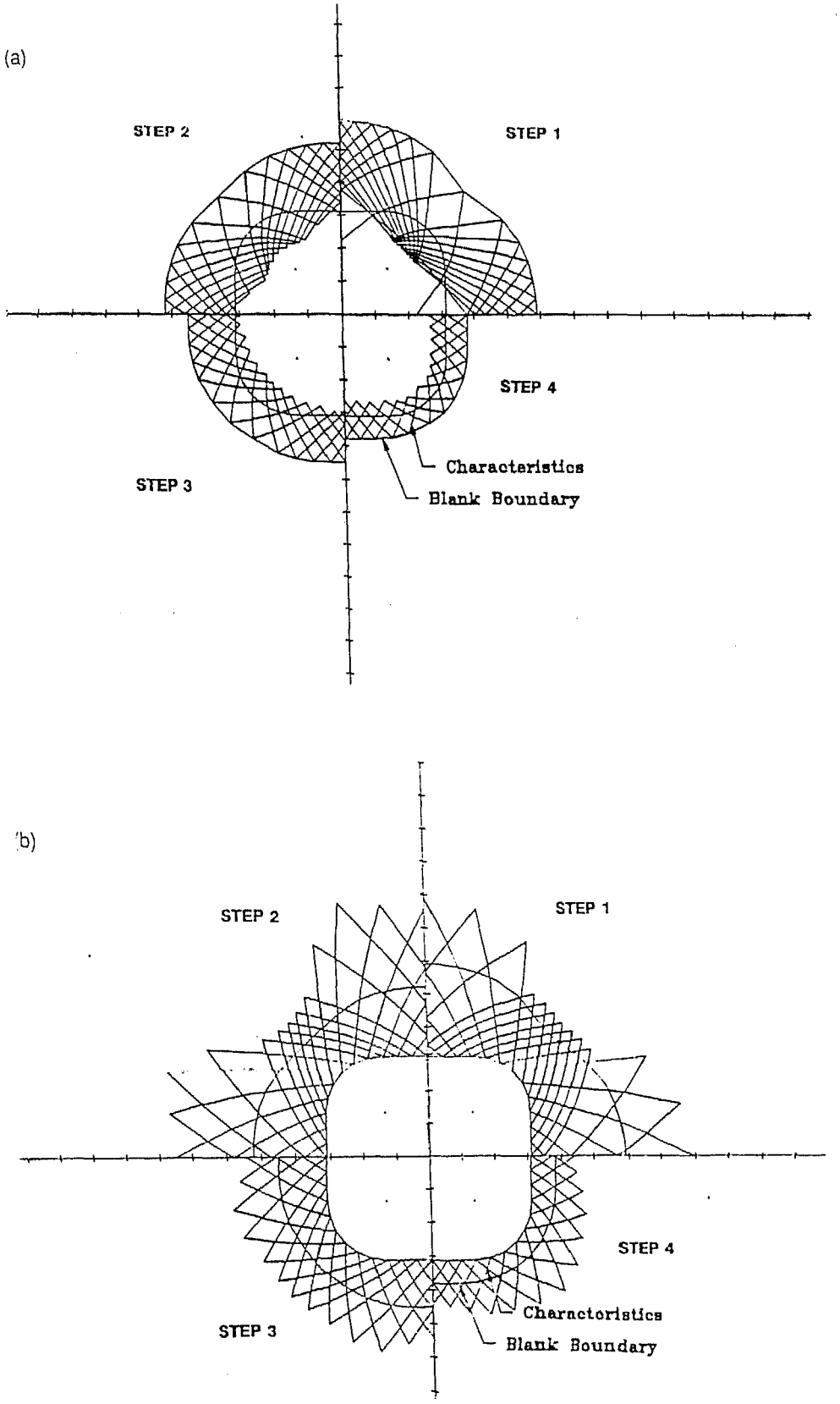

Fig. 1.2 Set of characteristics generated at different stages of drawing a) Inward moving characteristics b) Outward moving characteristic (Chen and Sowerby, 1991)

that the deformation velocity at the die contour is uniform and it is the same as punch velocity. The deformation of the flange is analyzed by considering a two-dimensional stress field (plane stress field) existing in the flange. The effect of strain hardening of material and thickness variation during the drawing operation is also accounted for. In this work also, the process is broken into a number of stages and in each stage, the finite element mesh is updated for the next stage after giving appropriate movement to the punch. The part thus obtained is compared with the part required and the blank size is modified accordingly. An optimum flat pattern can be obtained by iterating over the same procedure till the size of the flat pattern converges. For faster convergence, a near optimum flat pattern obtained by some other method like slip line field method can be used as an initial solution.

Toh and Kobayashi (1985) have also used *finite element analysis based on membrane theory,* to find the flat pattern for square cups. In the analysis, it is assumed that the material follows Hill's anisotropic yield criterion and Ludwik's strain hardening relationship. It is also assumed that the material in the flat bottom region undergoes very small plastic deformation and the stresses are varying linearly in each incremental step. The problem for three different shapes of initial blank is solved and the final products obtained are compared. Based on these results, an optimum blank shape is obtained for each case. Fig. 1.3 shows the optimum shapes for different starting blank shapes. Experiments were also conducted by the authors for these initial blank shapes and the results were found to be in good agreement with the predictions of the analysis. Here, the net material flow is represented by the distance between the initial and final locations of the same point on the periphery. The blank size is modified such that all the points on the periphery of the blank, come to the flange periphery at the end of the process. The initial blank size is very important in getting an optimum blank in a minimum number of iterations.

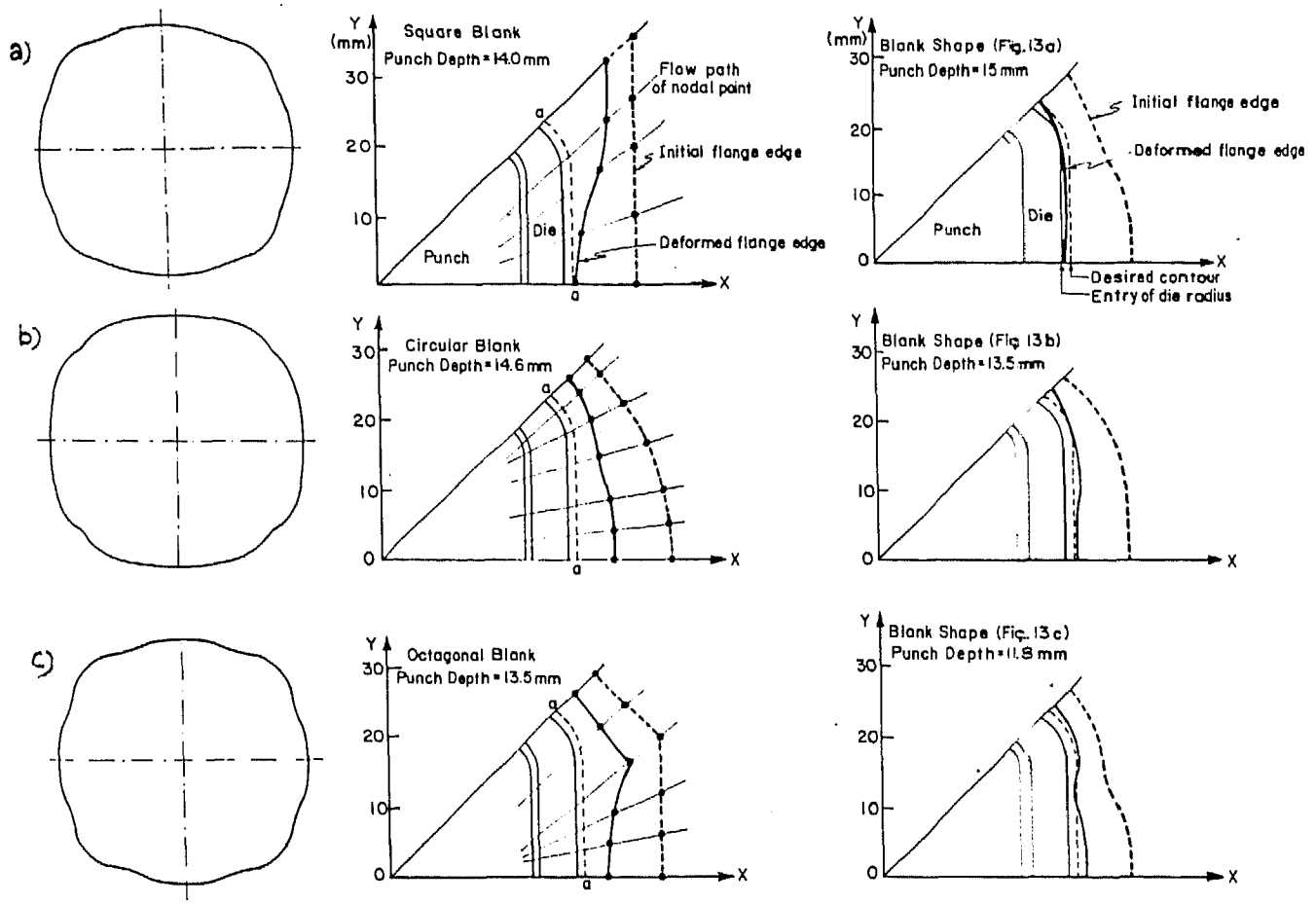

Optimum blank shape | Deformed flange shape after first iteration | Deformed flange shape using optimum blank

Fig. 1.3 Optimum blank shapes for different initial blanks. a) Square blank, b) Circular blank, c) Octagonal blank (Toh and Kobayashi, 1985)

1.3 STATEMENT OF PURPOSE

Above review of the literature has indicated that the ample work is not available in this field although the accuracy of the final product mainly depends on the accuracy of the flat pattern dimensions.

Literature on the flat pattern development for bent components has revealed that a detailed analysis of the problem is needed as the available works are based on the simplifying assumptions. At the same time, for flat pattern development for deep drawing, the finite element analysis based methods are detailed and accurate but they are computationally expensive and cumbersome to implement.

Based on these observations, in this work, we have proposed to develop methods for flat pattern development of bending and deep drawing which are accurate as well as computationally inexpensive.

The main objectives of this work are following:

1) To develop a prototype system for finding the flat pattern development for bent components considering the thinning effect and material hardening during bending and assuming plane strain field in the bend zone.

2) To develop a prototype system for finding the flat pattern development for a deep drawn component assuming plane stress field and considering the thinning of the sheet and strain hardening of material during drawing.

1.4 ORGANIZATION OF REPORT

Chapter 2 of this report gives the details of procedure for finding the flat pattern for bent components. It includes the

relevant mathematical formulations as well as the algorithm followed for finding the flat pattern.

In the next chapter, the operation of deep drawing is discussed in details. Various steps involved in finding the flat pattern for a deep drawn component are described along with appropriate theoretical background. A step-by-step iterative procedure for this purpose is also presented in this chapter.

In chapter 4, the results obtained for some example cases, by the developed prototype systems have been presented. For example on bent components, the part drawing and the flat pattern obtained are shown. The results in terms of bend allowance for each bend plane are also reported. In case of deep drawing, the desired and obtained part drawings are compared. The progressive flat pattern, i.e., the flat pattern found after every iteration along with the corresponding part dimensions obtained are also presented.

In the last chapter, the entire report have been summarized and the limitations of this work along with the scope for improvement are presented.

CHAPTER 2

FLAT PATTERN DEVELOPMENT FOR A BENT COMPONENT

2.1 INTRODUCTION

The basic objective of this chapter is to evolve a methodology for finding out the flat pattern for sheet metal components having one or more bend planes. The flat pattern for a bend plane of such a component is evaluated in terms of bend allowance for every bend. Bend allowance, as we have earlier defined, is the length of the unstretched fiber in the bend zone (BC in Fig. 2.1). So, the length required to produce the component will be the sum of the two flat planes adjacent to the bend plane, and the bend allowance for the bend zone.

Thus, by finding the bend allowance for each bend zone of the component and adding them, after proper geometrical transformations, to the lengths of adjacent flat planes, the original dimensions of that component can be found.

Fig. 2.1 shows a simple bent component and its flat pattern after development.

First step in finding the flat pattern is to select a plane having the maximum number of edges as a reference plane. The wireframe model is made in such a manner that it corresponds to the mean axis of the component. The bend allowance, accounting for thinning effect, is calculate by the algorithm given in the following section. The development with respect to any bend plane is found by first rotating the planes subsequent to the bend plane. The common edge between the reference plane and the bend plane is taken as the axis of rotation, and the planes are rotated by an angle equal to the included angle of the bend zone. After this, all these planes are translated by a distance equal to bend allowance in the development direction. After making these

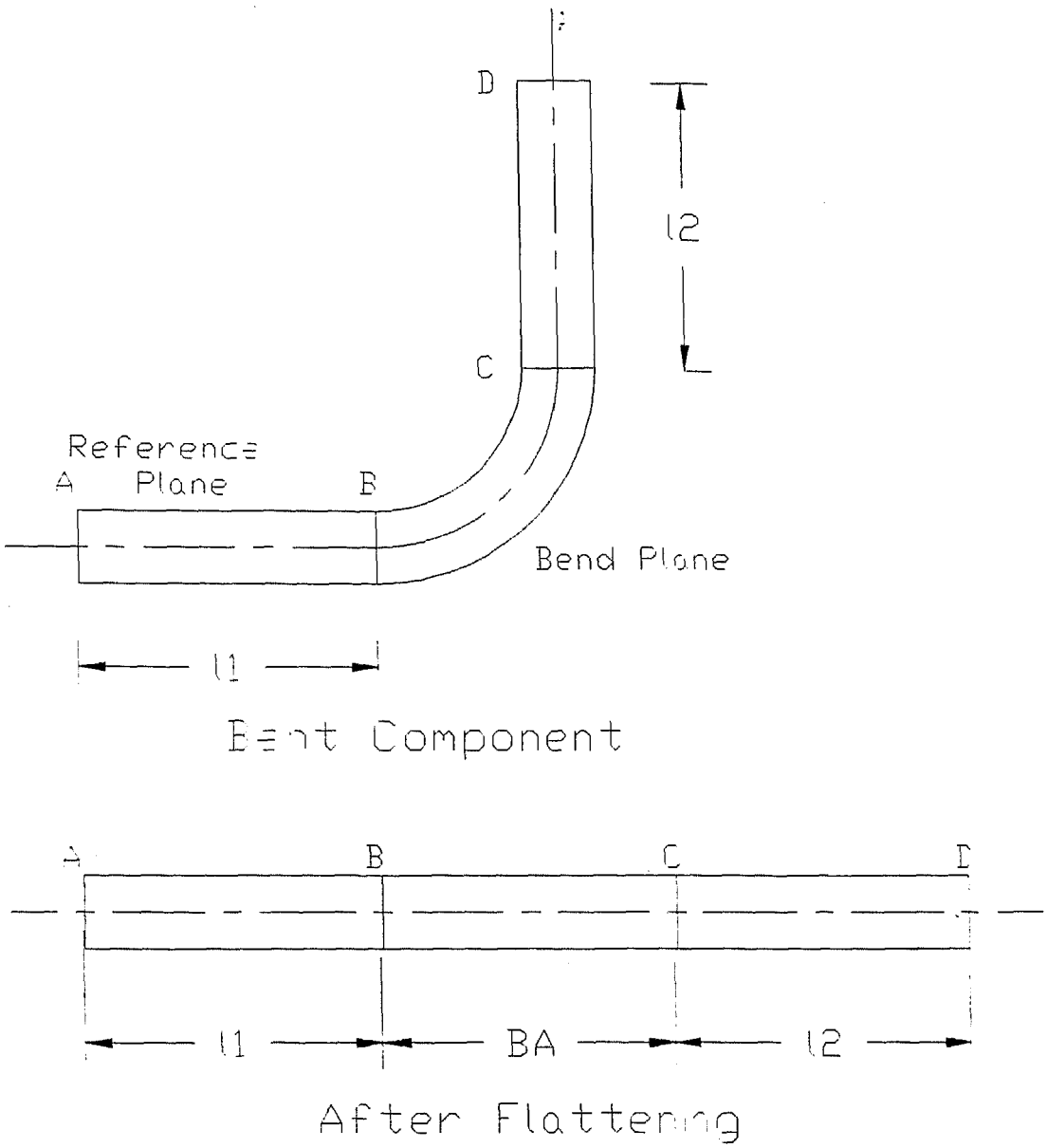

Fig. 2.1 Flat pattern development for a simple bent component (Nnaji et. al., 1991)

transformations, the developed bend plane and the plane next to it become coplaner with the reference plane. Now, the previous reference plane and the two newly added planes combined together make the new reference plane for developing other bend planes.

The same procedure is repeated for all the bend planes present in a component. After completing the procedure, all the points on the mean axis of the component will be in the reference plane. This graph will give the mean axis of the flat pattern required to produce the component. This flat pattern is in the reference plane, so, a final rotation is given to bring it into x-y plane.

In section 2.2, various steps involved in finding a flat pattern, and in the following section 2.3 its algorithm are given. The formats of input and output files are also discussed in the same section.

2.2 STEPS FOR FINDING A FLAT PATTERN

The main steps involved in finding the flat pattern for any bend plane are following :

1. Finding a reference plane.
2. Finding the axis of rotation.
3. Determination of development direction.
4. Estimation of bend allowance.
5. Rotation of subsequent planes.
6. Translation of subsequent planes.
7. Modification of part geometry databases.

The details of these steps are discussed below.

2.2.1 Finding A Reference Plane

In general, any plane can be taken as a reference plane without affecting the final result, but the time taken for

geometrical transformations can be significantly reduced if a plane having the maximum number of edges is used as the reference plane. This is so because, during the flat pattern development, all the planes are transformed to bring them into the reference plane.

To find the reference plane, the sum of number of edges in all the features in each plane is compared and the plane having the maximum number of edges is selected as the reference plane.

In Fig. 2.2, plane P_1 has the maximum number of edges (seven edges, e_1, e_2, .., e_7), so, it is taken as the reference plane.

2.2.2 Finding The Axis Of Rotation

The axis of rotation is defined as the unit vector along the edge which is common to both the bend plane and the reference plane. For finding this common edge, the lists of the edges for these two planes are compared and the edge present in both the lists is selected. The program segment used for this purpose, in pseudo code, is given as follows :

```
start_of_the edge_list_for_bend_plane
loop_1  :
  start_of_the_edge_list_for_the_reference_plane
  loop_2  :
       if (edge_of_bend_plane = edge_of_reference_plane)
            common_edge = edge_of_bend_plane
            exit
       else
            next_edge_of_the_list_for_reference_plane
  continue loop_2
  next_edge_of_the_list_for_bend_plane
continue loop_1
```

The loop terminates at "exit" as soon as an edge common

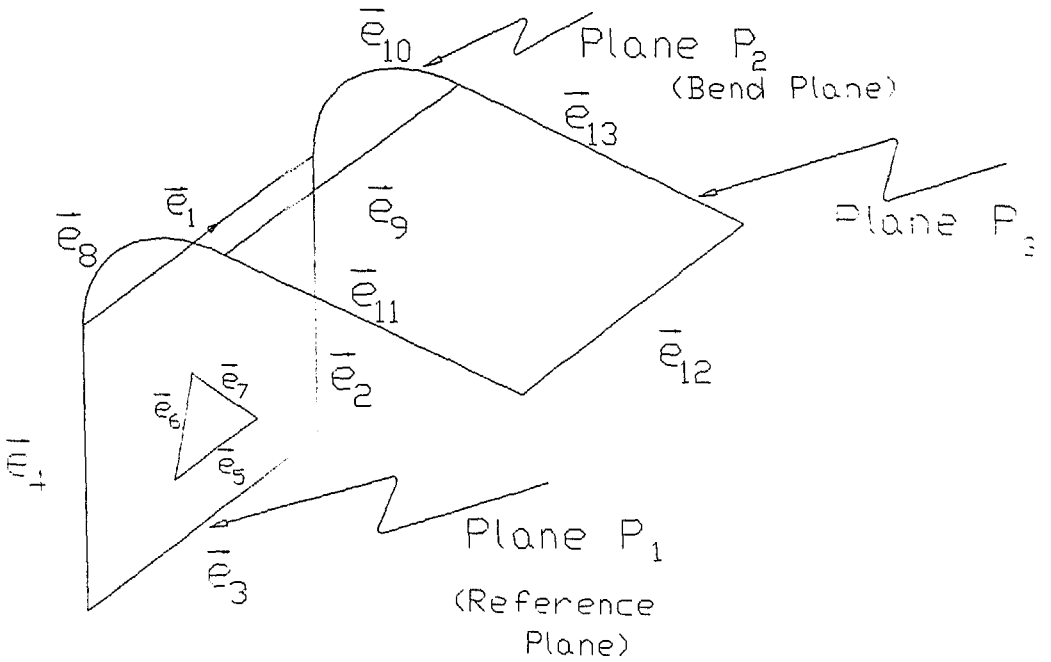

a) Before Development

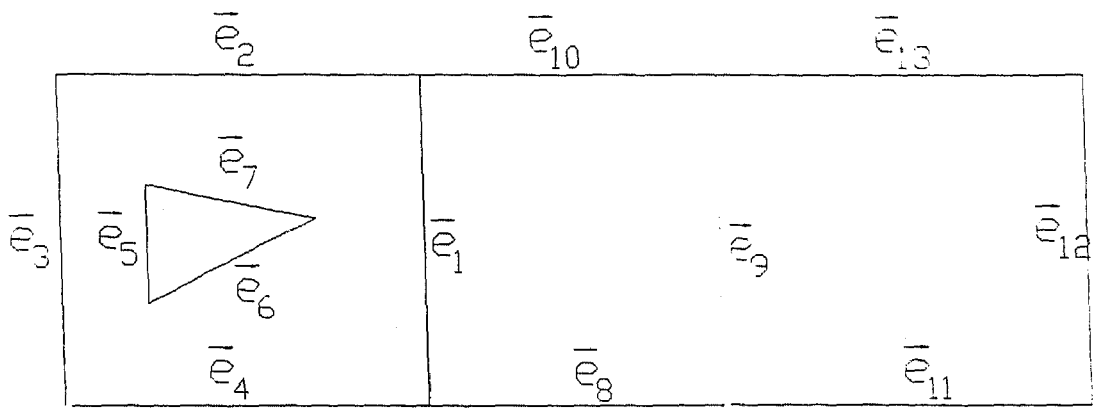

b) After Development

Fig. 2.2 Location of common edge between reference plane and bend plane

to both the planes is found. After identifying the common edge, the axis of rotation is determined by finding the unit vector along the common edge.

Table 2.1 gives the list of edges of the reference plane (P_1) and bend plane (P_2) for the component shown in Fig. 2.2. As is evident from the Table 2.1, the edge $\vec{e}_1$ is common to both the planes. So, the edge $\vec{e}_1$ is taken as a common edge. The location of the common edge $\vec{e}_1$ is shown in Fig. 2.2.

List of edges for reference plane	List of edges for bend plane
$\vec{e}_1$ $\vec{e}_2$ $\vec{e}_3$ $\vec{e}_4$ $\vec{e}_5$ $\vec{e}_6$ $\vec{e}_7$	$\vec{e}_1$ $\vec{e}_8$ $\vec{e}_9$ $\vec{e}_{10}$

Table 2.1 List of edges for reference plane and bend plane for the component shown in Fig. 2.2

2.2.3 Determination Of Development Direction

The development direction is the direction in which the bend plane is to be oriented after the development. It is normal to the common edge in the reference plane and projecting out of it. In Fig. 2.3, the vector $\vec{v}_1$ represents the direction of development, as it is normal to the common edge ($\vec{e}_1$) and coming out of the reference plane (P_1).

The vector $\vec{v}_1$ is found using the two mutually perpendicular vectors namely the vector normal to the reference plane ($\vec{v}_3$) and the vector associated with the common edge $\vec{e}_1$ (Fig.

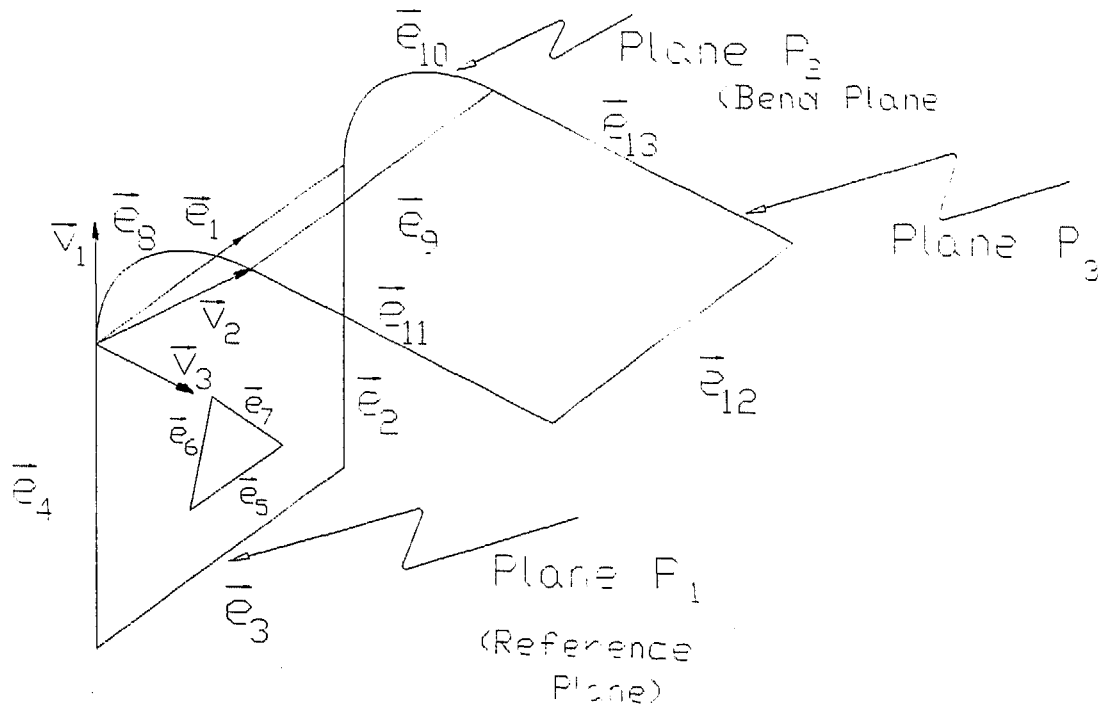

Fig. 2.3 Direction of development

2.3). The direction of development, being in the third mutually perpendicular direction, is found by taking vector product of the two previously mentioned vectors ($\vec{e}_1$ and $\vec{v}_3$). To ensure that the vector $\vec{v}_1$ is always coming out of the reference plane, the scalar product of the vector $\vec{v}_1$ and the vector $\vec{v}_2$ (Fig. 2.3), associated with the start and end vertices of the bend edge, is checked and a decision is taken on the basis of the magnitude of this scalar product and included angle of the bend.

The following special cases are also considered (Fig. 2.4) :

CASE 1 If scalar product $\vec{v}_1 \cdot \vec{v}_2$ is +ve and angle $\theta \leq 180^\circ$, take $\vec{v}_1$ as it is.

CASE 2 If scalar product $\vec{v}_1 \cdot \vec{v}_2$ is -ve and angle $\theta \leq 180^\circ$, take $\vec{v}_1$ as $-\vec{v}_1$.

CASE 3 If scalar product $\vec{v}_1 \cdot \vec{v}_2$ is -ve and angle $\theta \geq 180^\circ$, take $\vec{v}_1$ as it is.

CASE 4 If scalar product $\vec{v}_1 \cdot \vec{v}_2$ is +ve and angle $\theta \geq 180^\circ$, take $\vec{v}_1$ as $-\vec{v}_1$.

After finding the vector $\vec{v}_1$, the direction of development is found by taking the unit vector in the direction of the vector $\vec{v}_1$.

2.2.4 Estimation Of Bend Allowance

For estimating bend allowance, i.e., development of any bend plane, the formulation and algorithm given by Prasad and Somasundaram (1993) is used. Unlike other works, this formulation treats the unstretched fiber and neutral fiber differently and finds the radii (r_u and r_n respectively) at which they are located. It uses geometry of the bend and various material properties like initial yield stress (σ_o), strain hardening properties like strength coefficient (k), and strain hardening exponent(n) as input. It returns the length of the unstretched fiber (L_o) in the bend as output.

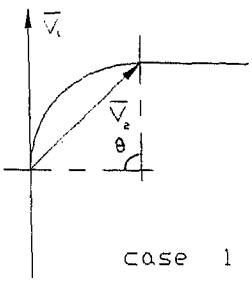

case 1
Included Angle θ = 180
$\overline{V_1} \cdot \overline{V_2} > = 0$

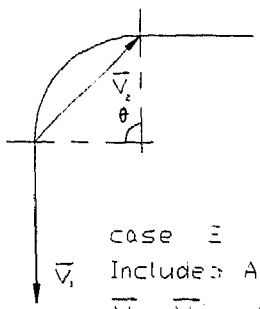

case 2
Included Angle θ = 180
$\overline{V_1} \cdot \overline{V_2} = 0$

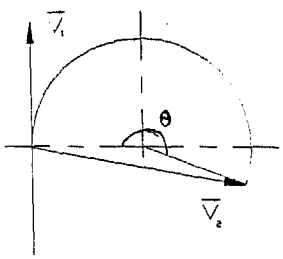

case 3
Included Angle θ = 180
$\overline{V_1} \cdot \overline{V_2} < = 0$

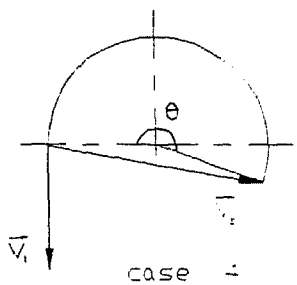

case 4
Included Angle θ = 180
$\overline{V_1} \cdot \overline{V_2} = 0$

Fig. 2.4 Fixing direction of development

The main geometrical parameters used in this formulation for finding the bend allowance are shown in Fig. 2.5.

After identifying the bend plane for development, the corresponding bending parameters like inner radius of bend (r_i), included angle (θ) etc. are found. Using thickness of the sheet, (t), the outer radius (r_o) and radius of mid fiber (r_m) of the bend zone are also calculated.

The formulation for finding the bend allowance given by Prasad and Somasundaram (1993) is described in the next section.

2.2.4.1 Formulation

This formulation is based on the following assumptions :

i) The material is rigid-plastic and strain hardening. It is assumed to follow the Ludwik's strain hardening rule.
ii) The deformations are occurring under plain-strain conditions.
iii) The material is incompressible.
iv) Bauschinger effect is negligible.
v) The process is quasi-static.
vi) End effects are negligible.

Various stages for finding the bend allowance using this formulation is shown in Fig. 2.6 and their details are given in Fig. 2.7 (a), (b) and (c).

The differential equation for equilibrium can be written as

$$\frac{d\sigma_r}{dr} = \frac{\sigma_\theta - \sigma_r}{r} \quad ; \qquad \text{(A)}$$

where, σ_θ and σ_r are the stresses in circumferential and radial directions respectively.

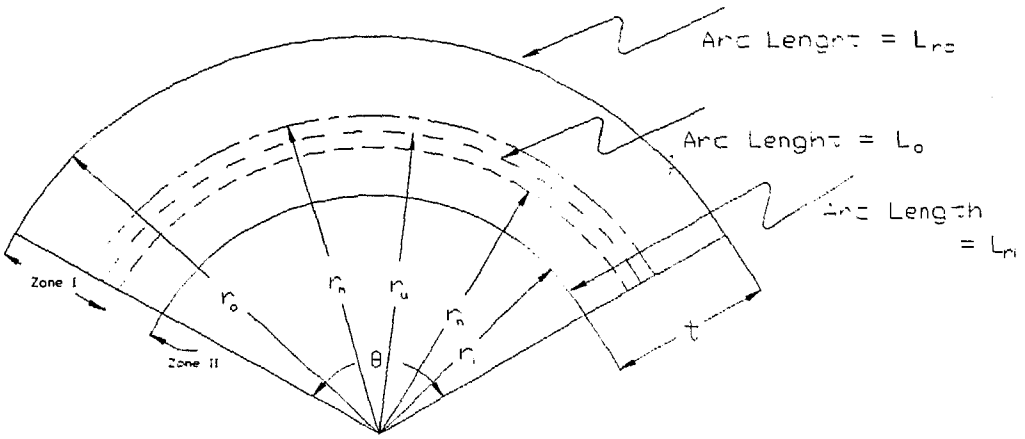

Fig. 2.5 Location of important fibers and other parameters of bend (Prasad et. al., 1993)

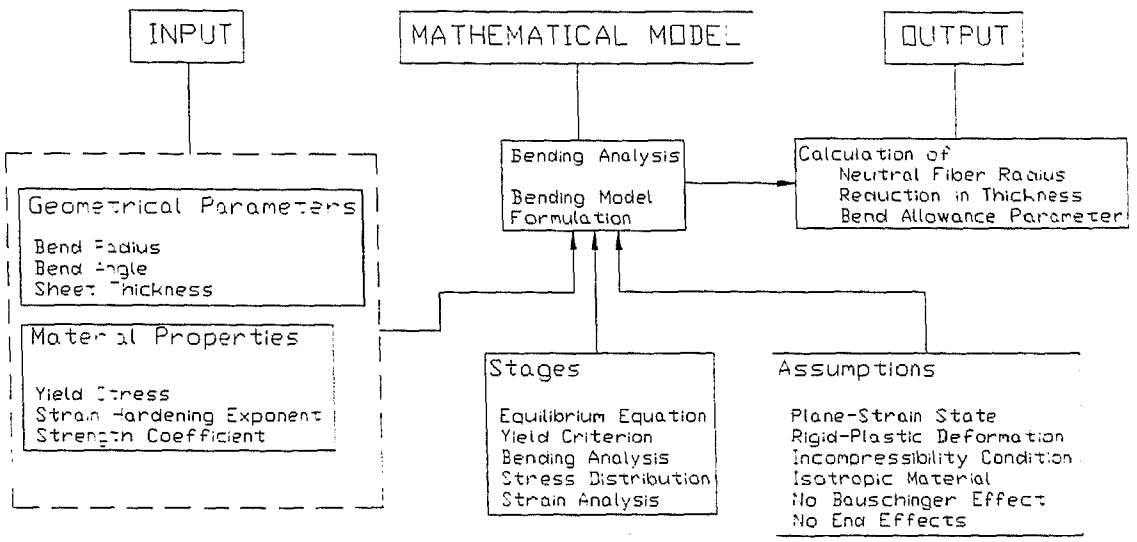

Fig. 2.6 Stages of bend allowance calculation (Prasad et. al., 1993)

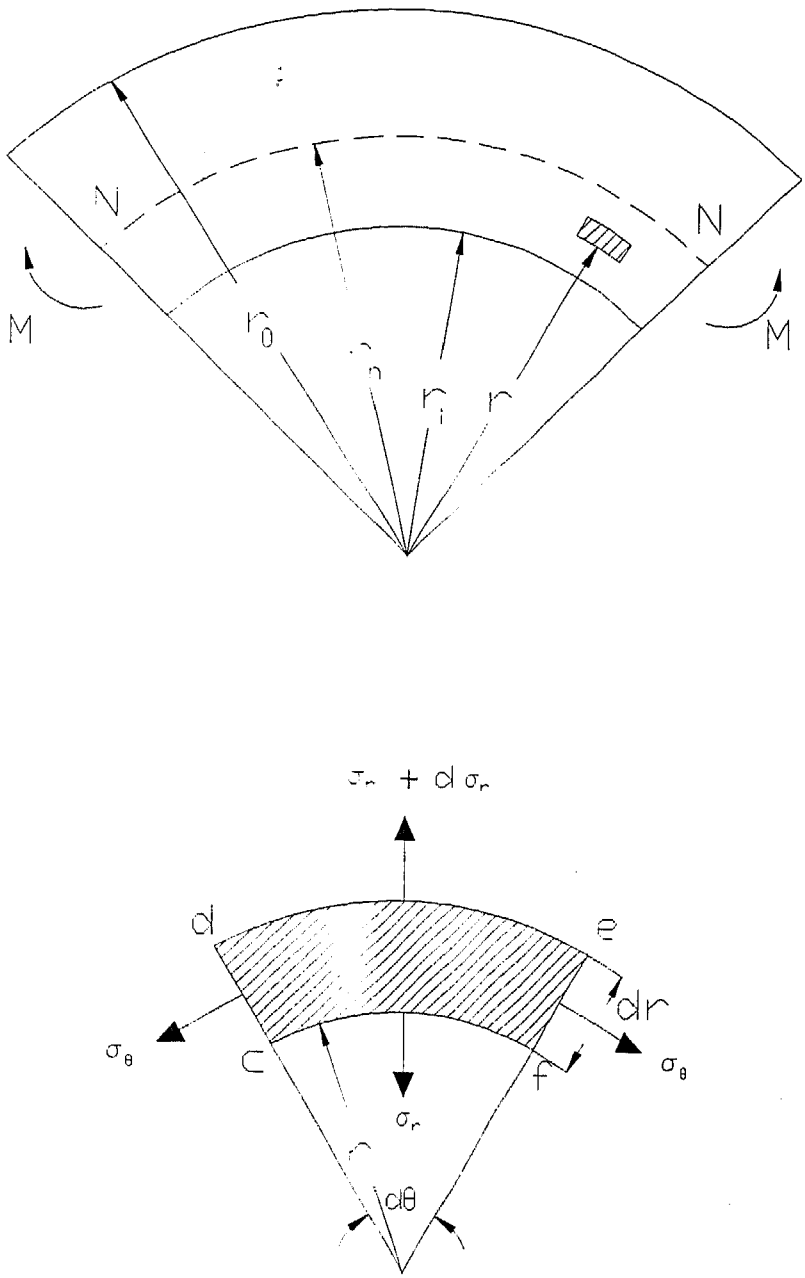

Fig. 2.7(a) Stresses on an element in bend zone (Prasad et. al., 1993)

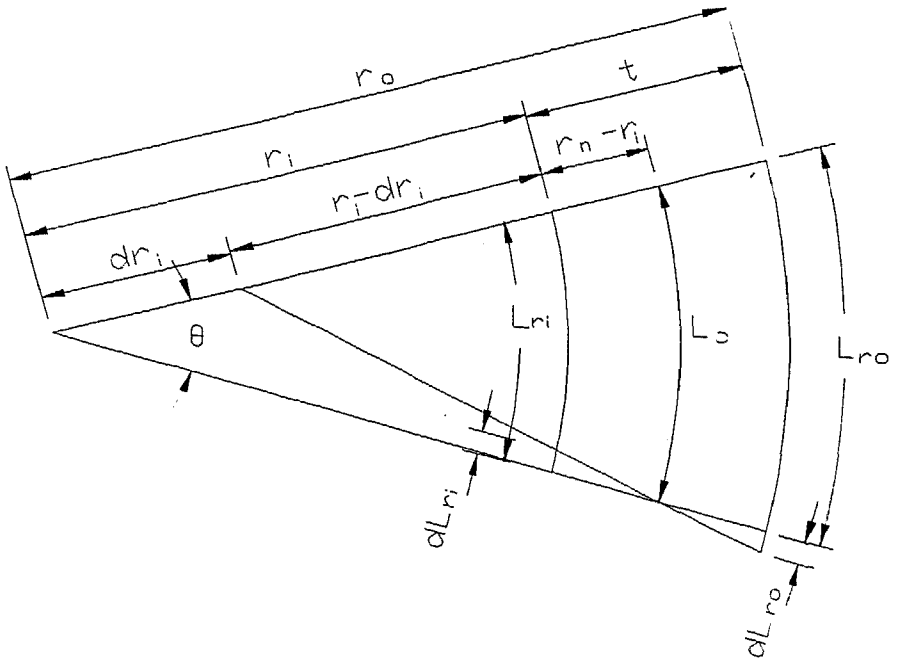

Fig. 2.7(b) Geometrical changes during a small incremental bend (Prasad et. al., 1993)

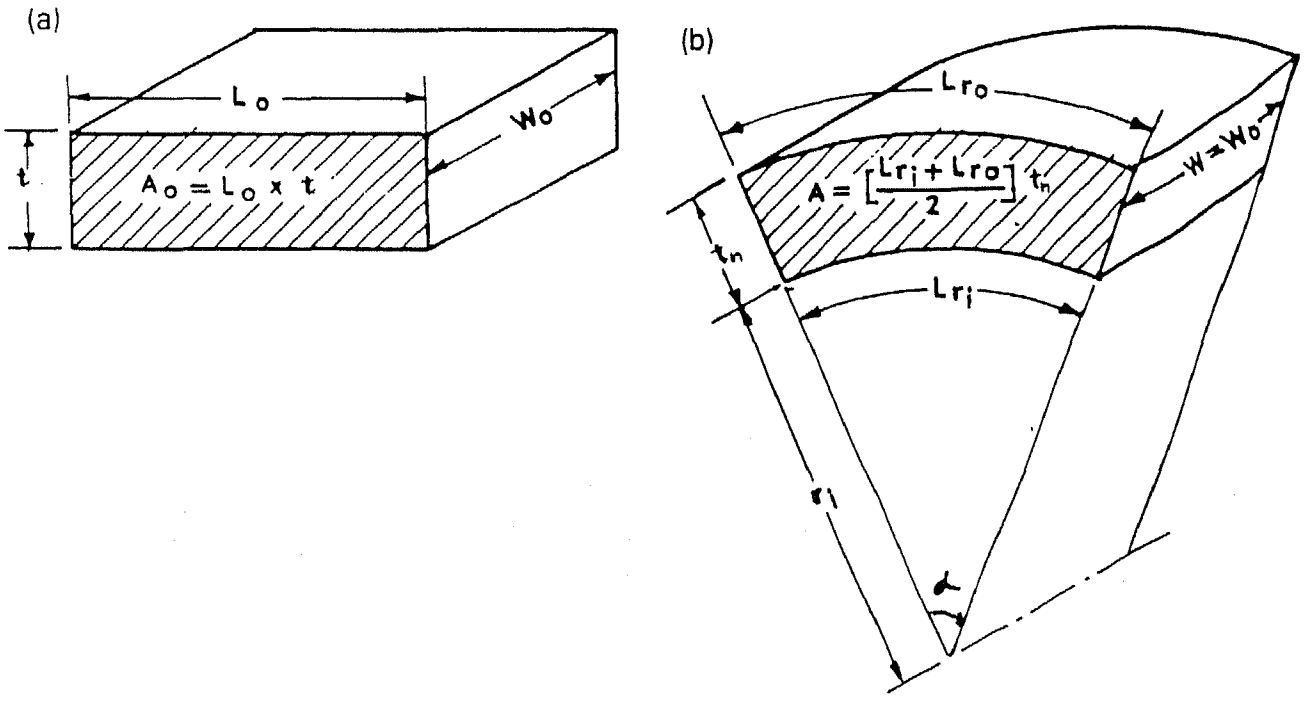

Fig. 2.7(c) Incompressibility condition (Prasad et. al., 1993)

The strain (ε_θ) in the θ direction will be

$$\varepsilon_\theta = \ln (r / r_u) . \qquad (B)$$

The equivalent strain ($\bar{\varepsilon}$) is

$$\bar{\varepsilon} = 2 / \sqrt{3}\ \varepsilon_\theta . \qquad (C)$$

The von Mises yield criteria using the plane strain condition will be

$$\bar{\sigma} = \sqrt{3} / 2\ (\sigma_\theta - \sigma_r) ;$$

where $\bar{\sigma}$ is the equivalent stress after considering strain hardening according to Ludwik's formula which can be written as

$$\bar{\sigma} = \sigma_o + k\ \bar{\varepsilon}^{\,n}$$

$$\text{or,}\quad \sigma_\theta - \sigma_r = 2 / \sqrt{3}\ (\sigma_o + k\ \bar{\varepsilon}^{\,n}) .$$

Substituting this in the equilibrium equation (eq. (A)) and using the definitions of ε_θ and $\bar{\varepsilon}$ (eq. (B) and (C)), we obtain

$$d\sigma_r = \frac{1}{r} \left[\frac{2\ \sigma_o}{\sqrt{3}} \pm k \left(\frac{2}{\sqrt{3}}\right) \left\{ \ln \left(\frac{r}{r_u}\right)\right\}^n \right] dr ;$$

where + stands for the zone I $r_n < r < r_o$
and - stands for the zone II $r_i < r < r_n$ in Fig. 2.5.

Solving above differential equation with boundary condition that the stresses are zero at free surfaces and equating the values of σ_r at the neutral fiber ($r = r_n$) for both the zones, we obtain,

$$\frac{(2 / \sqrt{3})^n\ k}{(n + 1)\ \sigma_y} \left\{ \left[\ln \left(\frac{r_u}{r_i}\right)\right]^{n+1} - \left[\ln \left(\frac{r_o}{r_u}\right)\right]^{n+1} \right\} + \left[\ln \left(\frac{r_n^{\,2}}{r_i r_o}\right)\right]^{n+1} = 0 . \qquad (2.1)$$

This relation can be used to find the location of the neutral fiber (r_n). Further, the incompressibility condition (Fig.

2.7c) is given as below

$$t_n \left(\frac{L_{r_i} + L_{r_o}}{2} \right) = t\, L_o \quad ; \qquad (2.2a)$$

where, L_{r_i} and L_{r_o} are the lengths of the innermost and outermost fibers respectively and t_n and t are final and initial thicknesses respectively.

Again, by considering the geometry and the incompressibility of the material, the change in thickness can be estimated using eq. (2.2a).

$$\frac{t}{t_n} = \frac{1}{2} \left(\frac{L_{r_i}}{L_o} + \frac{L_{r_o}}{L_o} \right)$$

$$= \frac{1}{2} \left(e_{r_i} + e_{r_o} \right) + 1 \; ; \qquad (2.2b)$$

where e_{r_i} and e_{r_o} are the strains at the innermost and outermost fibers respectively and the thickness of the sheet is changing from t to t_n.

Here, $\frac{L_{r_i}}{L_o}$ and $\frac{L_{r_o}}{L_o}$ can be calculated by integrating the ratios of the incremental changes in the lengths and the original lengths as given below :

$$e_{r_i} = L_o \int^{L_{r_i}} \frac{dL_{r_i}}{L_o} \; ;$$

and $$e_{r_o} = L_o \int^{L_{r_o}} \frac{dL_{r_o}}{L_o} \; .$$

Again, from the geometry (Fig. 2.7b)

$$\frac{dL_{r_i}}{L_o} = \frac{dr_i}{r_i} - \frac{dr_i}{r_n} \; ;$$

$$\text{and} \quad \frac{dL_{r_o}}{L_o} = \frac{dr_i}{r_o} - \frac{dr_i}{r_n} .$$

$$\text{So,} \quad e_{r_i} = \int_{\infty}^{r_i} \left(\frac{dr_i}{r_i} - \frac{dr_i}{r_n} \right) \quad ;$$

$$\text{and} \quad e_{r_o} = \int_{\infty}^{r_o} \left(\frac{dr_i}{r_o} - \frac{dr_i}{r_n} \right) \quad . \qquad (2.3)$$

Based on this formulation an algorithm was developed by Prasad and Somasundaram (1993) to find the bend allowance.

2.2.4.2 The algorithm

The step by step procedure to compute the length of the unstretched fiber using above formulation is given here. In this procedure, the problem is solved assuming that the thickness of the sheet remains constant during the period the bending takes place. After solving the problem with the constant thickness in a perticular iteration, we find the change in thickness using the relation (eq. (2.2b)). It is assumed that the thickness of the sheet remains uniform across the length of the bend plane. This new thickness is used as the initial thickness for solving the problem in the next iteration. We continue till no significant change in thickness is observed between two consecutive iterations. The main steps of this algorithm are following :

STEP 1 : Take $t = t_o$ (the initial thickness), $r_u = r_n =$ radius of the mid fiber, r_m $(= r_i + t / 2)$.

STEP 2 : Solve eq. (2.1) to get r_n.

STEP 3 : Integrate eq. (2.3) for constant t to obtain e_{r_i} and e_{r_o}.

STEP 4 : Calculate next approximation of thickness t_n using eq. (2.2b).

STEP 5 : If $| t_n - t | \geq \varepsilon$ $(= 0.001$, assumed for present work) Go to step 7.

STEP 6 : Calculate L_o from the incompressibility condition

(eq. (2.2a)), STOP.

STEP 7 : Substitute $t = t_n$.

STEP 8 : Repeat the steps 2 - 7 till the value of t converges (Difference in initial and final thickness in a perticular iteration is less than or equla to ε).

The flow chart for this algorithm is given in Fig. 2.8.

2.2.5 Rotation Of Subsequent Planes

For flattening, first of all, the bend plane and all the subsequent planes are rotated by an angle equal to the included angle of the bend plane. Orientation of the various planes before and after the rotation is shown in Fig. 2.9.

This rotation is acquired by applying the transformation for rotation about any arbitrary axis (Rogers and Adams, 1990). This arbitrary axis of rotation is nothing but the axis of rotation found in the step 2 (sect. 2.2.2). For getting the required transformation, the axis of rotation is transformed such that it coincides with the z-axis (the choice of z-axis is arbitrary, any other axis, x or y could have been selected) and passes through the origin of co-ordinate system. Now, any rotation about the z-axis is the rotation about the original axis of rotation, if proper reverse transformations are given to bring the axis back to its original position.

Let the direction cosines of the arbitrary axis of rotation be $[c_x \quad c_y \quad c_z \quad 0]$ and the length of its projection in y-z plane be d (Fig. 2.10), then,

$$d = \sqrt{(c_y^2 + c_z^2)} \quad .$$

The procedure for complete transformation is given below (Fig. 2.10) :

1) Translate the common edge $\vec{e}_1$ (Fig. 2.10a) such that its

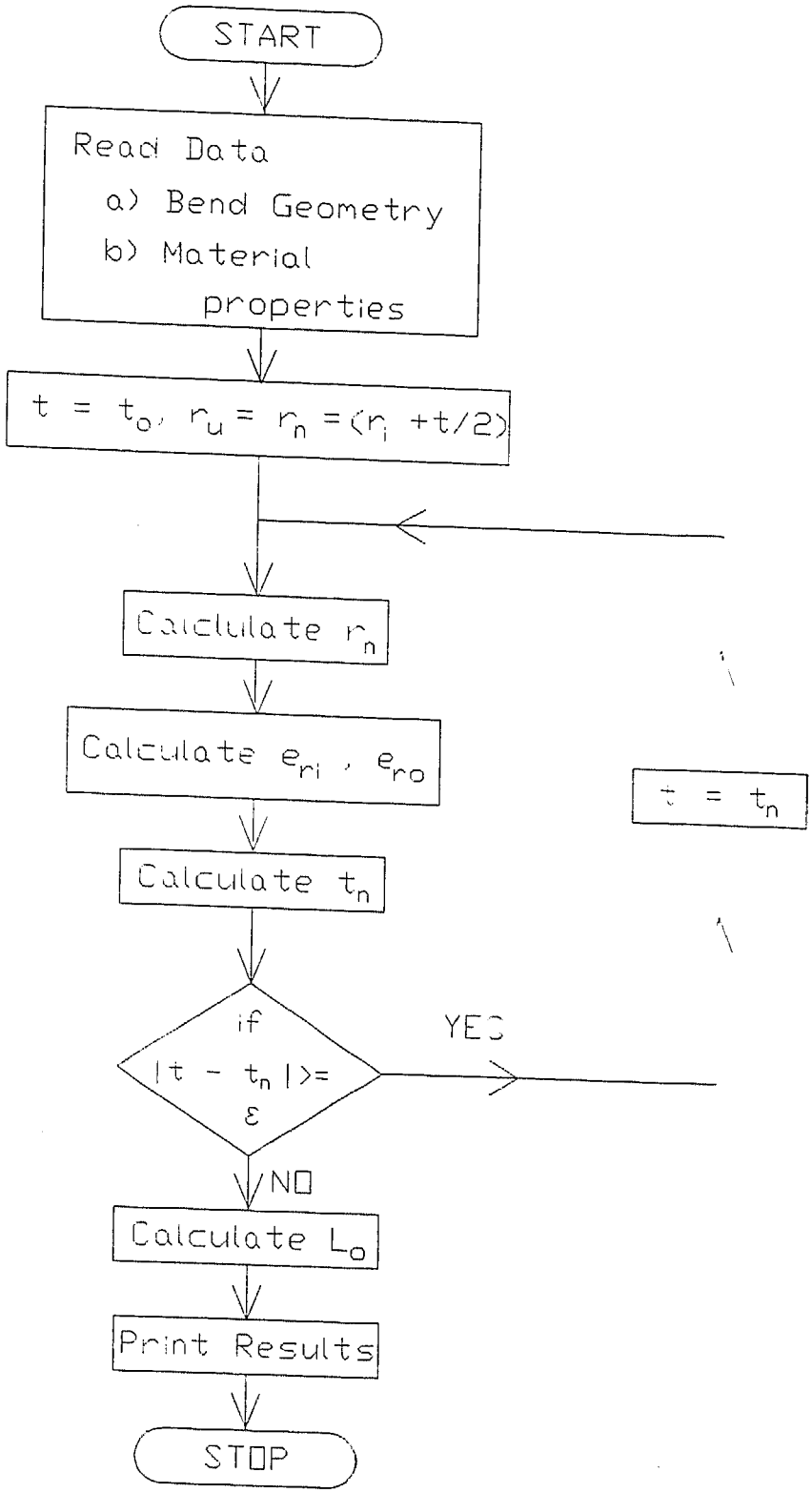

2.8 Flow chart for finding bend allowance

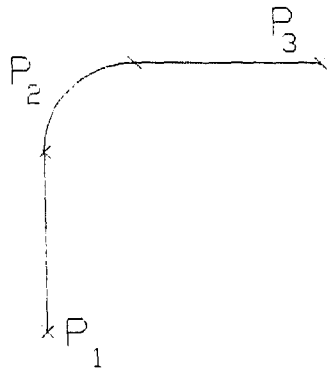

Planes Before Rotation

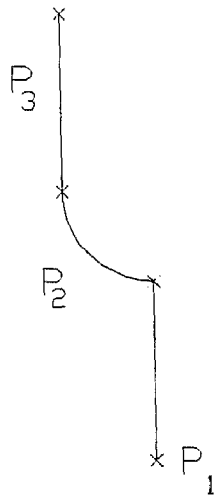

Planes After Rotation

Fig. 2.9 Orientation of planes before and after rotation

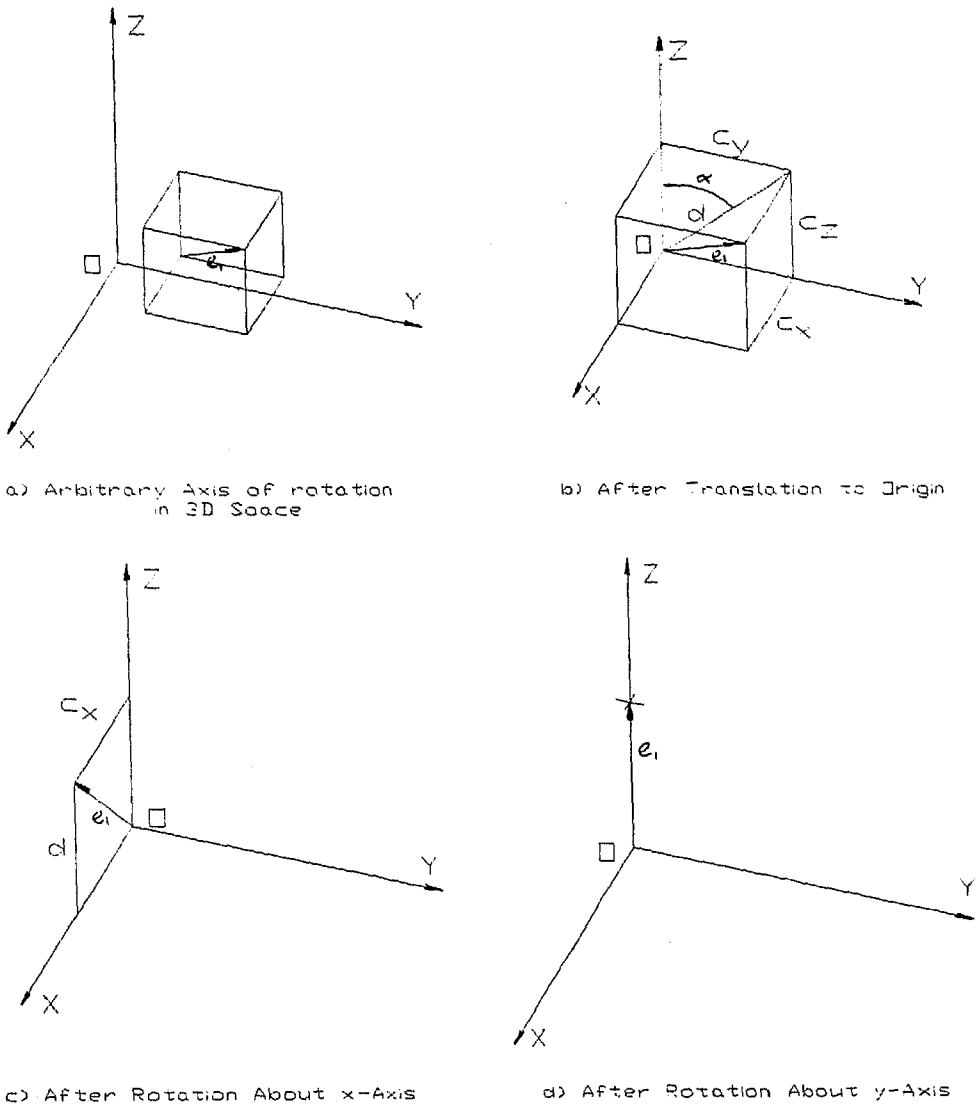

a) Arbitrary Axis of rotation in 3D Space

b) After Translation to Origin

c) After Rotation About x-Axis

d) After Rotation About y-Axis

Fig. 2.10 Rotation about an arbitrary axis

starting vertex coincides with the origin of the co-ordinate system (Fig. 2.10b). If the co-ordinates of the starting vertex of the edge $\vec{e}_1$ are $[x_o\ y_o\ z_o]$, the corresponding transformation matrix will be

$$[T] = \begin{bmatrix} 1 & 0 & 0 & 0 \\ 0 & 1 & 0 & 0 \\ 0 & 0 & 1 & 0 \\ -x_o & -y_o & -z_o & 1 \end{bmatrix}.$$

2) Rotate the common edge about the x-axis such that it falls in the x-z plane (Fig. 2.10c). The corresponding transformation matrix will be following :

$$[R_x] = \begin{bmatrix} 1 & 0 & 0 & 0 \\ 0 & \cos\alpha & \sin\alpha & 0 \\ 0 & -\sin\alpha & \cos\alpha & 0 \\ 0 & 0 & 0 & 1 \end{bmatrix} = \begin{bmatrix} 1 & 0 & 0 & 0 \\ 0 & c_z/d & c_y/d & 0 \\ 0 & -c_y/d & c_z/d & 0 \\ 0 & 0 & 0 & 1 \end{bmatrix}.$$

3) Rotate the common edge $\vec{e}_1$ about y-axis such that it coincides with the z-axis (Fig. 2.10d). The corresponding transformation matrix will be

$$[R_y] = \begin{bmatrix} d & 0 & c_x & 0 \\ 0 & 1 & 0 & 0 \\ -c_x & 0 & d & 0 \\ 0 & 0 & 0 & 1 \end{bmatrix}.$$

4) Rotate about the z-axis. This is the rotation which is to be given about the original axis. The corresponding matrix of rotation to give a rotation by an angle θ about the z - axis will be following

$$[R_z] = \begin{bmatrix} \cos\theta & \sin\theta & 0 & 0 \\ -\sin\theta & \cos\theta & 0 & 0 \\ 0 & 0 & 1 & 0 \\ 0 & 0 & 0 & 1 \end{bmatrix}.$$

5) Reverse rotation about y-axis $[R_y]'$.
6) Reverse rotation about x-axis $[R_x]'$.
7) reverse translation $[T]'$.

So, the complete transformation matrix will be

$$[R] = [T] [R_x] [R_y] [R_z] [R_y]' [R_x]' [T]'. \quad (2.4)$$

For rotating any plane, all the points of that plane were premultiplied with the transformation matrix $[R]$ (eq. (2.4)). The same transformation is applied to all the points of all the planes subsequent to the bend plane being developed. This completes the rotation of planes.

2.2.6 Translation Of Subsequent Planes

After making the transformations discussed in the previous section, the plane next to the bend plane, P_3, (Fig. 2.11) becomes parallel to the reference plane (P_1). Now, we have to translate it in such a manner that it comes into the reference plane and the distance between the two planes is equal to the bend allowance (BA) for the bend plane under consideration.

Now, we extend the common vertex, v_1, between the reference plane (P_1) and the bend edge (Fig. 2.12) in the direction of the unit vector defined as the direction of development ($\vec{v}_1$) in section 2.2.3. The magnitude of extension is equal to the bend allowance (BA) already found. This brings the vertex v_1 at v_2'. This is the new location of the vertex v_2 after development. So, the vertex v_2 has to be translated to v_2' and the same translation has to be given to all the points of plane P_3 to bring it in the reference plane.

The distance to be translated is the straight line distance between the points v_2' and v_2. But, the point v_2' is nothing but the vertex v_1 extended in the direction of development

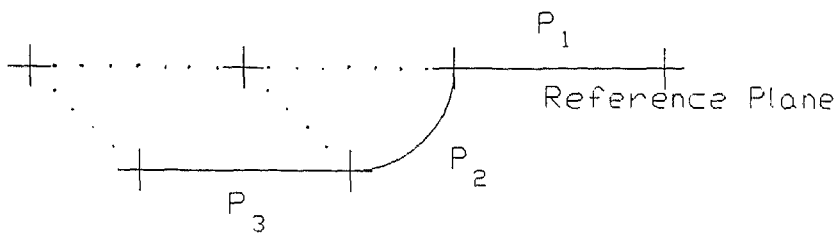

Planes Before Translation

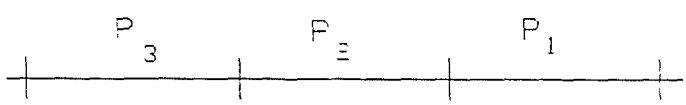

Planes After Translation

Fig. 2.11 Orientation of planes before and after translation

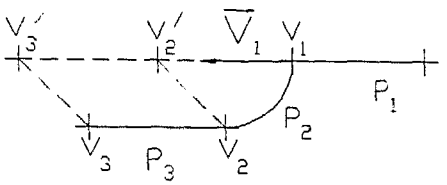

$$V_2' - V_2 =$$

$$[x_1 - x_2 + lL \quad y_1 - y_2 + mL \quad z_1 - z_2 + nL \quad 0]$$

Fig. 2.12 Location of vertices before and after translation

/ a distance equal to bend allowance. If the direction of evelopment is given by the unit vector [l m n 0] and L be ne bend allowance, then the co-ordinates of the points v_2' can be ound as

$$v_2' = v_1 + L \times [\ l \quad m \quad n \quad 0\ ] \ .$$

If $v_1 = [\ x_1 \quad y_1 \quad z_1 \quad 0\ ]$

then, the co-ordinates of v_2' will be

$$v_2' = [\ x_1 + l\ L \quad y_1 + m\ L \quad z_1 + n\ L \quad 0\ ] \ .$$

So, the distance to be translated will be

$$v_2' - v_2 = [\ x_1 - x_2 + l\ L \quad y_1 - y_2 + m\ L \quad z_1 - z_2 + n\ L \quad 0] \ ;$$

where $[\ x_2 \quad y_2 \quad z_2 \quad 0\ ]$ are the co-ordinates of the point v_2.

The corresponding translation matrix will be as follows :

$$[\ T\ ] = \begin{bmatrix} 1 & 0 & 0 & 0 \\ 0 & 1 & 0 & 0 \\ 0 & 0 & 1 & 0 \\ x_1 - x_2 + l\ L & y_1 - y_2 + m\ L & z_1 - z_2 + n\ L & 1 \end{bmatrix} . \qquad (2.5)$$

All the points of the planes subsequent to the bend plane are translated by this matrix. After this transformation, the bend plane and the plane next to it are flattened and made co-planner to the reference plane.

2.2.7 Modification Of Part Geometry Databases

While making the transformations discussed in previous sections, all the mathematical operations are done on

database for vertices. So, after making changes in the database for vertices, the database for edges is also modified. For every edge, its start and end vertices are traced and the old values are replaced with the changed values. The bent edges, which were initially listed as arcs are now listed as straight lines after their development.

The list of edges of the reference plane is also modified such that it incorporates the newly added planes to it. After development of a bend plane, the bend plane and the plane next to it come into the reference plane, and all the three jointly form the new reference plane for the development of the next bend plane. For this, the lists of edges for these two planes being added to the reference plane are merged with the list of edges of the reference plane. While making this merger, the common edges are not repeated.

Table 2.2 shows the list of edges on planes for the component shown in Fig. 2.2. It also gives the list of edges in the component after the development.

Plane No.	List of edges
1	e_1 e_2 e_3 e_4
2	e_1 e_8 e_9 e_{10}
3	e_9 e_{11} e_{12} e_{13}
1 (Inside feature)	e_5 e_6 e_7

a)

Plane No.	List of edges
1	e_1 e_2 e_3 e_4 e_8 e_9 e_{10} e_{11} e_{12} e_{13}
1 (Inside feature)	e_5 e_7 e_6

b)

Table 2.2 List of edges for each plane for component shown in Fig. 2.2. a) Before development, b) After development.

It can be seen in the Table 2.2 that the common edges $\vec{e}_1$ and $\vec{e}_9$) appear only once in the edge list for the component after development.

This stage completes the development for any bend plane and makes the database ready for taking on development of the next bend plane.

With these steps discussed in details, we need an algorithm as shown below for finding the complete flat pattern.

2.3 THE ALGORITHM

The step by step procedure for finding the complete flat pattern is as follows :

STEP	1	Read the data about geometrical information and material characteristics.
STEP	2	Identify the reference plane.
STEP	3	Select a bend plane attached to reference plane.
STEP	4	Using the logic given in section 2.2.2, find the corresponding axis of rotation.
STEP	5	Find the direction of development as given in sect. 2.2.3.
STEP	6	Find the bend allowance for the bend plane considering thinning effect.
STEP	7	Rotate the planes subsequent to the bend plane by an angle equal to the angle of bend using the rotation matrix (eq. (2.4)).
STEP	8	Translate the planes subsequent to the bend plane by a distance equal to the bend allowance using the translation matrix given in eq. (2.5).
STEP	9	Modify the part geometry database.
STEP	10	Modify the reference plane by adding the developed bend plane and the planes next to it.
STEP	11	Repeat the steps 3 - 10 till there is no more bend plane undeveloped.

STEP 12 Stop.

The flow chart used for developing the prototype system for the flat pattern development for a bent component is given in Fig. 2.13.

Based on this flow chart, the appropriate prototype systems are developed in the programming language Turbo C. The input to the system is the wireframe model of the mean axis of the component to be developed. It contains the list of the vertices with their co-ordinates in World Co-ordinate System (WCS). Table 4.3 and 4.4 show the list of vertices before and after the development for the component taken as Example 1 in chapter 4. The list of edges contains the information on the type of edge (entity), i.e., whether it is a line or an arc or a circle. It also contains the number of starting and end vertices along with their co-ordinates. In case of an arc, the co-ordinates of the starting vertex are replaced by the co-ordinates of its center and the co-ordinates of the end vertex are replaced with the information on the radius and the start and end angles of the arc. In case of a circle, the start vertex number and co-ordinates are replaced with the vertex number of the center and its co-ordinates. The space for the end vertex is left blank for the circles. The format of this list can be seen in Table 4.5 and 4.6 which show the list of edges before and after the development for the same component. The input file also contains the list of all the loops present along with the list of edges constituting that loop. Table 4.7 and 4.8 show the list of loops in different planes before and after the development for the component previously considered.

The input file for this program is obtained from the separate feature extraction system (Jagirdar, 1995) which gives the input file in a compatible form.

The output of the system is also given in the same form with proper changes in the values. Appropriate .dxf files are also

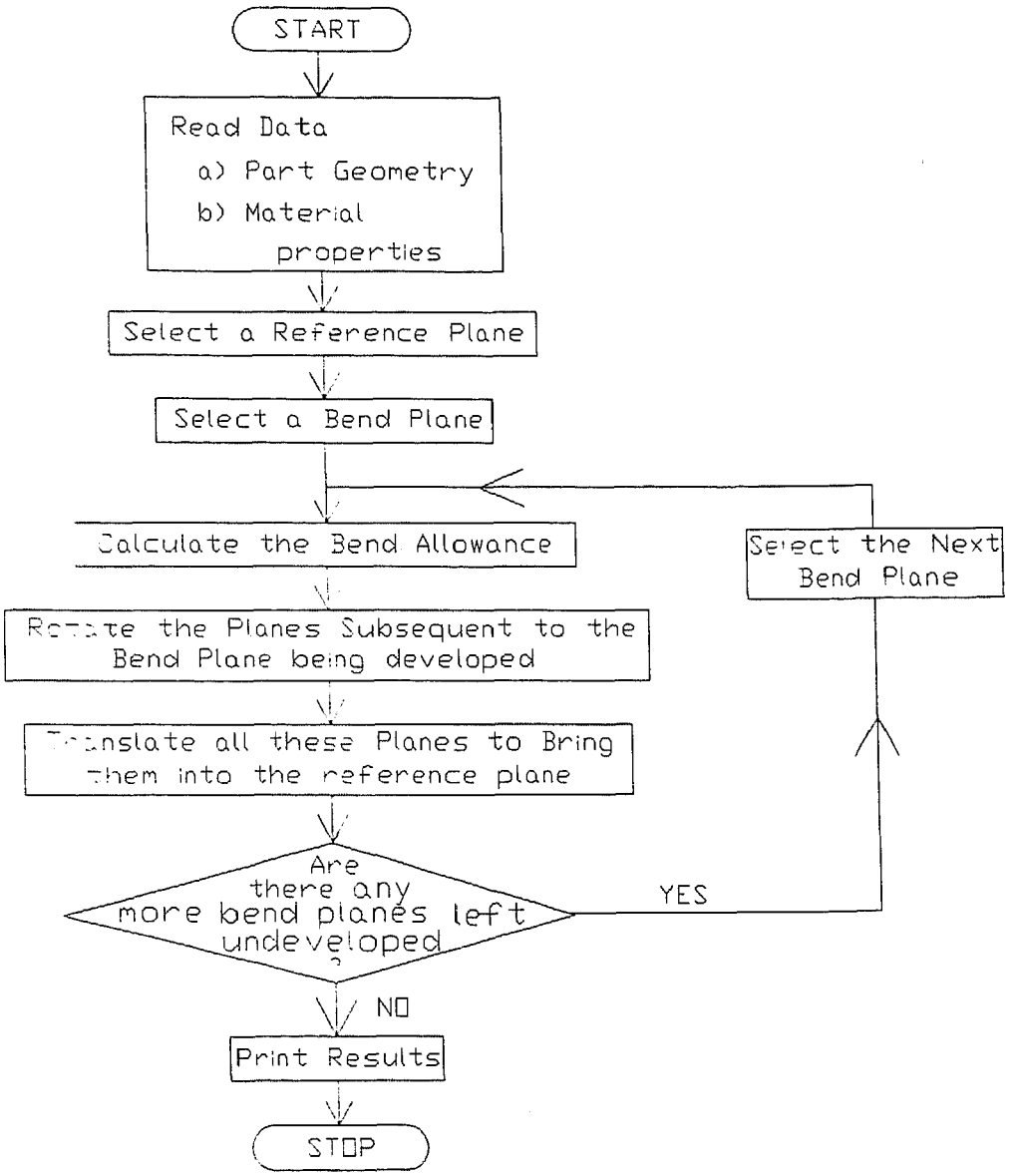

Fig. 2.13 Flow chart for finding the flat pattern for a bent component

created by the system itself for drawing the flat pattern obtained in ACAD. This helps in displaying as well as getting the hard copy of the output.

The prototypes are run on 80386 machine in DOS environment. The execution time was about 90 sec. for each bend plane. The results obtained for the example problem solved are listed separately in the chapter for Results and Discussion.

CHAPTER 3

FLAT PATTERN DEVELOPMENT FOR A DEEP DRAWN COMPONENT

3.1 INTRODUCTION

Drawing is a process which can be broken into a number of successive elementary stages. The deformation parameters, like stresses and strains, can be calculated for each stage. Generally, the value of the deformation parameters for any stage will depend on the values for the preceding stage. This concept can be extended to evolve a methodology to find the flat pattern for axisymmetric deep drawn cups. A small movement is given to the punch in each stage and the stresses and strains are calculated using the above process. These values are again used for solving the problem for the next incremental movement of the punch. Various geometric parameters of a deep drawing system are shown in Fig. 3.1.

In the next section (sect. 3.2), a detailed analysis of the problem for a general three dimensional case is given. Section 3.3 lists the assumptions made to make this problem tractable. After making these assumptions, the analysis done in section 3.2 is modified accordingly. This modified analysis is given in the next two sections, namely, 3.4 and 3.5. Section 3.6 gives various steps involved in finding the flat pattern for an axisymmetric deep drawn cup. The next section (sect. 3.7) gives the algorithm used for finding the flat pattern.

3.2 THEORETICAL BACKGROUND

Deep drawing is a very complex problem in which three dimensional stress and strain fields exist in the flange as well as in the curved segments over the die and punch profiles. Various aspects of the plasticity problem for a general three dimensional

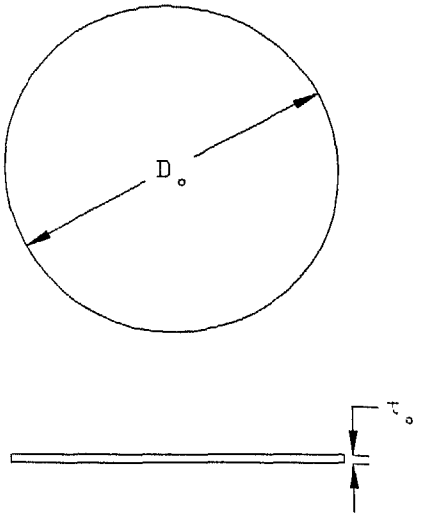

a) Blank for Deep Drawing

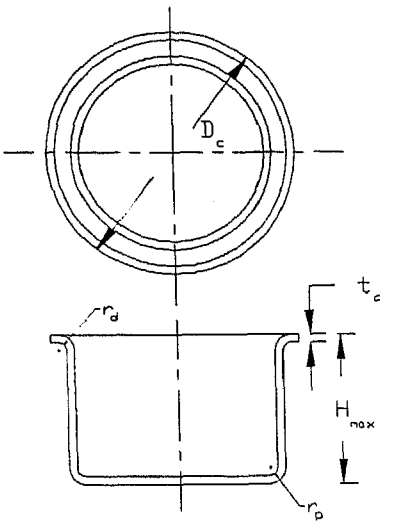

b) A Deep Drawn Cup

($D_C < D_0$, $t_C > t_0$)

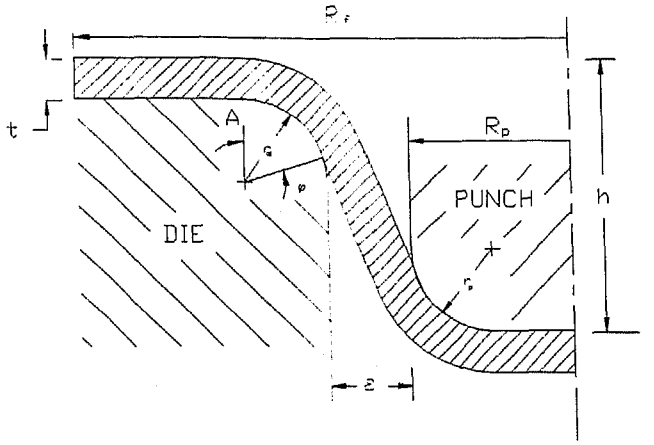

c) A Deep Drawing System

Fig. 3.1 Geometry of deep drawing system

case are given as follows :

3.2.1 Equilibrium Equation

Consider a small elemental volume of a sheet element of rotational symmetry (Jimma and Kuwabara, 1989) bounded by meridinal planes inclined at an angle $d\theta$ to each other and by radial planes inclined at an angle $d\phi$ to each other. Let this element be at radial distance R from the axis of symmetry and r from the center of curvature and the thicknesses at the two ends be t and (t + dt) respectively (Fig. 3.2). The stresses acting in the meridinal direction are σ_ϕ and $\sigma_\phi + d\sigma_\phi$. The uniform stress σ_θ acts in the circumferential direction, whereas, σ_{t1} and σ_{t2} are the two stresses that act in the direction normal to the surface of the element and τ_1 and τ_2 are the stresses which act on the surface of the sheet in the meridinal direction (Fig. 3.2). Various forces acting on this element are balanced as follows :

a) *Force Balance in Meridinal Direction* yields the following equation :

$$\{\sigma_\phi (R + dR)\, d\theta\, t - (\sigma_\phi + d\sigma_\phi)\, R\, d\theta\, (t + dt)\} \cos\frac{d\phi}{2} - 2\,\sigma_\theta\, r\, d\phi\, t \sin\frac{d\theta}{2} \cos\phi + (\tau_1 - \tau_2)\, r\, R\, d\phi\, d\theta = 0. \quad (D)$$

Since angles $d\theta$ and $d\phi$ are very small, $\sin\frac{d\theta}{2}$ and $\cos\frac{d\phi}{2}$ can be approximated as $\frac{d\theta}{2}$ and 1 respectively.

After this approximation, equation (D) can be written as,

$$\sigma_\phi (R + dR)\, d\theta\, t - (\sigma_\phi + d\sigma_\phi)\, R\, d\theta\, (t + dt) - \sigma_\theta\, r\, d\phi\, t\, d\theta \cos\phi + (\tau_1 - \tau_2)\, r\, R\, d\phi\, d\theta = 0.$$

This can be further simplified as

$$\sigma_\phi\, dR\, t - \sigma_\theta\, dR\, t - R(\sigma_\phi dt + d\sigma_\phi t) + (\tau_1 - \tau_2)\, r\, R\, d\phi = 0.$$

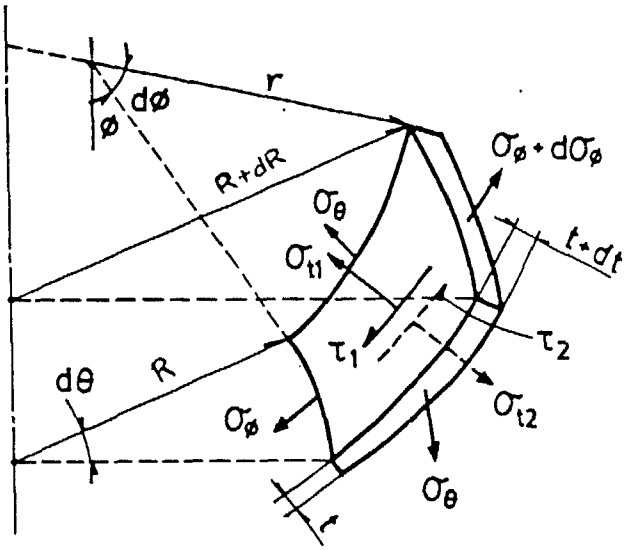

Fig. 3.2 Three dimensional stress field on a sheet element (Jimma et. al. 1989)

$$\text{or,} \quad (\sigma_\phi - \sigma_\theta)\, dR\, t - R\, d(\sigma_\phi t) + (\tau_1 - \tau_2)\, r\, R\, d\phi = 0.$$

After dividing the above equation by (dR t), it can be written as,

$$\text{or,} \quad (\sigma_\phi - \sigma_\theta) - \frac{R\, d(\sigma_\phi t)}{dR\, t} + \frac{(\tau_1 - \tau_2)\, r\, R\, d\phi}{dR\, t} = 0 .$$

As the length of the arc in the meridinal direction is small, it can be approximated as a straight line. This approximation gives $dR = r \cos \phi\, d\phi$. Making this substitution in the third term of the above equation, it can be written as,

$$\text{or,} \quad (\sigma_\phi - \sigma_\theta) - \frac{R\, d(\sigma_\phi t)}{dR\, t} + \frac{(\tau_1 - \tau_2)\, r\, R\, d\phi}{r \cos \phi\, d\phi\, t} = 0 .$$

Division of above equation by -(t / R) and rearrangement yields,

$$\text{or,} \quad \frac{d(\sigma_\phi t)}{dR} - \frac{t(\sigma_\theta - \sigma_\theta)}{R} - \frac{(\tau_1 - \tau_2)}{\cos \phi} = 0 . \qquad (3.1)$$

This is the equation of equilibrium in the meridinal direction.

b) *Force balance in the direction normal to tangent plane* results in following relationship :

$$(\sigma_{t1} - \sigma_{t2})(r + t)\, d\phi\, R\, d\theta - 2\, \sigma_\theta\, r\, d\phi\, t \sin\frac{d\theta}{2} \sin\phi + \{\sigma_\phi (R + dR)\, d\theta\, t + (\sigma_\phi + d\sigma_\phi)(t + dt) R\, d\theta\} \sin\frac{d\phi}{2} = 0. \qquad (3)$$

Since the angles $d\theta$ and $d\phi$ are very small, the following approximations can be made

$$\sin\frac{d\theta}{2} \simeq \frac{d\theta}{2};$$

$$\text{and} \quad \sin\frac{d\phi}{2} \simeq \frac{d\phi}{2}.$$

Again, as r » t, (r + t) can be taken as r.

With these approximations, equation (E) can be written as,

$$(\sigma_{t1} - \sigma_{t2}) r\ R\ d\phi\ d\theta - \sigma_\theta\ r\ t\ \sin\phi\ d\phi\ d\theta + \{\sigma_\phi (R + dR)\ t + (\sigma_\phi + d\sigma_\phi)(t + dt) R\}\ \frac{d\phi}{2}\ d\theta = 0$$

or, $$(\sigma_{t1} - \sigma_{t2}) r\ R\ d\phi\ d\theta - \sigma_\theta\ r\ t\ \sin\phi\ d\phi\ d\theta + \frac{1}{2}\{\sigma_\phi R\ t + \sigma_\phi\ dR\ t + \sigma_\phi\ R\ t + \sigma_\phi\ R\ dt + d\sigma_\phi\ R\ t + d\sigma_\phi\ R\ dt\}\ d\phi\ d\theta = 0 .$$

In the above equation, neglecting third and higher order terms, following relationship can be obtained,

$$(\sigma_{t1} - \sigma_{t2}) r\ R - \sigma_\theta\ r\ t\ \sin\phi + \sigma_\phi\ R\ t = 0 ;$$

or, $$\frac{(\sigma_{t1} - \sigma_{t2})}{t} - \frac{\sigma_\theta\ \sin\phi}{R} + \frac{\sigma_\phi}{r} = 0 .$$

Substituting for $r = \frac{dR}{\cos\phi\ d\phi}$, we get the required equilibrium equation in the direction normal to the meridinal plane as,

$$\frac{(\sigma_{t1} - \sigma_{t2})}{t} - \frac{\sigma_\theta\ \sin\phi}{R} + \sigma_\phi\ \cos\phi\ \frac{d\phi}{dR} = 0 . \quad (3.2)$$

3.2.2 Logarithmic Strain

Consider a element (Fig. 3.3) at an initial mean radius "s" which moves to a mean radius "r" and during this movement its length changes to dl from ds in the meridinal direction. In this case, the incremental logarithmic strains in the meridinal and circumferential directions ($d\varepsilon_\phi$, $d\varepsilon_\theta$ respectively) can be given as,

$$d\varepsilon_\theta = \ln\left(\frac{r}{s}\right) \quad (3.3)$$

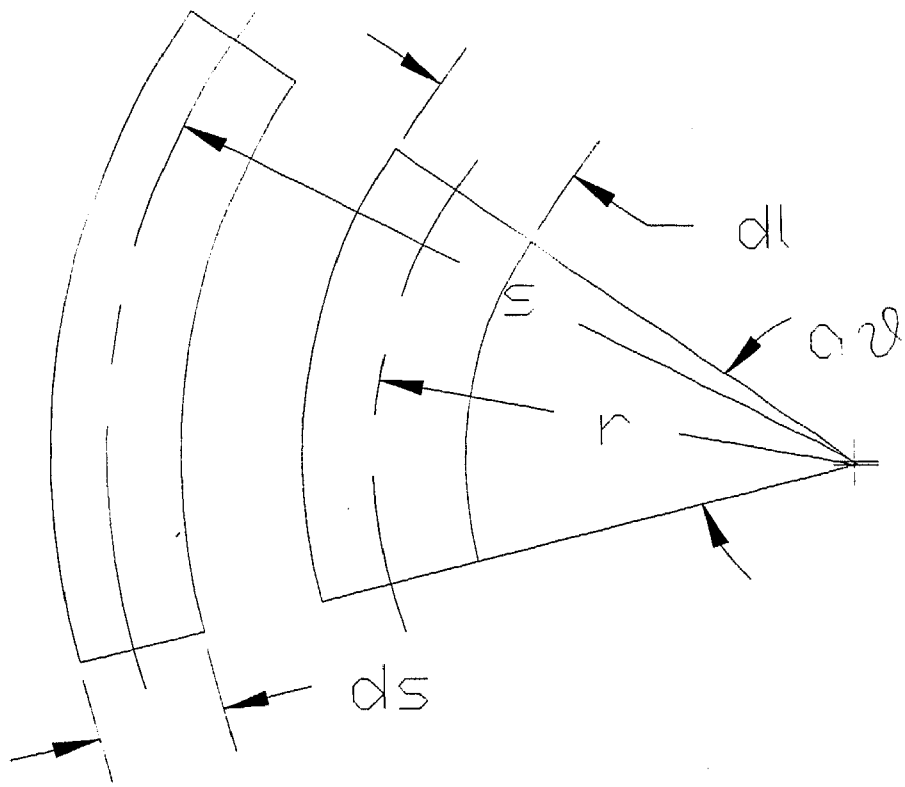

Fig. 3.3 Logarithmic strain

Considering the incompressibility condition,

$$d\varepsilon_t + d\varepsilon_\phi + d\varepsilon_\theta = 0$$

or $$d\varepsilon_t = -(d\varepsilon_\phi + d\varepsilon_\theta) = \ln\left(\frac{t}{t_o}\right) \qquad (3.5)$$

where $d\varepsilon_t$ is the incremental strain in thickness direction as the thickness of the element changes from t_o to t.

3.2.3 Stress - Strain Relationship

The flow rule associated with von Mises yield criterion can be written as

$$\varepsilon_{ij} = \lambda \frac{d\{(\sigma_1 - \sigma_2)^2 + (\sigma_2 - \sigma_3)^2 + (\sigma_3 - \sigma_1)^2\}^{1/2}}{d\sigma_{ij}} \quad ;$$

This equation gives,

$$\varepsilon_1 = 2\lambda\,(2\sigma_1 - \sigma_2 - \sigma_3) \quad ,$$

$$\varepsilon_2 = 2\lambda\,(2\sigma_2 - \sigma_3 - \sigma_1) \quad ,$$

and,

$$\varepsilon_3 = 2\lambda\,(2\sigma_3 - \sigma_1 - \sigma_2) \quad ;$$

where σ_1, σ_2, σ_3 and ε_1, ε_2, ε_3 are the stresses and strains in the three principal directions, and λ is a dimensionless parameter.

The above equation can also be written as :

$$\frac{\varepsilon_1}{(2\sigma_1 - \sigma_2 - \sigma_3)} = \frac{\varepsilon_2}{(2\sigma_2 - \sigma_3 - \sigma_1)} = \frac{\varepsilon_3}{(2\sigma_3 - \sigma_1 - \sigma_2)} = 2\lambda \; . \qquad (3.6)$$

This gives the required stress - strain relationship.

In addition, the equivalent stress ($\bar{\sigma}$) and strain ($\bar{\varepsilon}$) are defined as

$$\bar{\sigma} = \{(\sigma_1 - \sigma_2)^2 + (\sigma_2 - \sigma_3)^2 + (\sigma_3 - \sigma_1)^2\}^{1/2} \qquad (3.7)$$

$$\text{and} \quad \bar{\varepsilon} = \frac{\sqrt{2}}{3}\{(\varepsilon_1 - \varepsilon_2)^2 + (\varepsilon_2 - \varepsilon_3)^2 + (\varepsilon_3 - \varepsilon_1)^2\}^{1/2} \quad . \tag{3.8}$$

3.2.4 Strain Hardening Characteristic

In this work, the material is assumed to follow Ludwik's strain hardening rule. Mathematically, this can be written as,

$$\bar{\sigma} = \sigma_o + k\,(\bar{\varepsilon})^{n} \tag{3.9}$$

where, σ_o is the initial yield stress, k is the strength coefficient, n is the strain hardening exponent and $\bar{\sigma}$ is the equivalent stress after hardening.

This particular hardening rule is selected because it gives a better correspondence with the experimental results (Prasad and Somasundaram, 1993).

3.2.5 Instability Criterion

This condition is used to specify the limit up to which drawing can be done successfully. In this work Considere's Construction (Calladine, 1985) is used as the required limiting condition (fig 3.4). This criterion uses the nominal stress to estimate the drawing limit.

This criterion can be stated as "for successful drawing operation, the slope of the true stress - true strain curve (i.e., $(d\bar{\sigma} / d\bar{\varepsilon})$) should always be greater than the nominal stress (s)".

From the incompressibility condition, we know that,

$$A_o\, l_o = A\, l$$

$$\text{or,} \quad A_o / A = l / l_o \tag{F}$$

where, A_o and l_o are the initial area and length respectively in a uniaxial tensile test, and A and l are the area and length respectively at a certain stage of deformation. Let P be the drawing force at this stage, then the true stress (σ) and nominal stress can be defined as,

$$\sigma = \frac{P}{A}$$

and, $$s = \frac{P}{A_o} ;$$

or, $$\frac{\sigma}{s} = \frac{A_o}{A} .$$

Substituting for (A_o/A) from eq. (F), this can be written as

$$\frac{\sigma}{s} = \frac{l}{l_o}$$

$$= (1 + \varepsilon) .$$

The above relation can also be simplified as

$$s = \frac{\sigma}{(1 + \varepsilon)} .$$

Although, this formulation is done for uniaxial tensile stress field, it can be used for a three dimensional stress field by taking the equivalent stress and strain for the three dimensional stress field. So, this condition becomes

$$\bar{s} = \frac{\bar{\sigma}}{(1 + \bar{\varepsilon})} .$$

In Fig. 3.4, the intercept of line joining B to O' with the $\bar{\sigma}$ axis gives the equivalent nominal stress $\bar{s}$.

From the figure, it is evident that, the nominal stress increases up to a maximum till the point B moves to T. At this point, the slope of the true stress - true strain curve is the

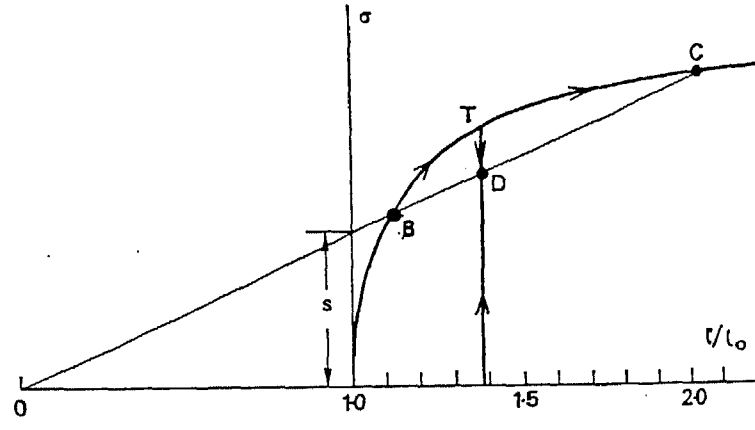

Fig. 3.4 Considère's construction (Calladine, 1985)

increases even if the nominal stress decreases. This means that the load can not be increased any more and further deformation has to be made with decreasing load. At this point the necking begins and the material subsequently fails.

Mathematically, this can be written as,

$$\frac{d\bar{\sigma}}{d\bar{\varepsilon}} \geq \frac{\bar{\sigma}}{(1 + \bar{\varepsilon})} \quad . \qquad (G)$$

Differentiation of the stress hardening rule (eq. (3.9)) w. r. t. $\bar{\varepsilon}$ gives

$$\frac{d\bar{\sigma}}{d\bar{\varepsilon}} = n\ k\ (\bar{\varepsilon})^{(n-1)} \quad .$$

Using this in eq. (G), the instability criterion becomes,

$$n\ k\ (\bar{\varepsilon})^{(n-1)} \geq \frac{\bar{\sigma}}{(1 + \bar{\varepsilon})} \quad .$$

Substituting for $\bar{\sigma}$ from eq. (3.9), the above equation becomes,

$$n\ k\ (\bar{\varepsilon})^{(n-1)} \geq \frac{(\sigma_o + k\ (\bar{\varepsilon})^n)}{(1 + \bar{\varepsilon})} \quad . \qquad (3.10)$$

This is the condition which is checked for ensuring successful drawing.

3.3 ASSUMPTIONS

We find that these equations ((3.1), (3.2), (3.5), (3.6) and (3.7)) are very complex and number of unknowns exceeds the number of equations. So, to make the problem tractable, certain simplifying assumptions are made as given below.

1) Problem is treated as a plane stress problem, i.e., σ_t = 0

are the principal directions.

3) Elastic deformations are negligible.
4) The flat part just below the punch and the segment in the unsupported annular zone between the die and the punch, do not undergo any plastic deformation.
5) Material follows Ludwik's strain hardening rule (eq. (3.9)).
6) Material is isotropic.
7) As soon as the punch starts moving down, the entire sheet becomes plastic at the same instant.
8) The thickness does not change during any incremental movement of the punch.
9) The process is quasi static.
10) Stresses and strains are uniform over the thickness in the flange.
11) Punch and die are rigid with circular profiles.

Based on these assumptions, equations ((3.1), (3.2), (3.6), (3.7) and (3.8)) are modified to make them simple. The effect of these assumptions on the various aspects of the problem in different regions are discussed in the next section.

3.4 SOLUTION FOR THE FLANGE

In case of a flange, we have a flat sheet being drawn into a die. So, here, the meridinal direction and the radial direction are the same (Fig. 3.5). The equation of equilibrium in the meridinal direction for the flange can be obtained by putting $\tau_1 = \tau_2 = 0$ in eq. (3.1) and taking t as constant. These substitutions give

$$\frac{d\sigma_\phi}{dR} + \frac{\sigma_\phi - \sigma_\theta}{R} = 0 \quad . \tag{3.11}$$

The yield criteria (eq. (3.7)) can be modified to the following form :

$$\bar{\sigma} = \sigma_\phi^2 - \sigma_\phi\sigma_\theta + \sigma_\theta^2 \quad ; \tag{3.12}$$

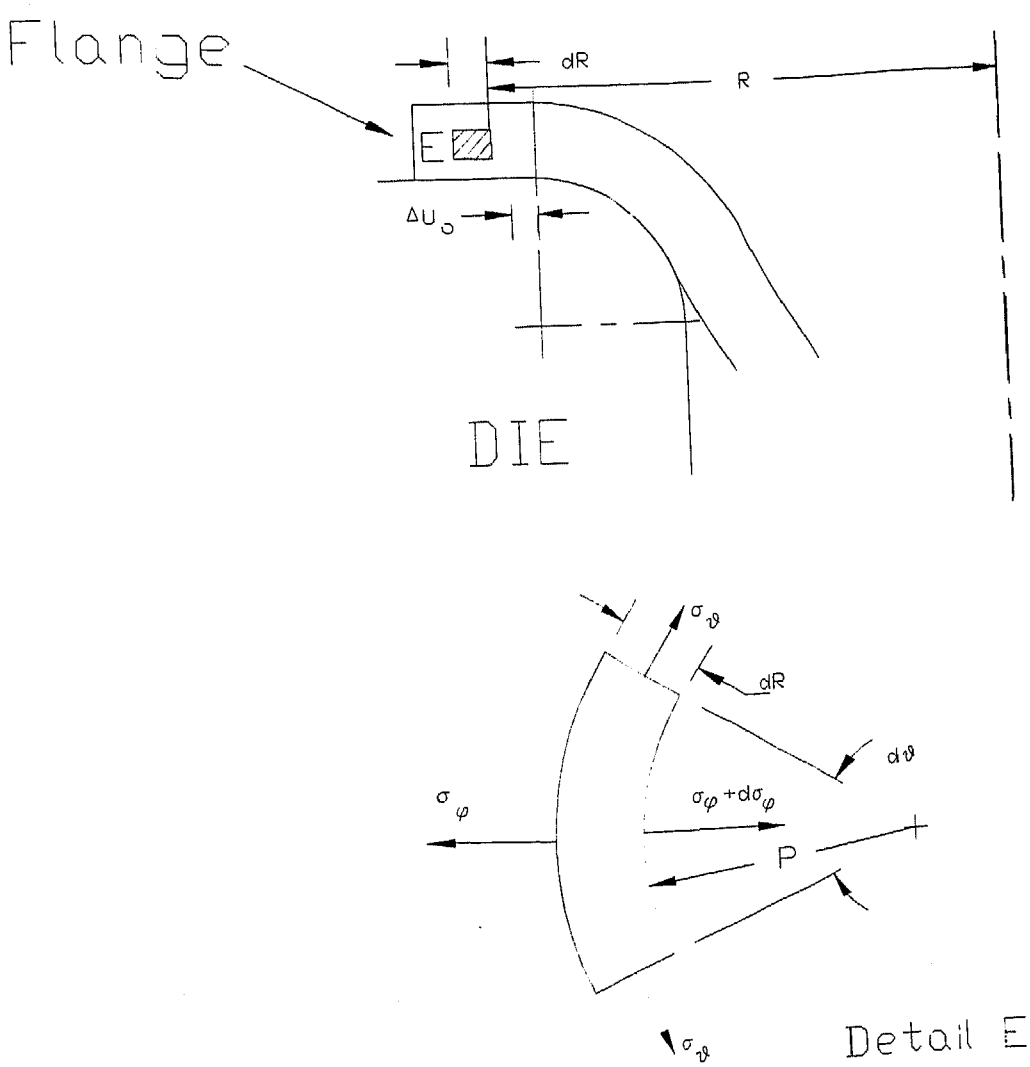

Fig. 3.5 Stresses on an element in flange

where $\bar{\sigma}$ is the yield stress obtained form the strain hardening rule (eq. (3.9)).

The stress - strain relationship can be obtained from the equation (3.6) by taking the ϕ, θ and t directions as the three principal directions and $\sigma_t = 0$. This gives the modified stress - strain relation in the following form :

$$\frac{\varepsilon_\phi}{2\sigma_\phi - \sigma_\theta} = \frac{\varepsilon_\theta}{2\sigma_\theta - \sigma_\phi} = -\frac{\varepsilon_t}{\sigma_\phi + \sigma_\theta} \quad . \qquad (3.13)$$

With these relations, the stresses were expressed in terms of another parameter $\omega = \omega(R)$ which represents of the stress state at any point on the yield locus (Szczepinski, 1966) as

$$\sigma_\phi = 2\ K \cos(\omega - \pi / 6) \qquad (3.14a)$$
$$\sigma_\theta = 2\ K \cos(\omega + \pi / 6) \qquad (3.14b)$$

where $K = \sigma_y / \sqrt{3}$.

Based on this, the stress and strain field was obtained by Zharkov (1992) for an incremental punch movement. The solution presented in the aforementioned work is given as follows

$$\omega = \omega_f + \frac{1}{\sqrt{3}} \ln\left(\frac{R^2}{R_f^2} \quad \frac{\sin\omega}{\sin\omega_f}\right) \quad . \qquad (3.15)$$

Here, ω_f is the value of ω at the periphery of the sheet, i.e., at $R = R_f$, where R_f is the instantaneous flange radius.

The equation (3.15) is solved numerically using Newton Raphson method to find the value of ω at any radius R. Using this ω, the stress values can be found easily from eq. (3.14).

The relations obtained for the evaluation of strains ar

as follows (Zharkov, 1992) :

$$d\varepsilon_{\phi} = \frac{\Delta U_o \sin(\omega + \pi/6)}{R \sin(\omega - \pi/6)} \left\{ \frac{\sin \omega_o}{\sin \omega_f} \exp[\sqrt{3}(\omega_o - 2\omega) + \frac{2}{\sqrt{3}}\pi] \right\}^{1/2} \quad (3.16a)$$

$$d\varepsilon_{\theta} = -\frac{\Delta U_o}{R} \left\{ \frac{\sin \omega_o}{\sin \omega_f} \exp[\sqrt{3}(\omega_o - 2\omega) + \frac{2}{\sqrt{3}}\pi] \right\}^{1/2} \quad (3.16b)$$

where, ω_f and ω_o are the values of ω at the periphery of the sheet and at die entry respectively, i.e., at $R = R_f$ and $R = R_o$ and ΔU_o is the inward movement of the sheet at the die entry.

Using these relationships (eq. (3.16a), (3.16b)), the strains at any radial distance from the axis of symmetry can be found by substituting the value of ω at that radius. These relations (eq. (3.14) and (3.16)) are also used to find the values of stresses and strains at the entry of the die (at the starting of the profile radius of the die), so that the solution for the curved profile can be obtained.

3.5 SOLUTION FOR THE CURVED SEGMENT

The basic geometry of an elemental volume in the curved segment remains the same as that of shown in the Fig. 3.2. Unlike the flange, in this segment, the variations in the meridinal and circumferential stresses in the thickness direction are considered. This is done mainly to take care of the variation in the stresses over the cross section due to bending of the sheet over the die profile. Based on this consideration and assumptions made previously, the stress field in the curved segment will be as shown in Fig. 3.6.

Consider an element of the sheet of radial thickness dr at a radial distance r from the center of the die profile (Fig. 3.6a). Let the element subtend an angle $d\phi$ at the center of die profile and an angle $d\theta$ at the axis of symmetry. Neglecting the normal stresses (σ_{t1} and σ_{t2}) and surface stress (τ_1 and τ_2), the

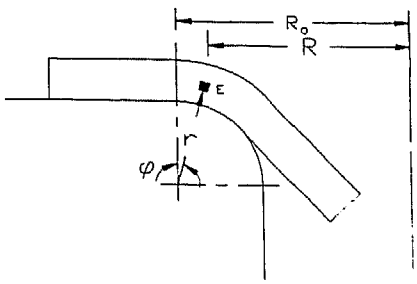

$$R_o = R_p + \varepsilon + r_d$$

a) Location of an Element in Curved Segment Over the Die

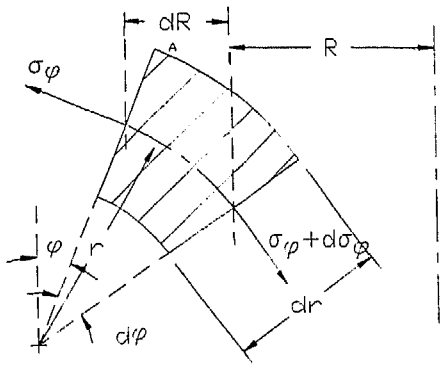

Details of Elemental Volume E

(Elevation View)

b) Meridinal Stresses

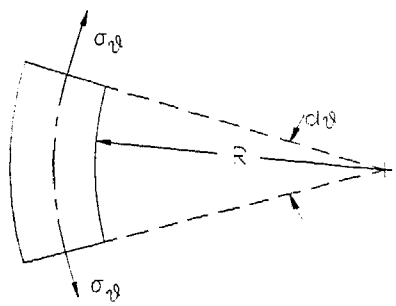

Details of Elemental Volume E

(Plan View)

c) Circumferential stresses

Fig. 3.6 Stress on an element in curved segment over the die profile

equation of equilibrium in the meridinal direction can be found as follows :

Force in the meridinal direction due to meridinal stresses can be written as (Fig. 3.6b) :

$$F_\phi = (\sigma_\phi + d\sigma_\phi)\ R\ d\theta\ dr \cos\frac{d\phi}{2} - \sigma_\phi (R + dR)\ d\theta\ dr \cos\frac{d\phi}{2}$$

$$= \{(\sigma_\phi + d\sigma_\phi)\ R - \sigma_\phi (R + dR)\}\ d\theta\ dr \cos\frac{d\phi}{2} \quad .$$

As $d\phi$ is very small, the following approximation can be made

$$\cos\frac{d\phi}{2} \simeq 1.$$

By substituting this value in the above relation becomes,

$$F_\phi = \{(\sigma_\phi + d\sigma_\phi)\ R - \sigma_\phi (R + dR)\}\ d\theta\ dr$$

$$= \{d\sigma_\phi\ R - \sigma_\phi\ dR\}\ d\theta\ dr \quad .$$

Similarly, force in the meridinal direction due to circumferential stresses can be expressed as (Fig. 3.6c) :

$$F_\theta = 2\ \sigma_\theta\ r\ d\phi\ dr \sin\frac{d\theta}{2} \cos\phi \ .$$

Again, since $d\theta$ is very small, $\sin\frac{d\theta}{2}$ can be taken as $\frac{d\theta}{2}$. So the above equation becomes,

$$F_\theta = \sigma_\theta\ r\ d\phi\ dr\ d\theta \cos\phi \quad .$$

For equilibrium, the total force on the element E (Fig. 3.6a) in the meridinal direction should be zero. So,

$$F_\phi + F_\theta = 0$$

$$\text{or,} \quad \{d\sigma_\phi \, R - \sigma_\phi \, dR\} \, d\theta \, dr + \sigma_\theta \, r \, d\phi \, dr \, d\theta \cos\phi = 0$$

$$\text{or,} \quad d\sigma_\phi = \frac{\sigma_\phi \, dR - \sigma_\theta \, r \cos\phi \, d\phi}{R} \quad .$$

Substituting $R = R_o - r \sin\phi$ and $dR = r \cos\phi \, d\phi$, we get

$$d\sigma_\phi = \frac{(\sigma_\phi - \sigma_\theta) \, r \cos\phi \, d\phi}{(R_o - r \sin\phi)} \quad . \qquad (3.17)$$

Similar equation (eq. (3.18)) is obtained for the deformation of an element over the punch profile (Fig. 3.7).

$$d\sigma_\phi = \frac{(\sigma_\phi + \sigma_\theta) \, r \cos\phi \, d\phi}{(A' + r \sin\phi)} \quad . \qquad (3.18)$$

If the stresses at any point A (Fig. 3.6b) are known, the increment in meridinal stress can be found using these relations.

Based on the concepts discussed above, a step by step procedure is evolved for developing a flat pattern for a deep drawn cup.

3.6 PROCEDURE FOR FLAT PATTERN DEVELOPMENT

Following are the six main steps to be followed for flat pattern development of a deep drawn cup :

1) Finding initial flat pattern size.
2) Calculation of thicknesses along the curved segments over die/punch profile for an incremental movement of the punch.
3) Evaluation of stresses and strains in the flange area for an incremental movement of the punch.
4) Checking instability criterion.
5) Determination of reduction in the flange radius.

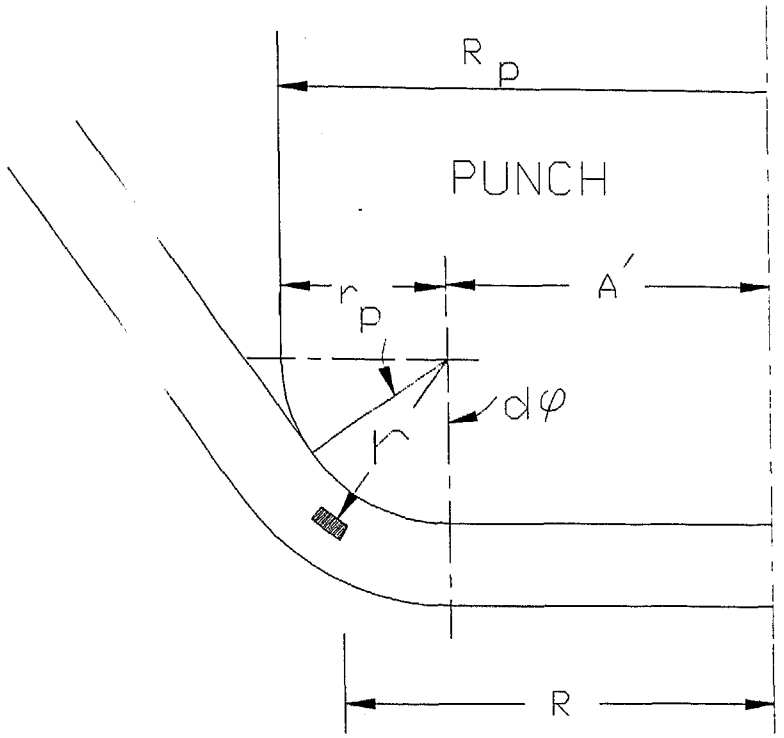

$$A' = R_p - r_p$$

Fig. 3.7 An element in curved segment over the punch profile

6) Modification in the flat pattern size after complete punch travel.

These steps are elaborated below one by one.

3.6.1 Finding Initial Flat Pattern Size

In this method, as stated above, the procedure starts with some value of flat pattern size, completes the computational deep drawing operation, compares the part obtained with the part desired and modifies the flat pattern size accordingly. So, finding an appropriate starting flat pattern size is very important. The starting flat pattern size should be such that it converges fast with a least number of iterations. In this work, the initial flat pattern size is obtained by neglecting the thickness changes during the drawing operation, i.e., by taking the surface area of the flat pattern to be equal to the surface area of the part required. Let, a_1, a_2, a_3, a_4 and a_5 be the surface areas of the various segments of the required part drawing as shown in Fig. 3.8, The initial flat pattern radius (R_i) can be calculated as

$$R_i = \sqrt{\left[\sum_{i=1}^{5} a_i / \pi \right]} \qquad (3.19)$$

where a_i is the area of the i^{th} segment of the cup as shown in Fig. 3.8 and can be found from the part drawing as follows :

$$a_1 = \pi (R_p - r_p)^2,$$
$$a_2 = \pi^2 (r_p + t/2) \{R_p + (2/\pi - 1)(r_p) + t/\pi\},$$
$$a_3 = 2 \pi (R_p + t/2)(H_{max} - r_p - r_d),$$
$$a_4 = \pi^2 (r_d + t/2) \{R_p - (2/\pi + 1)(r_d + t/2)\},$$
$$a_5 = \pi \{r_f^2 - (R_p + \varepsilon + r_d)^2\}.$$

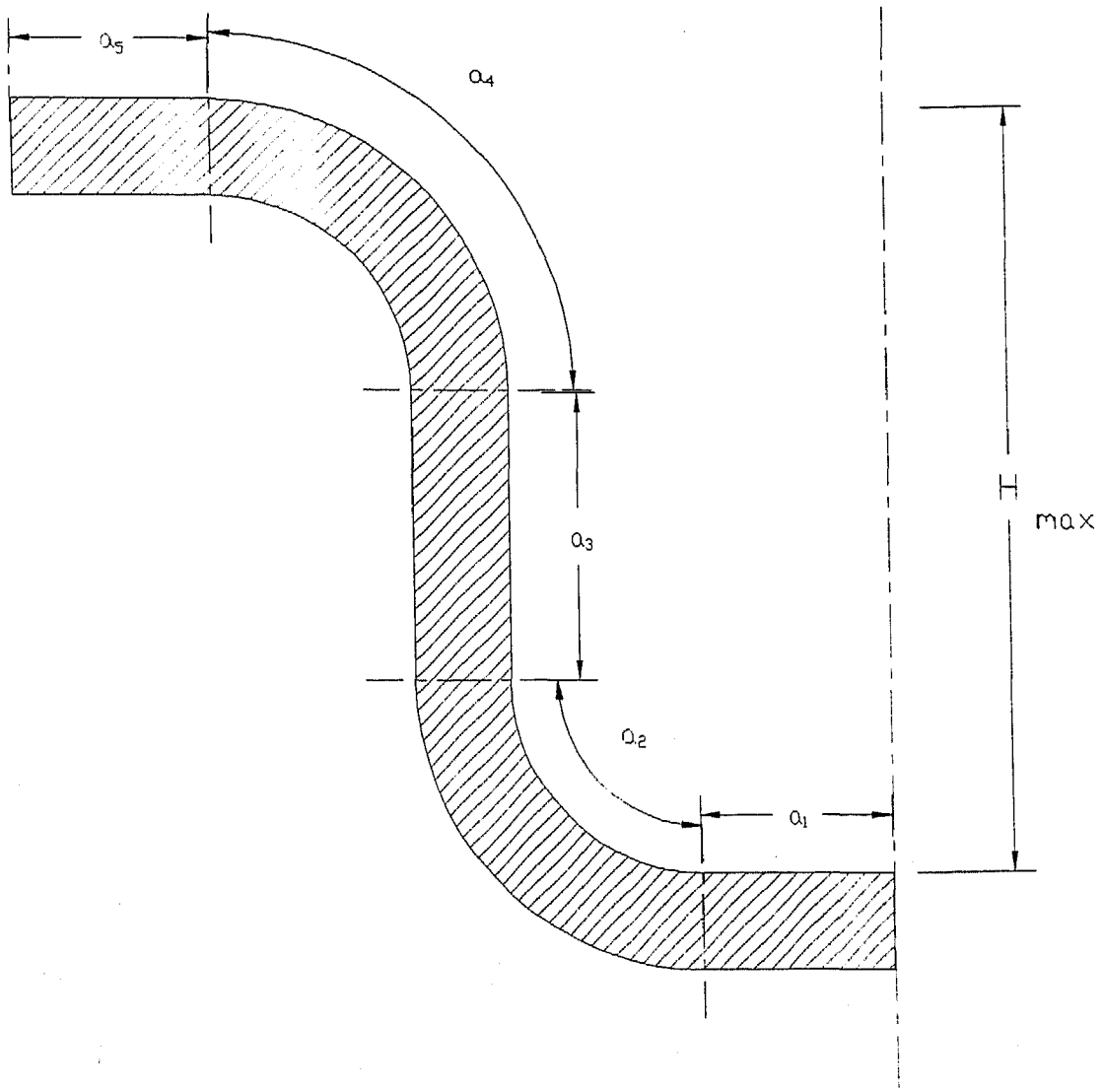

Fig. 3.8 Areas of various segments of the cup

Using these relations in eq. (3.19), the initial flat pattern size can be found. Based on this flat pattern size and the iterative procedure detailed below, the actual flat pattern size (within the accuracy of ε = 0.01 mm) for the part required is calculated.

3.6.2 Evaluation Of Thicknesses Along The Curved Segments

The objective of this section is to present a method to find the thickness of the sheet at various points on the curved profile over the punch and die.

The main steps to be followed for finding the thicknesses along the curved segments are following :

1) Finding the stresses and strains along the curved segment on the inner surface of the sheet.
2) Finding the stresses and strains along the curved segment on the outer surface of the sheet.
3) Calculation of thickness along the curved segment of the sheet.

3.6.2.1 Finding stresses and strains along the curved segment on the inner surface

Consider a stage, where the punch has travelled a distance h and the angle of wrap on the die and punch profile is ϕ (Fig. 3.1c). Let the stresses at the entry to the die (at point A) be $\sigma_{\phi o}$ and $\sigma_{\theta o}$ and the strains along the three principal directions be $\varepsilon_{\phi o}$, $\varepsilon_{\theta o}$ and ε_{to}. The thickness of the sheet at the entry to the die is t_o and the instantaneous flange radius is R_f. Now, an incremental movement dh is given to the punch, the corresponding increase in the angle of wrap will be given as

$$d\phi = \frac{dh \cos^2\phi}{B - R_o \sin \phi} \quad ; \qquad (3.20)$$

where B is $(r_p + r_d + t)$.

Let l_1, l_2, l_3 and l_1', l_2', l_3' (Fig. 3.9) be the lengths of the sheet segments over the die profile, unsupported annular zone and over the punch profile before and after the the incremental punch movement respectively. If we assume, for a moment, that there is no further elongation in the meridinal direction during this incremental movement of the punch, a point A (Fig. 3.10) will travel to a point B on the die profile, where the length (ΔL) of the arc AB, can be given as

$$\Delta L = (l_1' + l_2' + l_3') - (l_1 + l_2 + l_3)$$

and the corresponding angle of wrap can be calculated as

$$\Delta\phi = \frac{\Delta L}{(r_d + t/2)} \quad .$$

From this, it can be said that the element at A before the incremental punch movement has moved from a radial distance R_o to $\{R_o - r_d \sin(\Delta\phi)\}$ from the axis of symmetry.

So, the incremental compressive strain in circumferential direction ($d\varepsilon_\theta$) can be found using eq. (3.3) as :

$$d\varepsilon_\theta = \ln\left(\frac{R_o - r_d \sin(\Delta\phi)}{R_o}\right)$$

The total strains at the point B will be

$$\varepsilon_\phi = \varepsilon_{\phi o}, \qquad (3.21a)$$

(as we have assumed that there is no further elongation in meridinal direction.)

$$\varepsilon_\theta = \varepsilon_{\theta o} + d\varepsilon_\theta, \qquad (3.21b)$$

and from incompressibility condition (eq. (3.5))

$$\varepsilon_t = -(\varepsilon_\phi + \varepsilon_\theta).$$

Using the three components of the strain, the equivalent

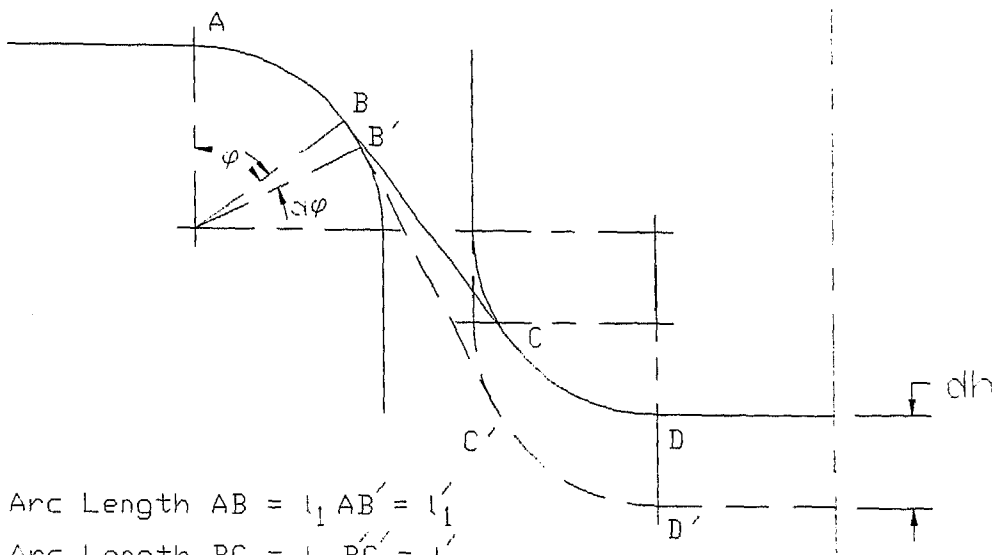

Arc Length AB = l_1 $\overset{\frown}{AB'}$ = l'_1

Arc Length BC = l_2 $\overset{\frown}{BC'}$ = l'_2

Arc Length CD = l_3 $\overset{\frown}{CD'}$ = l'_3

Thickness at B = t_1

Thickness at C = t_2

Fig. 3.9 Changes in the lengths of sheet segments due to incremental punch movement

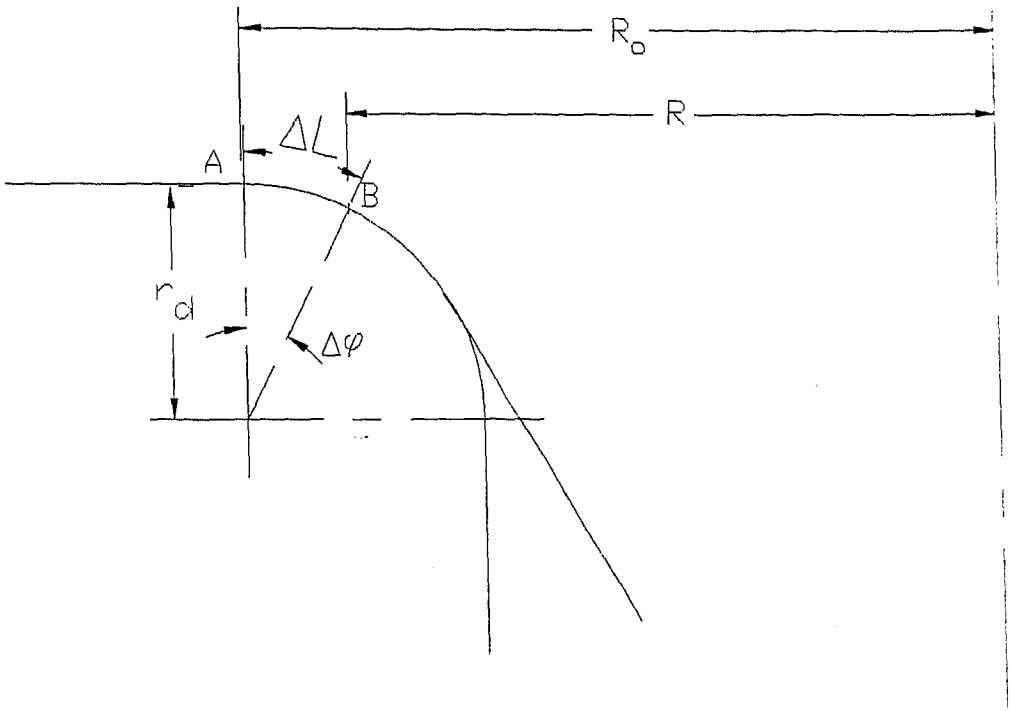

Fig. 3.10 Movement of sheet over the die profile

strain at the point B (Fig. 3.10) can be calculated using eq. (3.8). The corresponding yield stress after strain hardening can also be calculated using eq. (3.9). An increase in meridinal stress, $d\sigma_\phi$, is calculated using the equilibrium equation (eq. (3.17)) for the curved segment. The total meridinal stress at the point B will be

$$\sigma_\phi = d\sigma_\phi + \sigma_{\phi o} \ .$$

The additional stress at B due to friction over the die profile can be written as

$$d\sigma_{\phi_o} = \sigma_{\phi_o} e^{\mu\Delta\phi} - \sigma_{\phi_o}$$

$$= \sigma_{\phi_o} (e^{\mu\Delta\phi} - 1) \ .$$

So, the total meridinal stress at B will be,

$$\sigma_\phi = d\sigma_\phi + \sigma_{\phi_o} + d\sigma_{\phi_o}$$

$$= d\sigma_\phi + \sigma_{\phi_o} e^{\mu\Delta\phi} \ . \qquad (3.22)$$

Now, the equation of equivalent stress (eq. (3.12)), which is nothing but a quadratic equation in σ_θ, can be solved to find the value of σ_θ at point B in Fig. 3.10.

Using the above mentioned procedure and the values of stresses and strains at the point A (Fig. 3.10), the three strains (eq. (3.21) and (3.5)) and the two stresses (eq. (3.22) and (3.12)) at B can be evaluated. But, it has been assumed that the incremental strain in the meridinal direction is zero, which is not true. So, using the values of stress and strain at point B, the total strain in meridinal direction (ε_ϕ) can be obtained using the stress - strain relationship (eq (3.13)) as

$$\varepsilon_\phi = \frac{2\,\sigma_\phi - \sigma_\theta}{2\,\sigma_\theta - \sigma_\phi}\ \varepsilon_\theta$$

and the incremental strain in the meridinal direction $d\varepsilon_\phi$ is given as

$$d\varepsilon_\phi = \varepsilon_\phi - \varepsilon_{\phi o} .$$

Using this value of incremental strain, the distance travelled by the point A is modified as

$$\Delta L = \Delta L \; / \; \exp(d\varepsilon_\phi)$$

Above process is repeated till the value of the incremental strain in the meridinal direction converges, i.e., the difference between any two consecutive values of $d\varepsilon_\phi$ is less than a prespecified limiting value. In present work, the limiting value is taken to be 0.0001. This gives the final location of the point A after the incremental punch movement.

Using the thickness strain ε_t at point B (Fig. 3.10), the incremental thickness strain $d\varepsilon_t$ is obtained as

$$d\varepsilon_t = \varepsilon_t - \varepsilon_{to} .$$

Values of the stresses and strains at the point B are stored in the proper database. Similar procedure is repeated to find the stresses and strains at the point C and D (Fig. 3.11) and so on. In this way, the entire curved segment is analyzed. If final angle is not the same as that of $(\phi + d\phi)$, then the values at the last two points are interpolated linearly to find the stresses, strains and thickness at the last point of contact between the die profile and the sheet.

This gives the stress and strain values at various points on the inner surface of the sheet which is in contact with the die surface (points A, B, C,.. in Fig. 3.11).

3.6.2.2 Finding stresses and strains along the curved segment on the outer surface

Same procedure, as described in previous section, is repeated with r_d replaced by $(r_d + t)$ to find the solution at the outer surface of the sheet. This solution gives the stresses and strains at the various points (A', B', C'.. in Fig. 3.11) on the outer surface of the sheet.

3.6.2.3 Calculation of thickness along the curved segment of the sheet

Since the stresses and strains for the inner and outer surface of the sheet are computed separately, the solution points of the two cases may be at different angular locations. To find the thickness of the sheet in the curved segment, the value of the thickness strain at the inner and outer surfaces at the same angular location should be known. As shown in fig 3.11, A, B, C... are the points on the inner surface of the sheet for which the stresses and strains are known, and A′, B′, C′ ... are the points on the outer surface of the sheet for which the stresses and strains are also known. To find the values at the same angular locations as in the inner surface, the adjacent values are interpolated. For example, to find the stresses and strains at a point corresponding to A, i.e., A″, the values at A′ and B′ are interpolated. After finding the values at A″ the point A′ is discarded. The final incremental thickness strain is taken as the arithmetic mean of the incremental thickness strains at the inner and outer fibers. The sheet thickness at A and A″ can be found using the final incremental thickness strain at A as follows

$$t = t_o \exp(d\varepsilon_t) \qquad (3.23)$$

where, $d\varepsilon_t$ is the arithmetic mean of the incremental thickness strains at A and A".

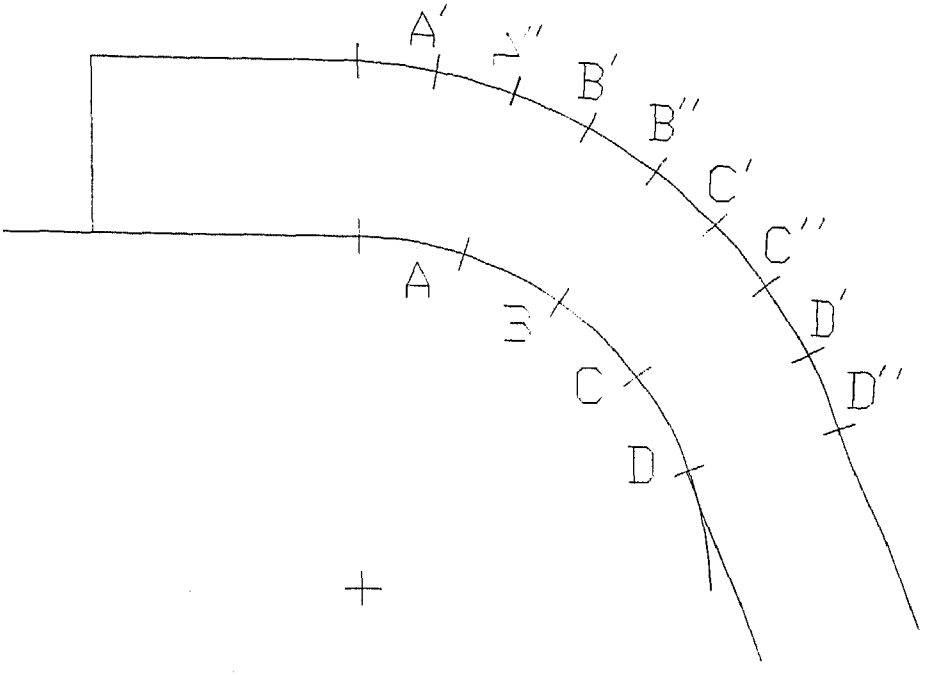

Fig. 3.11 Solution points on inner and outer surface of curved segment

Similarly, the final thickness of the sheet at all the points A, B, C... are found.

The solution for the curved segment over the punch profile can also be found in a similar way.

Finding the thickness of the sheet along the die and punch profiles at various points (eq. (3.23)) completes the solution for the curved segments over the die and punch profiles.

3.6.3 Evaluation of Stresses and Strains in the Flange

In case of flange, the interest lies in knowing the thickness, stresses and strains at the entry to the die. Thickness and strains are evaluated at the periphery as well. The stresses and strains at the entry to the die give the starting values for the next step.

As shown by eq. (3.16), the incremental strains are functions of the parameter ΔU_o which is the radial inward movement of the flange at the entry of the die. This movement of the sheet supplies material for the increase in the volume of the sheet in the die. So, to find ΔU_o, first the total increase in volume of the sheet in the die is calculated.

For finding the volume of the curved segment, each sector of the segment (AB, BC and so on in fig 3.11) is treated separately. The volume of any sector can be calculated as

$$v = 2 \pi R_m (\Delta\phi \; r_d \; t)$$

where, R_m is the mean radius for the sector under consideration.

or, $$R_m = R_o - \frac{1}{2}(r_d + t/2)\{\sin \phi + \sin(\phi + d\phi)\}.$$

By adding volumes of all the sectors, volume of the

curved segments, both on the die and the punch profiles can be found. The increase in the total volume of these segments can be found as the difference between the total volumes of these segments before and after the incremental movement of punch. Let, this increase in volumes be v_1 and v_3.

For the straight unsupported segment (BC in Fig. 3.9) between the two curved segments, an increase in volume is due to the length $\{(l_2' + l_3') - (l_2 + l_3)\}$ entering into it. At the same time, $(l_3' - l_3)$ goes over the punch, thus leaving the straight segment. So, an increase in the volume for the straight segment will be

$$v_2 = \{(l_2' + l_3') - (l_2 + l_3)\}\, t_1 * (2 * \pi * (R_o - r_m \sin\phi)) - (l_3' - l_3)\, t_2 * 2 * \pi * (R_p - r_m \sin\phi).$$

where t_1 and t_2 are the thicknesses at the last contact points between the sheet and the die and the sheet and the punch profiles respectively (thicknesses at points B and C respectively in Fig. 3.9).

The net increase in volume of the sheet within the die will be

$$V = (v_1 + v_2 + v_3)$$

This volume has to be supplied from the flange. Let, t_o be the thickness of the sheet at the entry of the die and ΔU_o be the radial inward movement of the sheet at the entry of the die, then,

$$V = \{\pi(R_p + \varepsilon + r_d)^2 - \pi[(R_p + \varepsilon + r_d) - \Delta U_o]^2\}\, t_o$$

$$\text{or, } \Delta U_o = \sqrt{\left\{\frac{V}{\pi t_o} + (R_p + \varepsilon + r_d)^2\right\}} - (R_p + \varepsilon + r_d) \qquad (3.24)$$

Now, eq. (3.15) is solved by putting $R = (R_p + \varepsilon + r_d)$

and $R = R_f$ to give the value of the parameter ω at die entry and at the periphery respectively. Let these values be ω_o and ω_f. The strains at the entry to the die are calculated by putting $\omega = \omega_o$ in eq. (3.16) and using the values of ω_o and ω_f. After finding $d\varepsilon_\phi$ and $d\varepsilon_\theta$, the third component of strain $d\varepsilon_t$ is calculated using incompressibility condition (eq. (3.5))

The changed thickness of the sheet at the entry to die can be found using the incremental thickness strain as

$$t_o = t_o \exp(d\varepsilon_t)$$

The thickness at the periphery can also be found in a similar way. Finding the thicknesses at the entry to the die and the periphery, completes the solution for the flange.

3.6.4 Checking Instability Criterion

After finding complete solution for each incremental movement of the punch, the instability condition is checked. For this, the $\bar{\varepsilon}$ value at the last point of contact between the die profile and the sheet is used to check the instability condition (eq. (3.10)). If this condition is satisfied, we go to the next incremental movement of the punch. Otherwise, the component has to be taken out and annealed before further drawing can be done. So, a message is sent to the output file that annealing is to be performed at this point and the process can be continued after stress relieving.

3.6.5 Determination of Reduction in the Flange Radius

If the inward radial movement at the die entry is ΔU_o and the thickness at the die entry and at the periphery are known, the corresponding reduction in the flange radius can be calculated. This is done by assuming that there is no change in the thickness during incremental movement of the punch. In this case, increase in volume of the sheet within the die will come

only from the periphery of the flange. If dR is a reduction in the flange radius corresponding to an incremental punch movement given, then increase in the volume within the die can be equated to the volume drawn from the flange, i.e.,

$$\pi \{R_f^2 - (R_f - dR)^2\} t_f = \pi \{(R_p + \varepsilon + r_d)^2 - [(R_p + \varepsilon + r_d) - \Delta U_o]^2\} t_o$$

where t_f and t_o are the thicknesses at the periphery and the die entry respectively.

Taking $(R_p + \varepsilon + r_d)$ as R_o, and simplifying

$$dR^2 - 2 R_f dR + (2 R_o \Delta U_o - \Delta U_o^2) \frac{t_o}{t_f} = 0 .$$

Neglecting dR^2 as dR is very small, the following relationship is obtained,

$$dR = \frac{(2 R_o \Delta U_o - \Delta U_o^2)}{2 R_f} \frac{t_o}{t_f} \qquad (3.25)$$

This gives the reduction in the radius for an incremental punch movement.

3.6.6 Modification in Flat Pattern Size for Next Iteration

In this step, the final size of the component obtained is compared to the final size specified in the drawing. The difference between the two decides the amount by which the flat pattern size is increased or decreased for the next iteration. Let, R_o, R_f and r_f be the initial radius, final radius obtained and final radius required respectively. The difference in the volume of the final part required and the final part obtained will be

$$\delta V = \pi (R_f^2 - r_f^2) t_f$$

So, the modified flat pattern size will be given as

$$R_i = \sqrt{\{(\pi R_i^2 t_i - \delta V) / t_i \pi\}}$$

or, $$R_i = \sqrt{[\{R_i^2 t_i - (R_f^2 - r_\phi^2) t_f\}/t_i]} \qquad (3.26)$$

This modified value of the flat pattern size is used as the flat pattern for the next iteration.

3.7 THE ALGORITHM

Based on the above steps, following algorithm was developed to find the flat pattern size.

The step wise procedure to find the flat pattern is given as follows :

STEP 1 Read data, Part geometry, Material specifications.

STEP 2 Calculate the initial flat pattern size.

STEP 3 Initialize counter count for counting number of iterations. Initialize angle of wrap and height (ϕ and h) to zero.

STEP 4 Find the thicknesses along the die profile for the incremental punch travel.

STEP 5 Find the thicknesses along the punch profile for the incremental punch travel .

STEP 6 Check instability criterion (eq. (3.10))

If instability criterion is satisfied

go to step 7.

else

go to step 8.

STEP 7 make all stresses and strains zero.

STEP 8 Find ΔU_o using new thicknesses along the curved profiles over the die and punch and the procedure given in sect. 3.6.3 (eq. (3.24)).

STEP 9 Using ΔU_o in eq. (3.25), find dR.

STEP 10 Modify the value of R_f as $R_f = R_f - dR$.

STEP 11 Find find stresses, strains and thickness at die entry and thickness at flange periphery.

STEP 12 Update the value of h as h = h + dh.

STEP 13 Repeat Steps 4 - 10 till h <= h_{max}.

STEP 14 If | R_f - r_f | < ε STOP.

STEP 15 Using eq. (3.26) calculate the modified flat pattern size.

STEP 16 Count = count + 1.

STEP 17 If count > 10 STOP.

STEP 18 Repeat Steps 3 - 17.

STEP 19 STOP.

The flow chart for this algorithm is given in fig 3.12.

Based on this algorithm, prototype systems were written in programming language Turbo C and run on a 80386 based machine in DOS environment. The results obtained for sample input are presented in separate chapter on Results and Discussion.

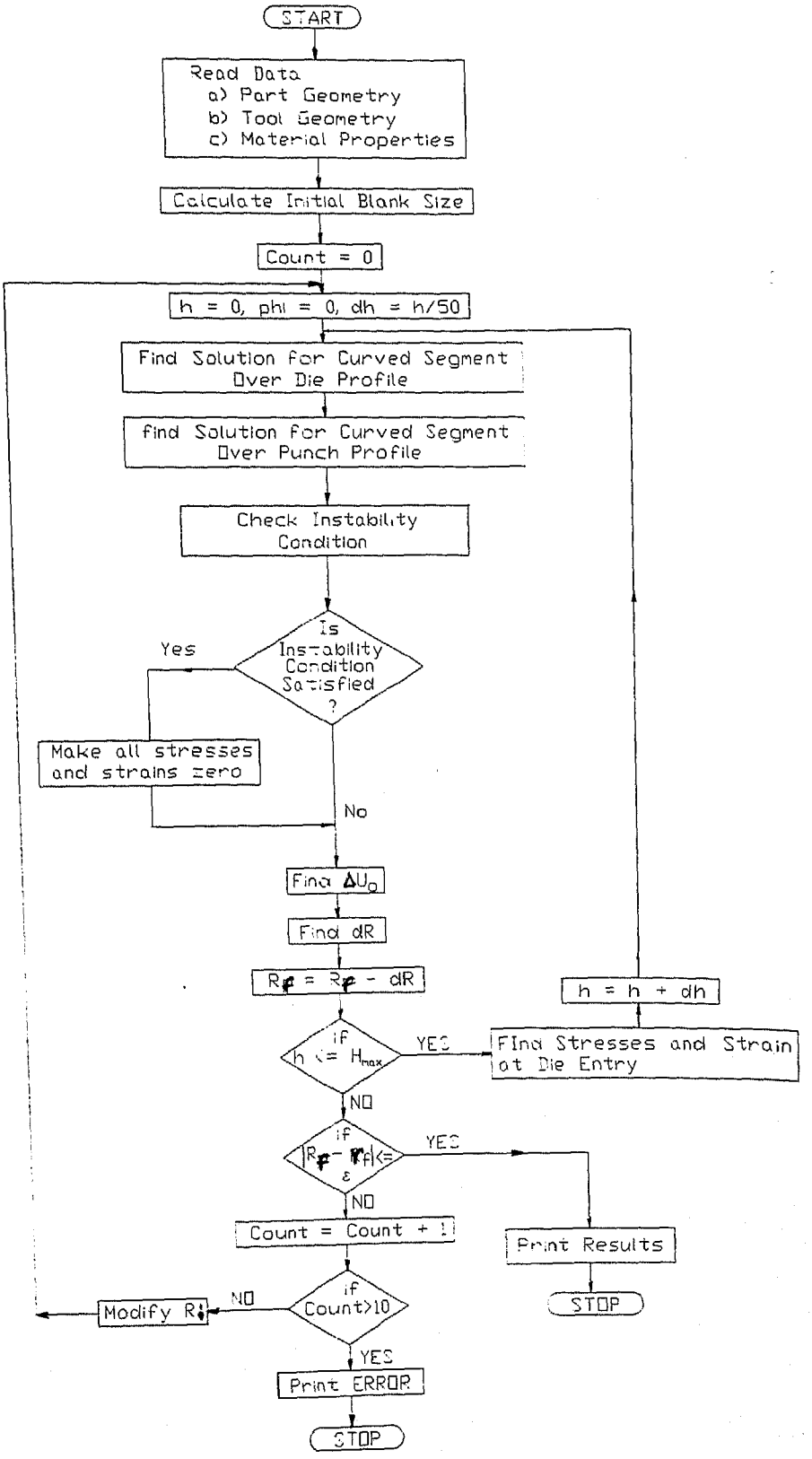

Fig. 3.12 Flow chart for finding the flat pattern for a deep drawn component

CHAPTER 4

RESULTS AND DISCUSSIONS

Based on the methods discussed in the previous chapters for finding the flat pattern development, prototype systems were developed and executed for a number of sample cases. Examples on bent as well as deep drawn components were considered.

In this chapter, a few examples on the flat pattern development for bent components followed by the results obtained for deep drawn components are presented.

4.1 FLAT PATTERN DEVELOPMENT FOR BENT COMPONENTS

To test the validity of the prototype systems developed based on the model discussed in the chapter on "Flat pattern development for bent components", the results obtained from this system are compared with those reported by Prasad and Somasundaram (1993). Prasad and Somasundaram (1993) have listed the radius of unstretched fiber and the changed thickness of the sheet after bending. In the Table 4.1, the results obtained by the present prototype system are compared with the results obtained by Prasad and Somasundaram (1993) for a bend of radius 2.5 mm in the sheets of different materials having thicknesses equal to 1 mm. The angle of bend is taken to be 90°.

Deviations between the two are insignificant as is evident from the Table 4.1. This validates the present prototype system for evaluating the radius in neutral fiber as well as the change in thickness of the sheet.

The results of flat pattern development for a bent component include the part drawing and the drawing of the flat pattern obtained. It also gives the bend allowance calculated for each bend plane along with the geometrical parameters of a bend

Material	Results (Prasad and Somasundaram)		Present System	
	r_u (mm)	t_n (mm)	r_u (mm)	t_n (mm)
AK Steel	2.42	0.972	2.42	0.973
High Strength Steel				
HS1	2.43	0.976	2.43	0.976
HS2	2.43	0.977	2.43	0.978
HS3	2.43	0.978	2.43	0.978
Aluminium 70:30	2.40	0.965	2.39	0.966
Brass - Aluminium	2.42	0.972	2.42	0.972

Table 4.1 Comparison of Results for Bend Allowance calculation (Angle of Bend 90°)

viz. radius and angle of bend and the new thickness of the bent section.

EXAMPLE PART 1

Fig. 4.1 shows a simple bent component (numbers in circles indicate the plane numbers) having one bend plane. The result of bend allowance calculations are shown in Table 4.2. The flat pattern obtained for this component is shown in Fig. 4.2. For this component, the detailed output, including various databases, is also presented. In Table 4.3 and 4.4 the list of vertices for the original component and the flat pattern obtained is presented respectively. In the next two tables, i.e., Table 4.5 and 4.6, the old and modified information on edges is shown. Finally, Table 4.7 and 4.8 contain the edge list for various planes in the original component and the flat pattern obtained respectively.

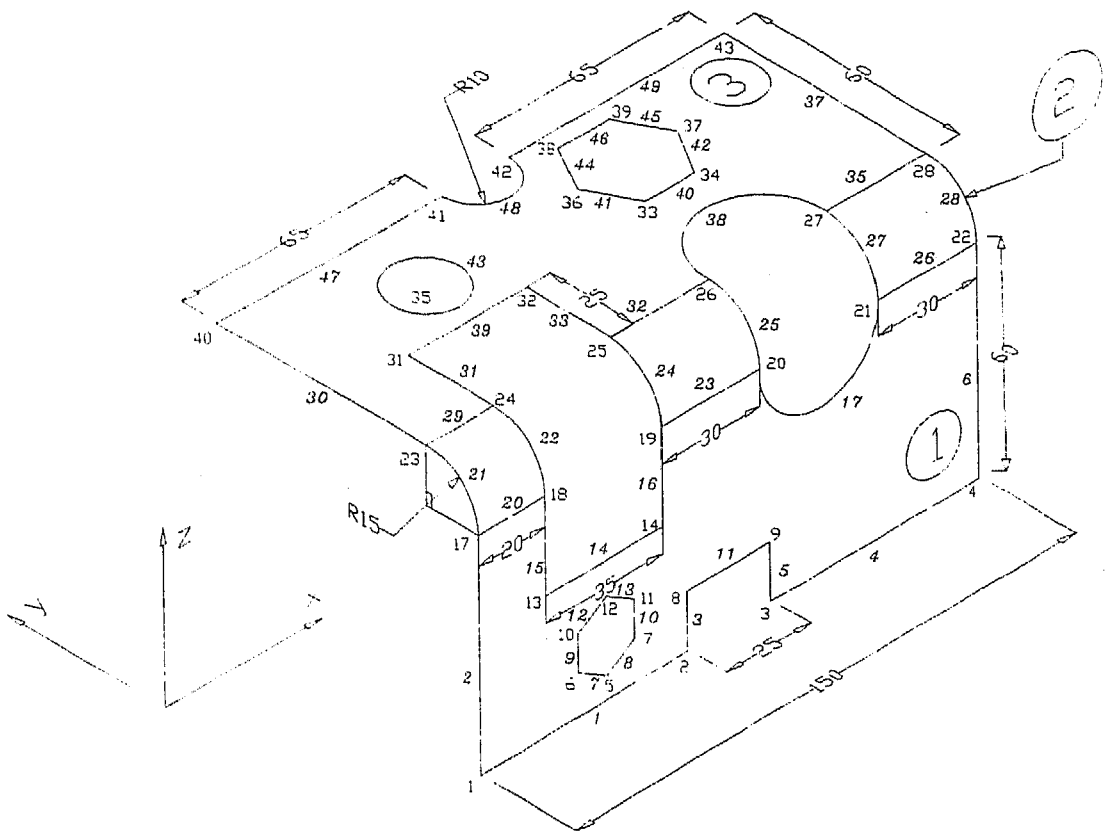

Fig. 4.1 Part drawing for the component in Example Part 1

SUMMARY RESULTS OF BEND ALLOWANCE CALCULATION

Material Properties

Material	:	Aluminium Killed steel
Yield Stress (sigma_o)	:	172.8 MPa
Exponent (n)	:	0.22
Strength Coefficient (k)	:	510.16 MPa
Ultimate Tensile Strength	:	840.0 MPa

****

INPUT DATA FOR BEND PLANE # 2

Bend Plane	:	2	
Inner Radius of Bend	:	12.5000	mm
Angle of Bend	:	1.5708	rad.
Initial Thickness	:	5.0000	mm

OUTPUT DATA FOR BEND PLANE # 2

Final Thickness	:	4.9828	mm
Rad. of unstretched fiber	:	14.9399	mm
Bend Allowance	:	23.4676	mm

****

Table 4.2 Results of Bend Allowance calculation for Example Part 1 of bending

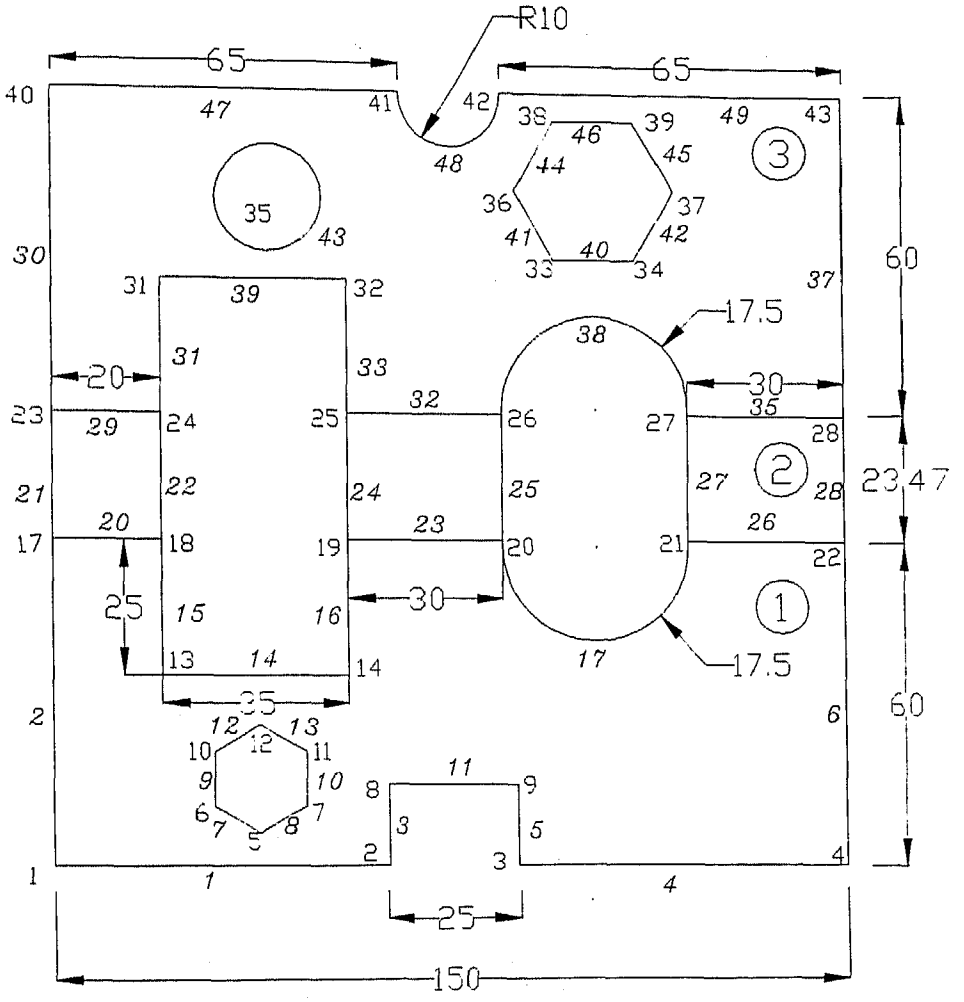

Fig. 4.2 Flat pattern for the component in Example Part 1

LIST OF VERTEX DATA

vert_no	x_cord	y_cord	z_cord
1	201.7701	108.7299	-32.2200
2	264.2701	108.7299	-32.2200
3	289.2701	108.7299	-32.2200
4	351.7701	108.7299	-32.2200
5	239.7701	108.7299	-26.2200
6	231.1098	108.7299	-21.2200
7	248.4303	108.7299	-21.2200
8	264.2701	108.7299	-17.2200
9	289.2701	108.7299	-17.2200
10	231.1098	108.7299	-11.2200
11	248.4303	108.7299	-11.2200
12	239.7701	108.7299	-6.2200
13	221.7701	108.7299	2.7800
14	256.7701	108.7299	2.7800
15	286.7701	108.7299	26.7800
16	321.7701	108.7299	26.7803
17	201.7701	108.7299	27.7800
18	221.7701	108.7299	27.7802
19	256.7701	108.7299	27.7800
20	286.7701	108.7299	27.7802
21	321.7701	108.7299	27.7800
22	351.7701	108.7299	27.7800
23	201.7701	123.7299	42.7800
24	221.7701	123.7299	42.7800
25	256.7701	123.7299	42.7800
26	286.7701	123.7299	42.7800
27	321.7701	123.7299	42.7800
28	351.7701	123.7299	42.7800
29	286.7701	124.7299	42.7800
30	321.7701	124.7299	42.7800
31	221.7701	148.7299	42.7800
32	256.7701	148.7299	42.7800
33	296.7701	152.7492	42.7800
34	311.7701	152.7492	42.7800
35	241.7701	163.7299	42.7800
36	289.2701	165.7395	42.7800
37	319.2701	165.7395	42.7800
38	296.7701	178.7299	42.7800
39	311.7701	178.7299	42.7800
40	201.7701	183.7299	42.7800
41	266.7701	183.7298	42.7800
42	286.7701	183.7299	42.7800
43	351.7701	183.7299	42.7800

Table 4.3 List of vertices for Example Part 1 before development

LIST OF VERTEX DATA AFTER DEVELOPMENT

vert_no	x_cord	y_cord	z_cord
1	201.7701	40.2623	42.7800
2	264.2701	40.2623	42.7800
3	289.2701	40.2623	42.7800
4	351.7701	40.2623	42.7800
5	239.7701	46.2623	42.7800
6	231.1098	51.2623	42.7800
7	248.4303	51.2623	42.7800
8	264.2701	55.2623	42.7800
9	289.2701	55.2623	42.7800
10	231.1098	61.2623	42.7800
11	248.4303	61.2623	42.7800
12	239.7701	66.2623	42.7800
13	221.7701	75.2623	42.7800
14	256.7701	75.2623	42.7800
15	286.7701	99.2623	42.7800
16	321.7701	99.2626	42.7800
17	201.7701	100.2623	42.7800
18	221.7701	100.2625	42.7800
19	256.7701	100.2623	42.7800
20	286.7701	100.2625	42.7800
21	321.7701	100.2623	42.7800
22	351.7701	100.2623	42.7800
23	201.7701	123.7299	42.7800
24	221.7701	123.7299	42.7800
25	256.7701	123.7299	42.7800
26	286.7701	123.7299	42.7800
27	321.7701	123.7299	42.7800
28	351.7701	123.7299	42.7800
29	286.7701	124.7299	42.7800
30	321.7701	124.7299	42.7800
31	221.7701	148.7299	42.7800
32	256.7701	148.7299	42.7800
33	296.7701	152.7492	42.7800
34	311.7701	152.7492	42.7800
35	241.7701	163.7299	42.7800
36	289.2701	165.7395	42.7800
37	319.2701	165.7395	42.7800
38	296.7701	178.7299	42.7800
39	311.7701	178.7299	42.7800
40	201.7701	183.7299	42.7800
41	266.7701	183.7298	42.7800
42	286.7701	183.7299	42.7800
43	351.7701	183.7299	42.7800

Table 4.4 List of vertices for Example Part 1 after development

LIST OF EDGE DATA BEFORE DEVELOPMENT

	start_x_cord	start_y_cord	start_z_cord	char_1	char_2
4	201.7701	183.7299	42.7800	266.7701	183.7299
4	351.7701	183.7299	42.7800	351.7701	123.7299
4	256.7701	123.7299	42.7800	256.7701	148.7299
4	256.7701	148.7299	42.7800	221.7701	148.7299
4	221.7701	148.7299	42.7800	221.7701	123.7299
4	201.7701	123.7299	42.7800	201.7701	183.7299
4	201.7701	108.7299	27.7800	201.7701	108.7299
4	201.7701	108.7299	-32.2200	264.2701	108.7299
4	351.7701	108.7299	-32.2200	351.7701	108.7299
4	221.7701	108.7299	27.7800	221.7701	108.7299
4	221.7701	108.7299	2.7800	256.7701	108.7299
4	256.7701	108.7299	2.7800	256.7701	108.7299
1	241.7701	163.7299	42.7800	10.0000	1.0000
4	296.7701	178.7299	42.7800	311.7701	178.7299
4	311.7701	178.7299	42.7800	319.2701	165.7395
4	319.2701	165.7395	42.7800	311.7701	152.7492
4	311.7701	152.7492	42.7800	296.7701	152.7492
4	296.7701	152.7492	42.7800	289.2701	165.7395
4	289.2701	165.7395	42.7800	296.7701	178.7299
4	239.7701	108.7299	-6.2200	248.4303	108.7299
4	248.4303	108.7299	-11.2200	248.4303	108.7299
4	248.4303	108.7299	-21.2200	239.7701	108.7299
4	239.7701	108.7299	-26.2200	231.1098	108.7299
4	231.1098	108.7299	-21.2200	231.1098	108.7299
4	231.1098	108.7299	-11.2200	239.7701	108.7299
3	201.7701	123.7299	27.7800	15.0000	0.0000
3	221.7701	123.7299	27.7800	15.0000	360.0000
3	256.7701	123.7299	27.7800	15.0000	0.0000
3	286.7701	123.7299	27.7800	15.0000	360.0000
3	321.7701	123.7299	27.7800	15.0000	0.0000
3	351.7701	123.7299	27.7800	15.0000	0.0000
4	201.7701	123.7299	42.7800	221.7701	123.7299
4	201.7701	108.7299	27.7800	221.7701	108.7299
4	256.7701	108.7299	27.7800	286.7701	108.7299
4	321.7701	108.7299	27.7800	351.7701	108.7299
4	256.7701	123.7299	42.7800	286.7701	123.7299
4	321.7701	123.7299	42.7800	351.7701	123.7299
4	264.2701	108.7299	-32.2200	264.2701	108.7299
4	289.2701	108.7299	-32.2200	289.2701	108.7299
4	264.2701	108.7299	-17.2200	289.2701	108.7299
4	289.2701	108.7299	-32.2200	351.7701	108.7299
3	276.7701	183.7299	42.7800	10.0000	180.0000
4	286.7701	183.7299	42.7800	351.7701	183.7299
3	304.2701	124.7299	42.7800	17.5000	0.0000
3	304.2701	108.7299	26.7800	17.5000	180.0000
4	286.7701	124.7299	42.7800	286.7701	123.7299
4	321.7701	124.7299	42.7800	321.7701	123.7299
4	321.7701	108.7299	27.7800	321.7701	108.7299
4	286.7701	108.7299	27.7800	286.7701	108.7299

Table 4.5 List of edges for Example Part 1 before

LIST OF EDGE DATA AFTER DEVELOPMENT

_no	ent_type	start_x_cord	start_y_cord	start_z_cord	char_1	char_2
	4	201.7701	183.7299	42.7800	266.7701	183.7298
	4	351.7701	183.7299	42.7800	351.7701	123.7299
	4	256.7701	123.7299	42.7800	256.7701	148.7299
	4	256.7701	148.7299	42.7800	221.7701	148.7299
	4	221.7701	148.7299	42.7800	221.7701	123.7299
	4	201.7701	123.7299	42.7800	201.7701	183.7299
	4	201.7701	100.2623	42.7800	201.7701	40.2623
	4	201.7701	40.2623	42.7800	264.2701	40.2623
	4	351.7701	40.2623	42.7800	351.7701	100.2623
	4	221.7701	100.2625	42.7800	221.7701	75.2623
	4	221.7701	75.2623	42.7800	256.7701	75.2623
	4	256.7701	75.2623	42.7800	256.7701	100.2623
	1	241.7701	163.7299	42.7800	10.0000	1.0000
	4	296.7701	178.7299	42.7800	311.7701	178.7299
	4	311.7701	178.7299	42.7800	319.2701	165.7395
	4	319.2701	165.7395	42.7800	311.7701	152.7492
	4	311.7701	152.7492	42.7800	296.7701	152.7492
	4	296.7701	152.7492	42.7800	289.2701	165.7395
	4	289.2701	165.7395	42.7800	296.7701	178.7299
	4	239.7701	66.2623	42.7800	248.4303	61.2623
	4	248.4303	61.2623	42.7800	248.4303	51.2623
	4	248.4303	51.2623	42.7800	239.7701	46.2623
	4	239.7701	46.2623	42.7800	231.1098	51.2623
	4	231.1098	51.2623	42.7800	231.1098	61.2623
	4	231.1098	61.2623	42.7800	239.7701	66.2623
	4	201.7701	100.2623	42.7800	201.7701	123.7299
	4	221.7701	100.2625	42.7800	221.7701	123.7299
	4	256.7701	100.2623	42.7800	256.7701	123.7299
	4	286.7701	100.2625	42.7800	286.7701	123.7299
	4	321.7701	100.2623	42.7800	321.7701	123.7299
	4	351.7701	100.2623	42.7800	351.7701	123.7299
	4	201.7701	123.7299	42.7800	221.7701	123.7299
	4	201.7701	100.2623	42.7800	221.7701	100.2625
	4	256.7701	100.2623	42.7800	286.7701	100.2625
	4	321.7701	100.2623	42.7800	351.7701	100.2623
	4	256.7701	123.7299	42.7800	286.7701	123.7299
	4	321.7701	123.7299	42.7800	351.7701	123.7299
	4	264.2701	40.2623	42.7800	264.2701	55.2623
	4	289.2701	40.2623	42.7800	289.2701	55.2623
	4	264.2701	55.2623	42.7800	289.2701	55.2623
	4	289.2701	40.2623	42.7800	351.7701	40.2623
	3	276.7701	183.7299	42.7800	10.0000	180.0000
	4	286.7701	183.7299	42.7800	351.7701	183.7299
	3	304.2701	124.7299	42.7800	17.5000	0.0000
	3	304.2701	99.2623	42.7800	17.5000	180.0000
	4	286.7701	124.7299	42.7800	286.7701	123.7299
	4	321.7701	124.7299	42.7800	321.7701	123.7299
	4	321.7701	100.2623	42.7800	321.7701	99.2626
	4	286.7701	100.2625	42.7800	286.7701	99.2623

Table A.6 List of edges for Example Part 1 after de

LIST OF PLANE DATA

_no	no of edges	list of edges ->					
1	16	1	2	3	4	5	6
		11	14	15	16	17	18
		19	20	23	26		
2	12	20	21	22	23	24	25
		26	27	28	29	32	35
3	14	29	30	31	32	33	34
		35	36	37	38	39	47
		48	49				
1	6	7	8	9	10	12	13
3	6	40	41	42	44	45	46
3	1	43					

Table 4.7 List of planes for Example Part 1 before development

LIST OF PLANE DATA AFTER DEVELOPMENT

_no	no of edges	list of edges ->					
3	36	29	30	31	32	33	34
		35	36	37	38	39	47
		48	49	20	21	22	23
		24	25	26	27	28	1
		2	3	4	5	6	11
		14	15	16	17	18	19
3	6	7	8	9	10	12	13
3	6	40	41	42	44	45	46
3	1	43					

Table 4.8 List of plane data for Example Part 1 after development

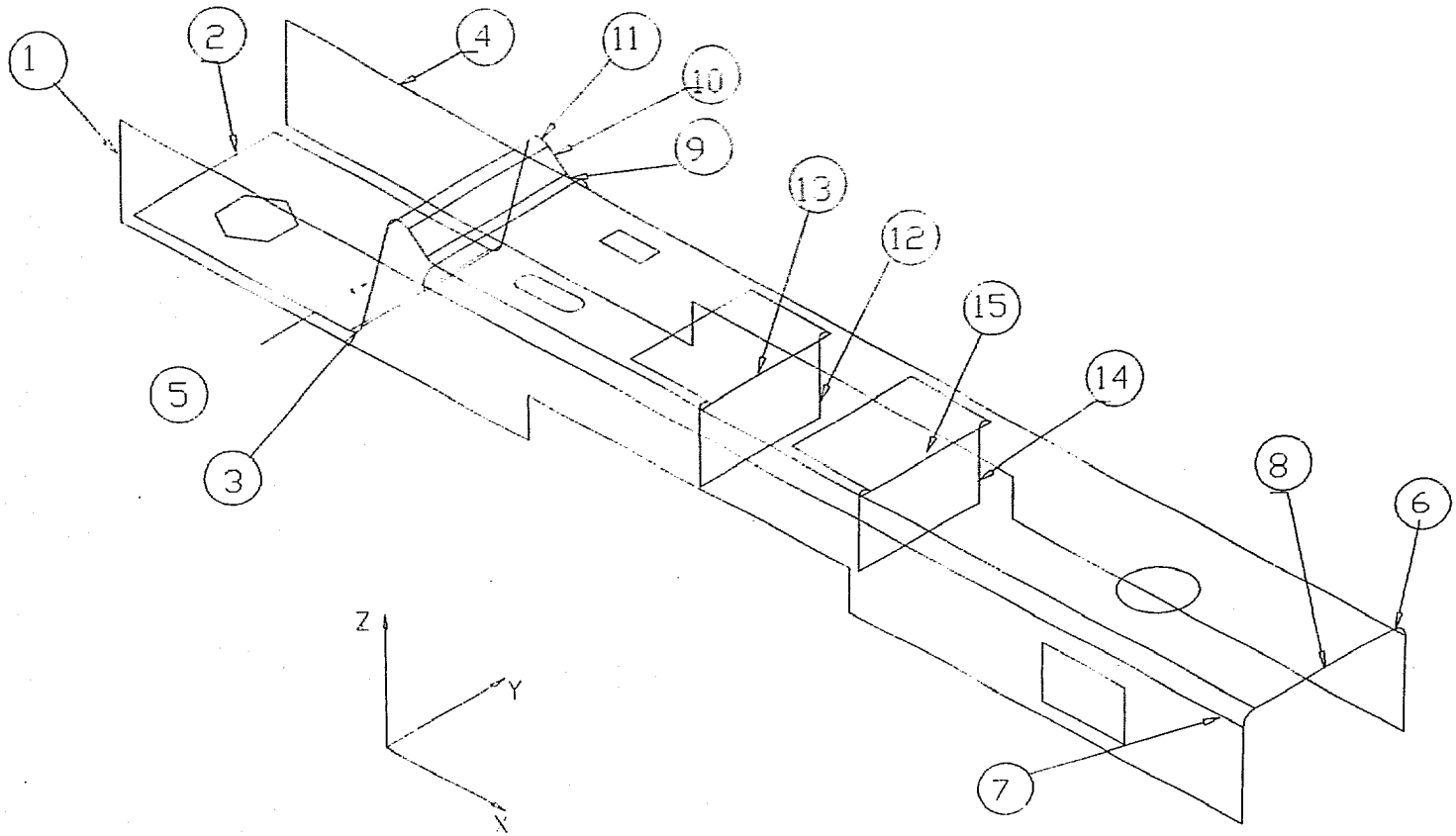

Fig. 4.3 Part drawing for the component in Example Part 2

SUMMARY RESULTS OF BEND ALLOWANCE CALCULATION

terial Properties

Material	:	Aluminium Killed Steel
Yield Stress (sigma_o)	:	172.8 MPa
Exponent (n)	:	0.22
Strength Coefficient (k)	:	510.16 MPa
Ultimate Tensile Strength	:	840.0 MPa

****

INPUT DATA FOR BEND PLANE # 6

Bend Plane	:	6	
Inner Radius of Bend	:	2.0000	mm
Angle of Bend	:	1.5708	rad.
Initial Thickness	:	2.0000	mm

OUTPUT DATA FOR BEND PLANE # 6

Final Thickness	:	1.9337	mm
Rad. of unstreched fiber	:	2.8685	mm
Bend Allowance	:	4.5059	mm

****

INPUT DATA FOR BEND PLANE # 9

Bend Plane	:	9	
Inner Radius of Bend	:	2.0000	mm
Angle of Bend	:	0.7330	rad.
Initial Thickness	:	2.0000	mm

OUTPUT DATA FOR BEND PLANE # 9

Final Thickness	:	1.9337	mm
Rad. of unstreched fiber	:	2.8688	mm
Bend Allowance	:	2.1028	mm

****

Table 4.9 Results of Bend Allowance calculation for Example Part 2 of bending (contd.)

INPUT DATA FOR BEND PLANE # 13

Bend Plane	:	13	
Inner Radius of Bend	:	2.0000	mm
Angle of Bend	:	1.5708	rad.
Initial Thickness	:	2.0000	mm

OUTPUT DATA FOR BEND PLANE # 13

Final Thickness	:	1.9337	mm
Rad. of unstreched fiber	:	2.8685	mm
Bend Allowance	:	4.5059	mm

****

INPUT DATA FOR BEND PLANE # 15

Bend Plane	:	15	
Inner Radius of Bend	:	2.0000	mm
Angle of Bend	:	1.5708	rad.
Initial Thickness	:	2.0000	mm

OUTPUT DATA FOR BEND PLANE # 15

Final Thickness	:	1.9337	mm
Rad. of unstreched fiber	:	2.8685	mm
Bend Allowance	:	4.5059	mm

****

INPUT DATA FOR BEND PLANE # 7

Bend Plane	:	7	
Inner Radius of Bend	:	2.0000	mm
Angle of Bend	:	1.5708	rad.
Initial Thickness	:	2.0000	mm

Table 4.9 Results of Bend Allowance calculation for Example Part 2 of bending (contd.)

UTPUT DATA FOR BEND PLANE # 7

Final Thickness	:	1.9337	mm
Rad. of unstreched fiber	:	2.8685	mm
Bend Allowance	:	4.5059	mm

****

INPUT DATA FOR BEND PLANE # 11

Bend Plane	:	11	
Inner Radius of Bend	:	2.0000	mm
Angle of Bend	:	2.0420	rad.
Initial Thickness	:	2.0000	mm

OUTPUT DATA FOR BEND PLANE # 11

Final Thickness	:	1.9337	mm
Rad. of unstreched fiber	:	2.8686	mm
Bend Allowance	:	5.8577	mm

****

INPUT DATA FOR BEND PLANE # 3

Bend Plane	:	3	
Inner Radius of Bend	:	2.0000	mm
Angle of Bend	:	1.3090	rad.
Initial Thickness	:	2.0000	mm

OUTPUT DATA FOR BEND PLANE # 3

Final Thickness	:	1.9337	mm
Rad. of unstreched fiber	:	2.8686	mm
Bend Allowance	:	3.7550	mm

****

Table 4.9 Results of Bend Allowance calculation for Example Part 2 of bending

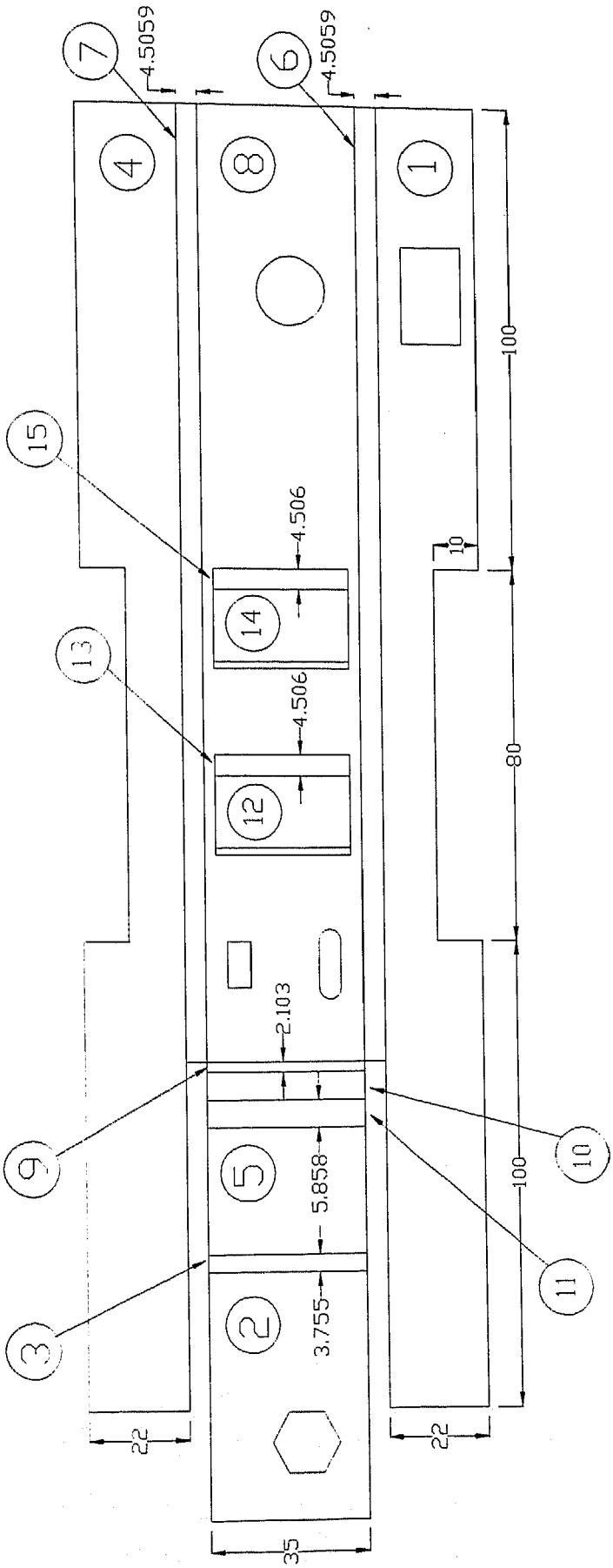

Fig. 4.4 Flat pattern for the component in Example Part 2

PART 3

The drawing of the part taken as the third example is in Fig. 4.5. It is the pin tray of a common stapler. The considered here is modified slightly because of the tions of the model considered. The original component had a ing feature which can not be analyzed by present prototype. it has been removed in this example. The original component wn in Fig. 4.6. This component has 13 planes in total and 6 are bend planes. The results of calculation are shown in 4.10 and flat pattern obtained is given in Fig. 4.7.

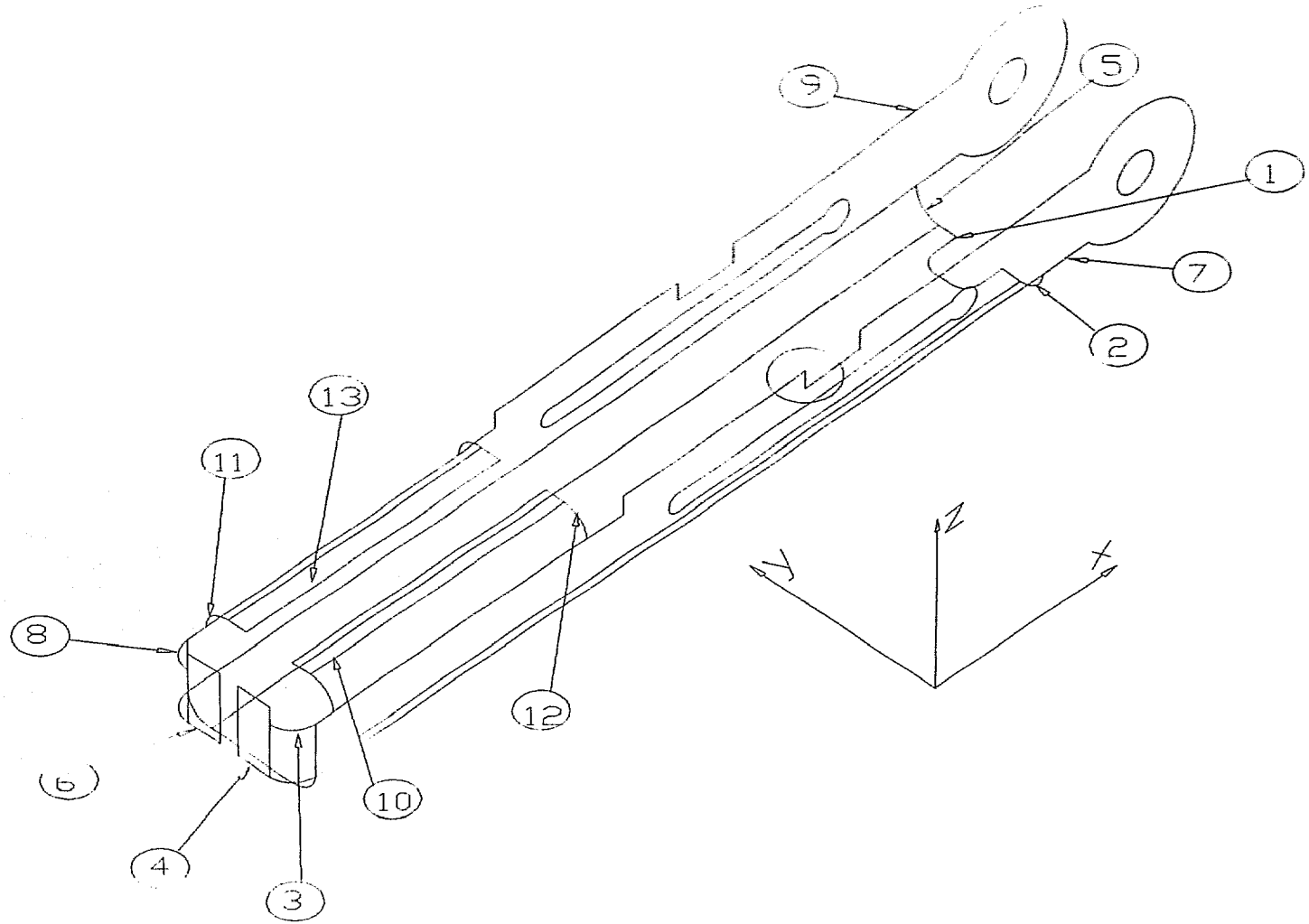

Fig. 4.5 Part drawing for the component in Example Part 3

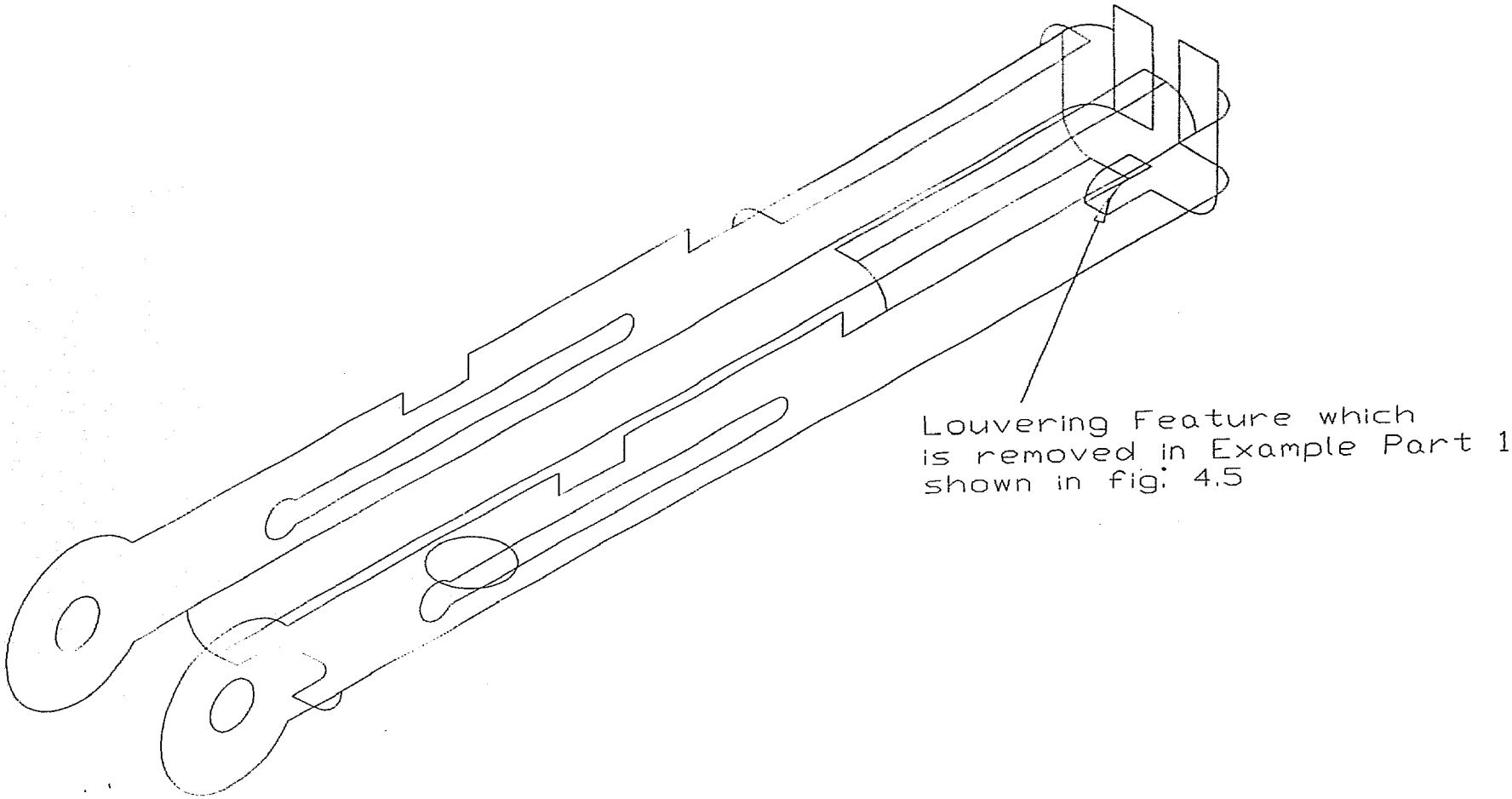

Fig. 4.6 Original component for Example Part 3

SUMMARY RESULTS OF BEND ALLOWANCE CALCULATION

terial Properties

Material	: Aluminium Killed Steel
Yield Stress (sigma_o)	: 172.8 MPa
Exponent (n)	: 0.22
Strength Coefficient (k)	: 510.16 MPa
Ultimate Tensile Strength	: 840.0 MPa

****

INPUT DATA FOR BEND PLANE # 8

Bend Plane	: 8
Inner Radius of Bend	: 2.0000 mm
Angle of Bend	: 1.5708 rad.
Initial Thickness	: 1.0000 mm

OUTPUT DATA FOR BEND PLANE # 8

Final Thickness	: 0.9906 mm
Rad. of unstretched fiber	: 2.4714 mm
Bend Allowance	: 3.8827 mm

****

INPUT DATA FOR BEND PLANE # 2

Bend Plane	: 2
Inner Radius of Bend	: 2.0000 mm
Angle of Bend	: 1.5708 rad.
Initial Thickness	: 1.0000 mm

OUTPUT DATA FOR BEND PLANE # 2

Final Thickness	: 0.9906 mm
Rad. of unstretched fiber	: 2.4714 mm
Bend Allowance	: 3.8827 mm

****

Table 4.10 Results of Bend Allowance calculation for Example Part 3 of bending (contd.)

INPUT DATA FOR BEND PLANE # 3

Bend Plane	:	3	
Inner Radius of Bend	:	1.0000	mm
Angle of Bend	:	1.5708	rad.
Initial Thickness	:	1.0000	mm

OUTPUT DATA FOR BEND PLANE # 3

Final Thickness	:	0.9906	mm
Rad. of unstretched fiber	:	2.4714	mm
Bend Allowance	:	3.8827	mm

****

INPUT DATA FOR BEND PLANE # 12

Bend Plane	:	12	
Inner Radius of Bend	:	2.0000	mm
Angle of Bend	:	1.5708	rad.
Initial Thickness	:	1.0000	mm

OUTPUT DATA FOR BEND PLANE # 12

Final Thickness	:	0.9906	mm
Rad. of unstretched fiber	:	2.4714	mm
Bend Allowance	:	3.8827	mm

****

INPUT DATA FOR BEND PLANE # 10

Bend Plane	:	10	
Inner Radius of Bend	:	2.0000	mm
Angle of Bend	:	1.5708	rad.
Initial Thickness	:	1.0000	mm

Table 4.10 Results of Bend Allowance calculation for Example Part 3 of bending (contd.)

OUTPUT DATA FOR BEND PLANE # 10

Final Thickness	:	0.9906	mm
Rad. of unstretched fiber	:	2.4714	mm
Bend Allowance	:	3.8827	mm

****

INPUT DATA FOR BEND PLANE # 5

Bend Plane	:	5	
Inner Radius of Bend	:	2.0000	mm
Angle of Bend	:	1.5708	rad.
Initial Thickness	:	1.0000	mm

OUTPUT DATA FOR BEND PLANE # 5

Final Thickness	:	0.9906	mm
Rad. of unstretched fiber	:	2.4714	mm
Bend Allowance	:	3.8827	mm

****

Table 4.10 Results of Bend Allowance calculation for Example Part 3 of bending

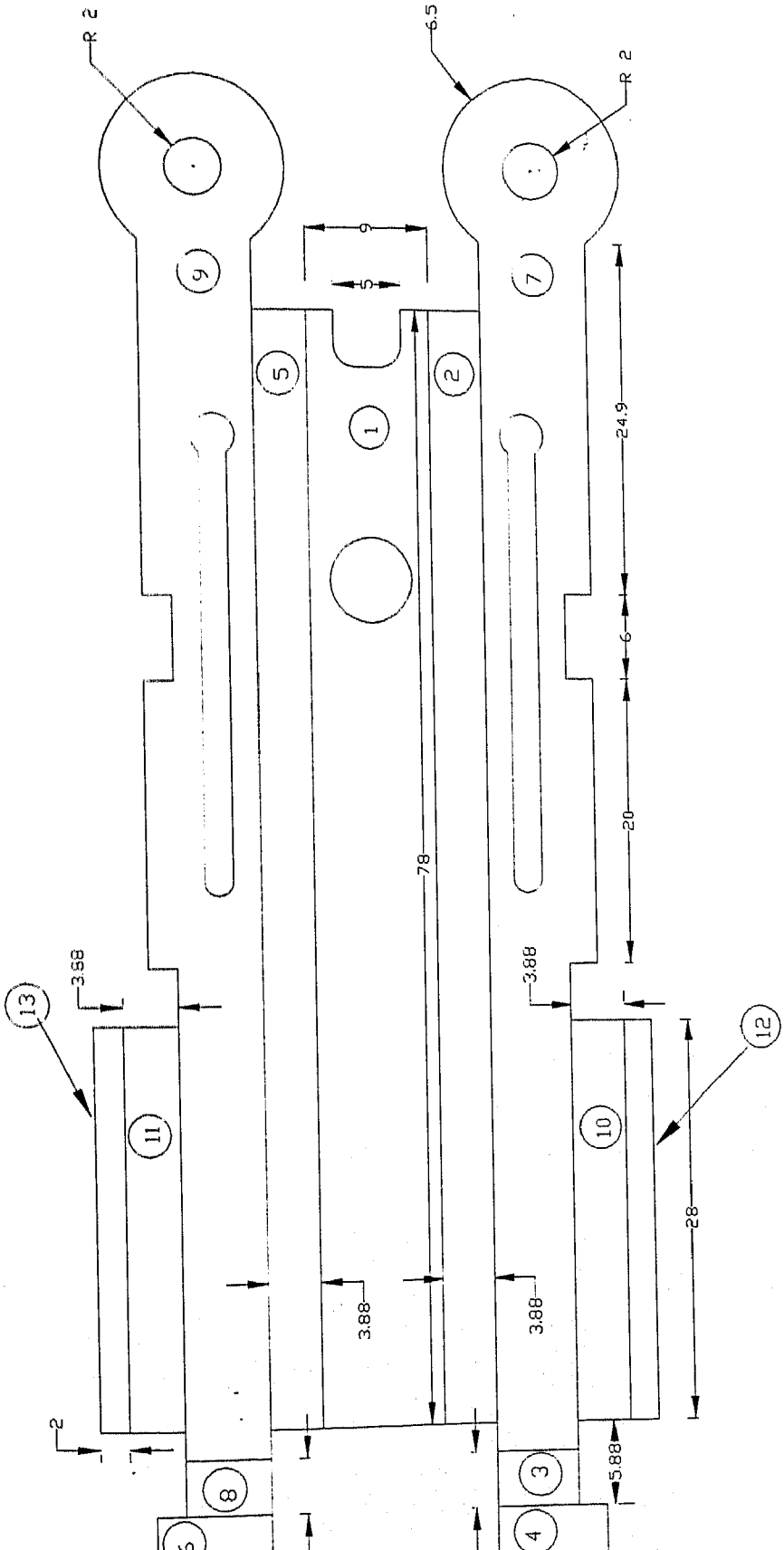

Fig. 4.7 Flat pattern for the component in Example Part 3

4.2 FLAT PATTERN DEVELOPMENT FOR DEEP DRAWN COMPONENTS

Similar to previous section, before presenting the complete results, a comparison between the results obtained by the present system and those available in the literature is made. No direct results are available on the flat pattern development for axisymmetric deep drawn components, hence, the results obtained for the components having shapes very close to the axisymmetric cup are chosen for comparison purpose. Flat pattern obtained by Toh and Kobayashi (1985) for square cups using FEM is compared with the results obtained by the present system. Here, the flat pattern obtained by the present system for maximum inscribing circular profile and minimum circumscribing circular profile are compared with those of square cups obtained by Toh and Kobayashi (1985). Figs. 4.8 and 4.9 show the two comparisons.

In Fig. 4.8(a), the square cup analyzed by Toh and Kobayashi (1985) and the maximum inscribing circular cup analyzed by present system is shown. Fig. 4.8(b) shows the flat patterns obtained for the two cases. The flat pattern obtained by present system is found to be smaller than that obtained by Toh and Kobayashi (1985). This is mainly because the cup analyzed by present system is smaller in terms of cross sectional area and flange size than the cup considered by Toh and Kobayashi.

Similarly, Fig. 4.9(a) shows the square cup analyzed by Toh and Kobayashi (1985) and the minimum circumscribing cup analyzed by present work. In Fig. 4.9(b), flat patterns obtained for the two cases are presented. In this case, the flat pattern obtained by present system is observed to be bigger than the flat pattern obtained by Toh and Kobayashi (1985) for square cup. This discrepancy is mainly because, the cup analyzed by the present system has a bigger cross-sectional area and flange radius than that considered by Toh and Kobayashi (1985).

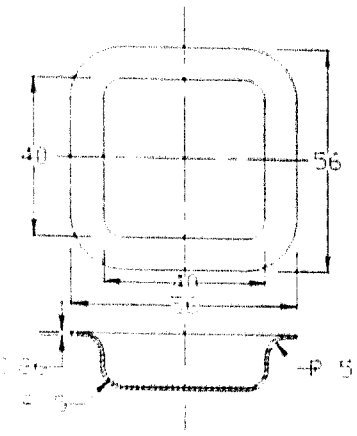

Square shaped component considered by Toh and Kobayashi (1985)

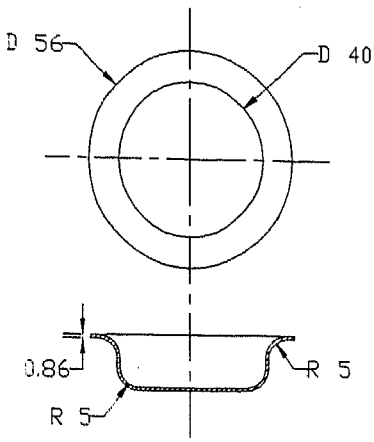

Inscribing circular component considered in the present work

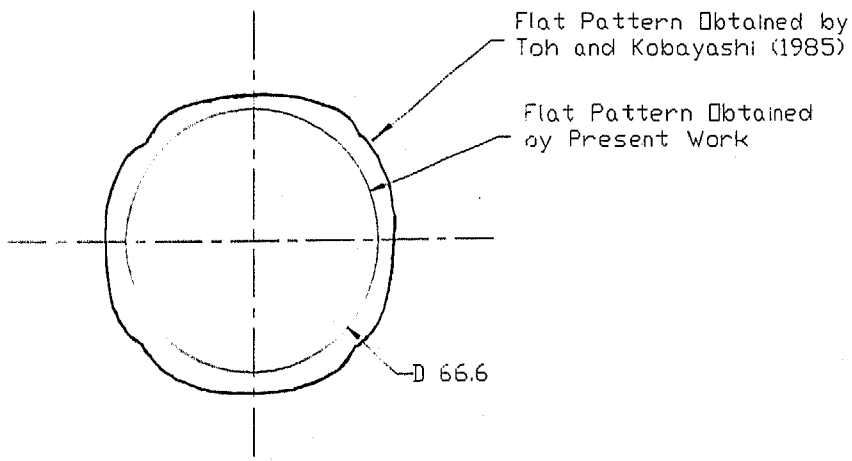

Comparison of flat pattern sizes obtained by Toh and Kobayashi (1985) and present work

Fig. 4.8 Comparison of results for inscribing circular profile

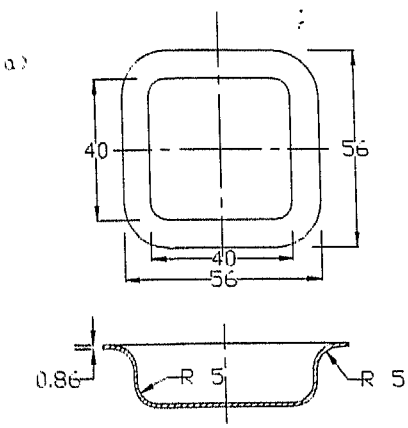

Square shaped component considered by Toh and Kobayashi (1985)

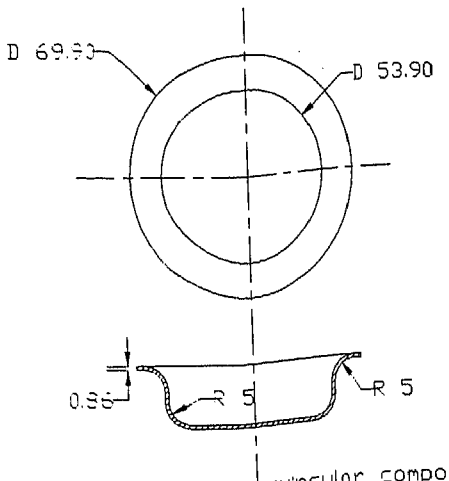

Circumscribing cuircular component considered in the present work

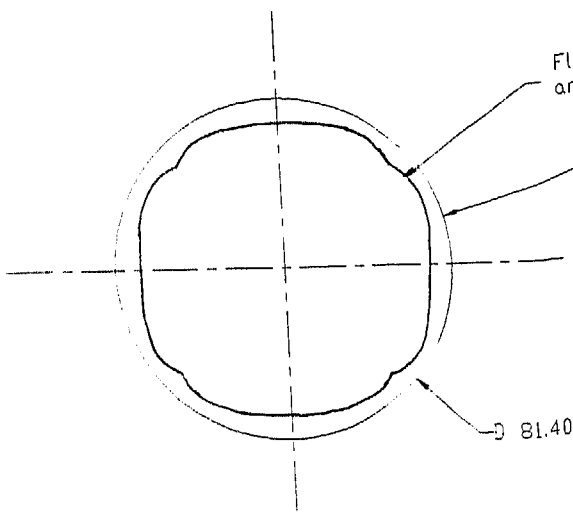

Comparison of flat pattern sizes obtained by Toh and Kobayashi (1985) and present work

Fig. 4.9 Comparison of results for circumscribing circular profile

:AMPLE PART 1

Table 4.11 gives the result sheet for the Example Part The component considered in this example is a cup a AK steel of :ight 20 mm and a flange radius of 32 mm. The initial sheet ıickness is given to be 2 mm. Detailed input data is presented ı this table. The results obtained are also shown on the same ıble. Firstly, the values of blank diameter, flange diameter ;ed, minimum and maximum thicknesses obtained for each iteration ; presented. Finally, the table gives the results of the flat ıttern development system. For this component, the size of flat ıttern was found to be 32.95 mm giving a flange radius of 32.008 ı. Since, this value of the flange radius is within the accuracy .mit (0.01 mm), no further iterations are made. The final ıickness was found to be 2.29 mm at the periphery and 1.72 at the ırved profile over the die.

Fig. 4.10 shown the drawing of the final flat pattern. ıe comparison between the desired and the obtained cups is also resented. Fig. 4.11 shows the instantaneous flange size of the up at different depths of the cup during the drawing operation or the last iteration.

SUMMARY RESULTS FOR DEEP DRAWING

EXAMPLE PART 1

****

INPUT DATA

Material Properties

Material Type	: Aluminium Killed Steel
Yield Stress (sigma_o)	: 172.8 MPa
Exponent (n)	: 0.22
Strength Coefficient (k)	: 510.16 MPa
Ultimate Tensile Strength	: 840.0 MPa

Part Geometry

Punch Diameter (R_p)	: 20 mm
Die Corner Radius (r_d)	: 3 mm
Punch Corner Radius (r_p)	: 3 mm
Height (H_max)	: 20 mm
Clearance (epsn)	: 5 mm
Flange Diameter (r_f)	: 32 mm
Sheet Thickness (t_0)	: 2 mm
Coeff. of Friction	: 0.02
Blank Holding Force	: 500 kgf

OUTPUT DATA

Blank Size	: 35.952 mm
Final Flange Size	: 32.008 mm
Maximum Thickness	: 2.290 mm
Minimum Thickness	: 1.718 mm

****

Table 4.11 Result and convergence history of Example Part 1 of deep drawing (contd.)

Convergence history of flat pattern for example 1

Iteration Number	Blank Rad. (mm)	Flange Rad. (mm)	Cup Thickness (mm)	Periphery Thickness (mm)
1	42.6965	35.0939	1.7829	2.2708
2	41.3567	33.5954	1.7508	2.2799
3	40.6684	32.8199	1.7345	2.2848
4	40.3153	32.4233	1.7266	2.2875
5	40.1346	32.2163	1.7225	2.2888
6	40.0420	32.1102	1.7199	2.2896
7	39.9947	32.0564	1.7188	2.2899
8	39.9704	32.0289	1.7182	2.2900
9	39.9580	32.0148	1.7179	2.2902
10	39.9516	32.0076	1.7177	2.2902

Table 4.11 Result and convergence history of Example Part 1 of deep drawing

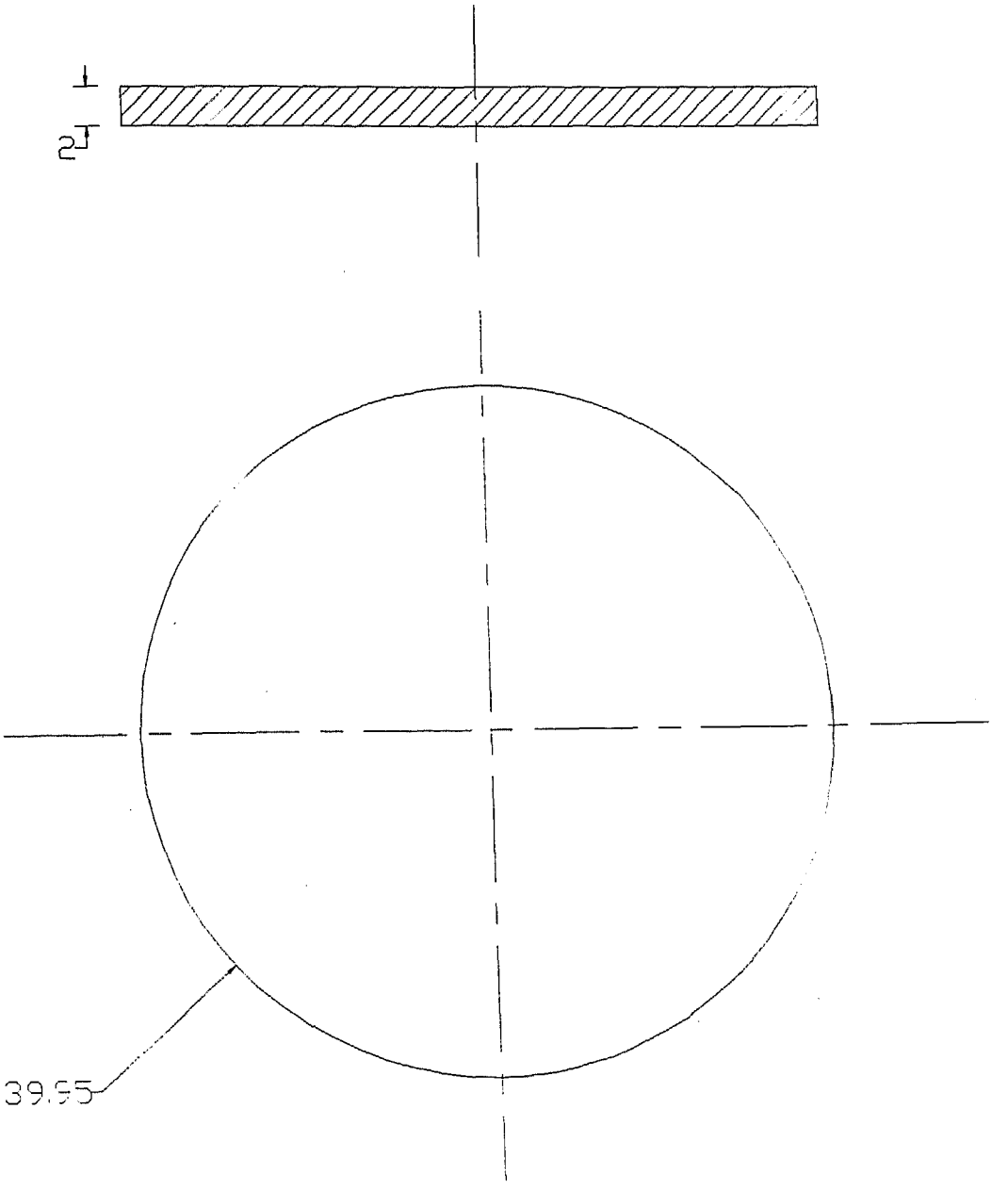

Fig 4.10 (a) Flat pattern obtained for Example Part 1

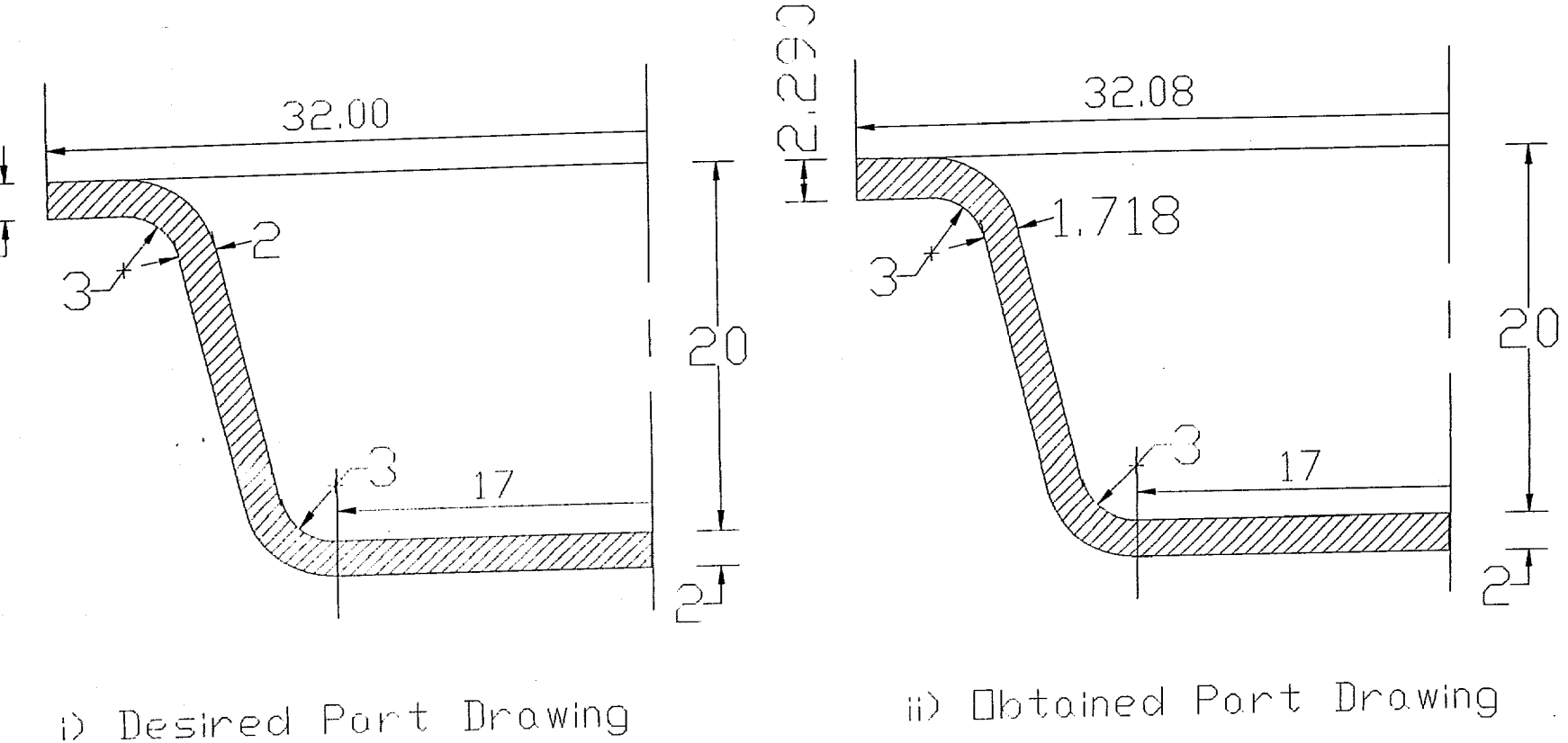

Fig. 4.10(b) Desired and obatined part drawings for the component in Example Part 1

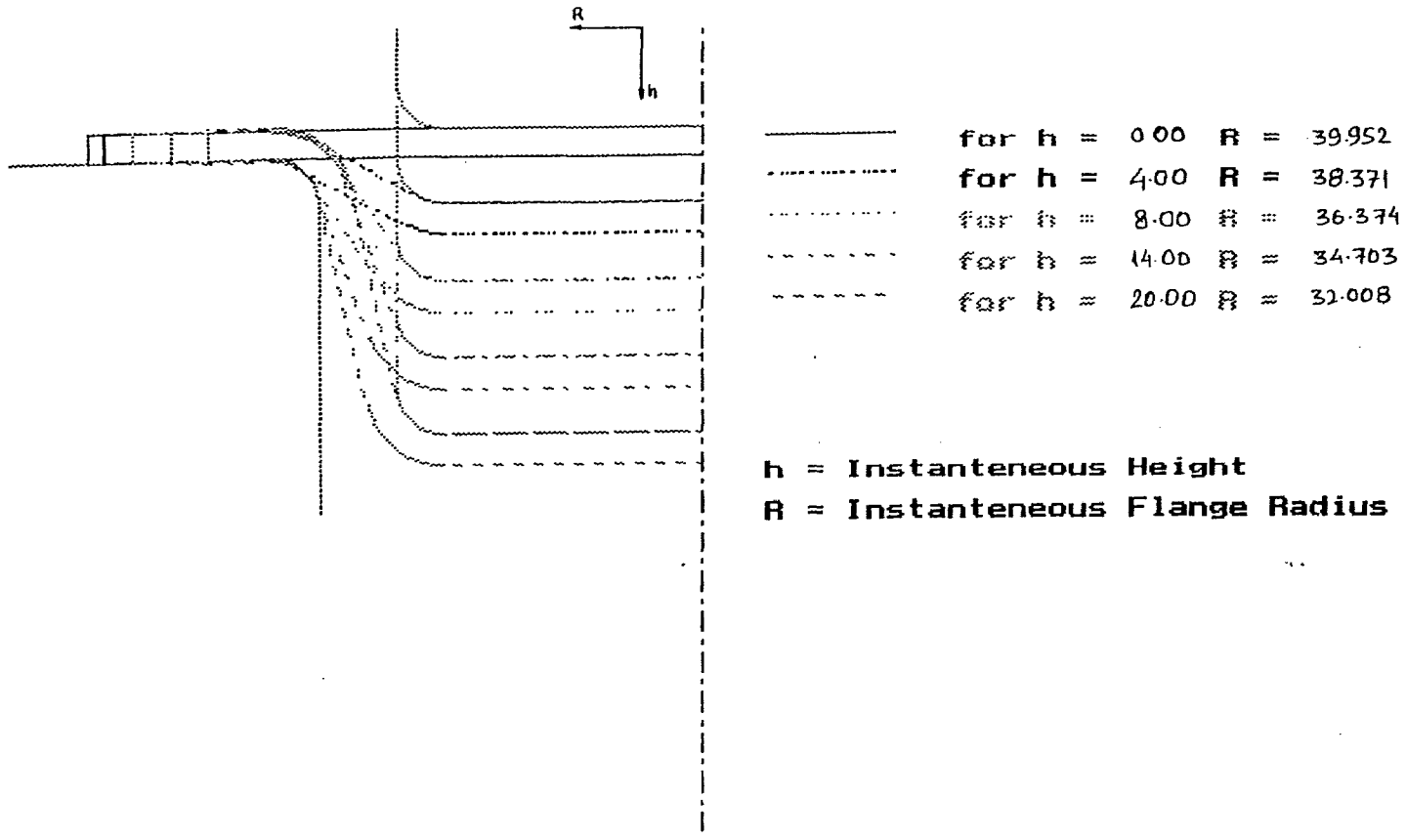

Fig. 4.11 Progressive stages for the component in Example Part 1

SUMMARY RESULT FOR DEEP DRAWING

EXAMPLE PART 2

****

INPUT DATA

Material Properties

Material	: Aluminium
Yield Stress (sigma_o)	: 113.0 MPa
Exponent (n)	: 0.50
Strength Coefficient (k)	: 785.92 MPa

Part Geometry

Punch Diameter (R_p)	: 20.00 mm
Die Corner Radius (r_d)	: 5.00 mm
Punch Corner Radius (r_p)	: 5.00 mm
Height (H_max)	: 13.50 mm
Clearance (epsn)	: 1.25 mm
Flange Diameter (r_f)	: 28.00 mm
Sheet Thickness (t_0)	: 0.86 mm
Coeff. of Friction	: 0.2
Blank Holding Force	: 500 kgf

OUTPUT DATA

Blank Size	: 33.270 mm
Final Flange Size	: 28.009 mm
Maximum Thickness	: 0.9463 mm
Minimum Thickness	: 0.7311 mm

****

The blank size obtaine for the component is 33.270 mm

Table 4.12 Result and convergence history for Example Part 2 of deep drawing (contd.)

Convergence history of flat pattern for example 2

eration umber	Blank Rad. (mm)	Flange Rad. (mm)	Cup Thickness (mm)	Periphery Thickness (mm)
1	36.0881	31.0681	0.7648	0.9370
2	34.7248	29.5974	0.7483	0.9414
3	34.0172	28.8239	0.7403	0.9436
4	33.6521	28.4240	0.7362	0.9447
5	33.4651	28.2195	0.7340	0.9454
6	33.3685	28.114	0.7327	0.9458
7	33.3179	28.0600	0.7320	0.9460
8	33.2924	28.0326	0.7316	0.9461
9	33.2781	28.0174	0.7313	0.9462
10	33.2707	28.0091	0.7351	0.9463

Table 4.12 Result and convergence history for Example Part 2 of deep drawing

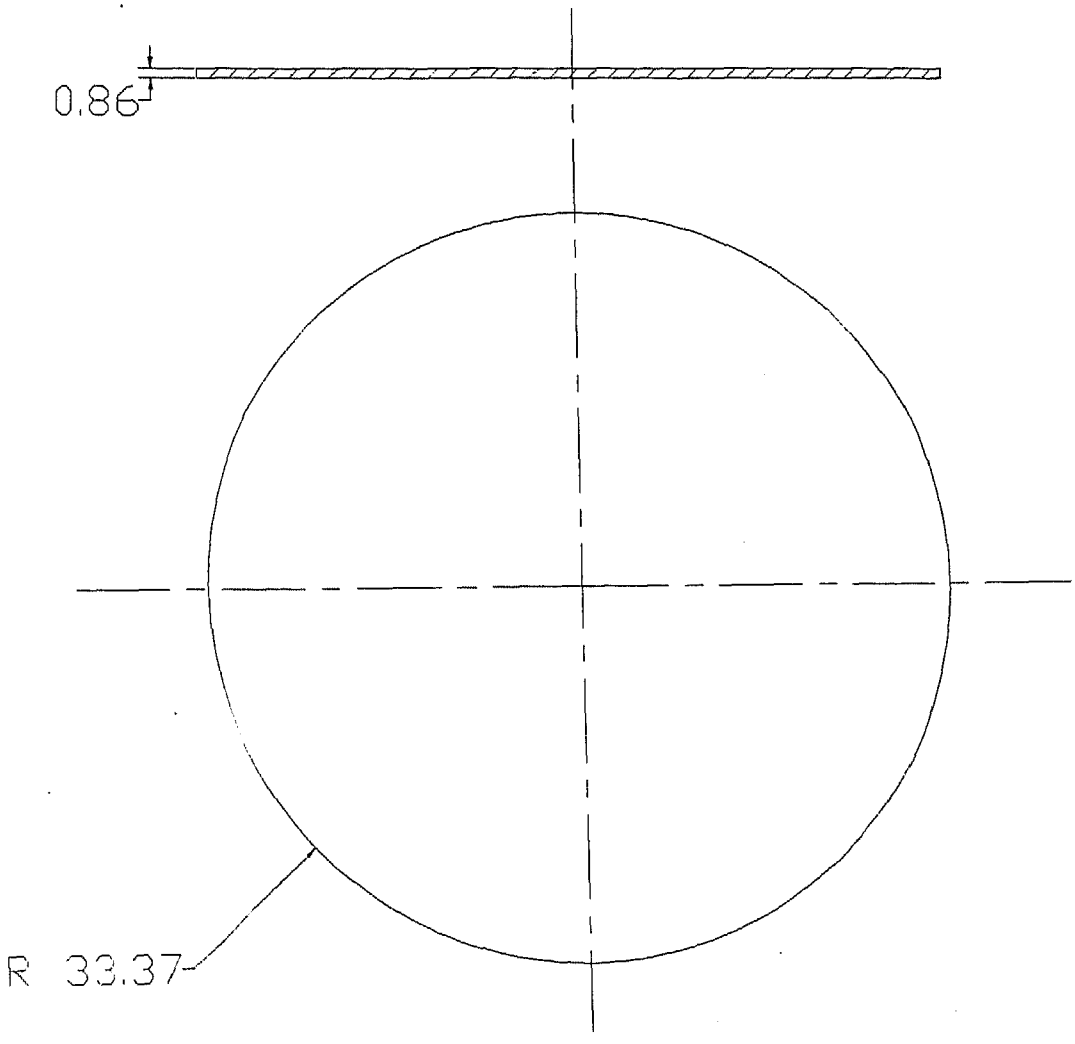

Fig. 4.12(a) Flat pattern obtained for Example Part 2

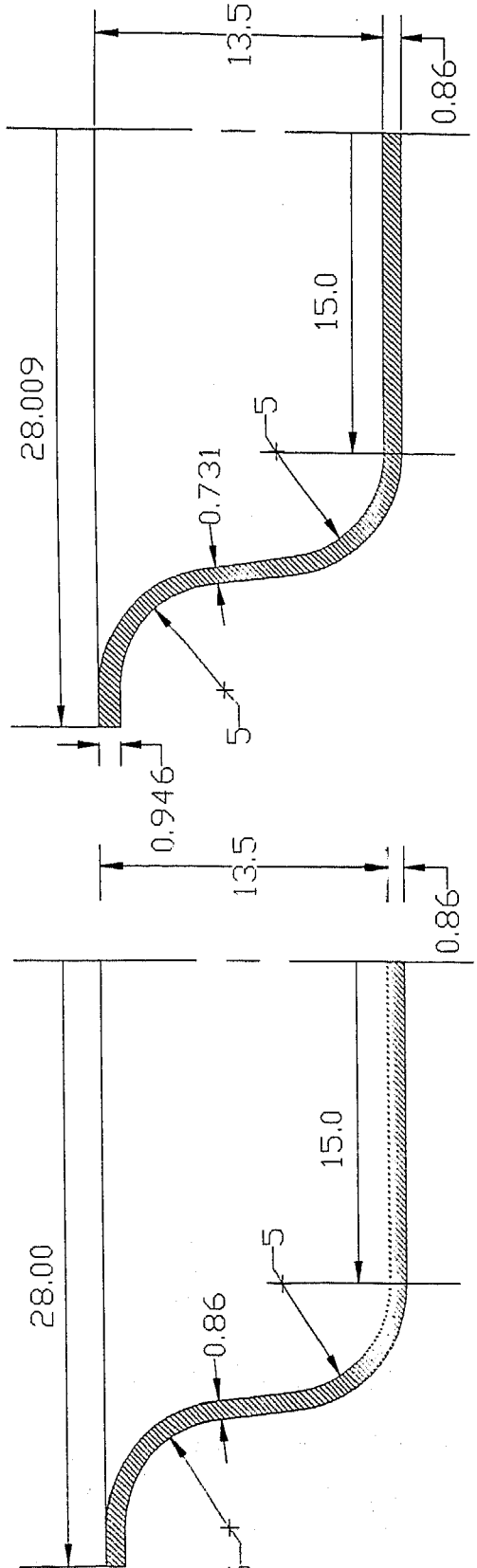

ii) Obtained part drawing

i) Desired part drawing

Fig. 4.12(b) Desired and obtained part drawings for the component in Example Part 2

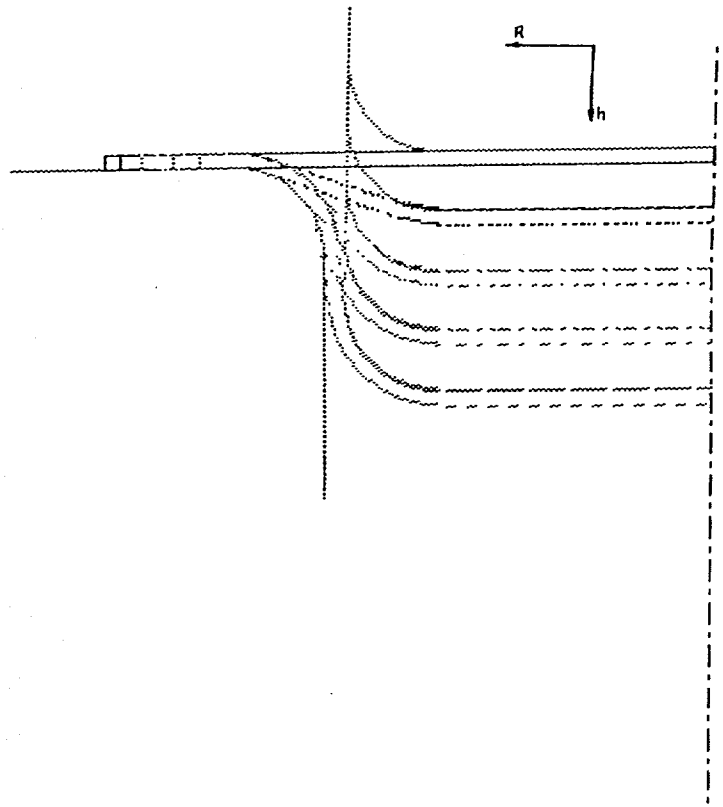

for h = 0·00 R = 33·271
for h = 3·51 R = 32·335
for h = 6·75 R = 31·159
for h = 10·26 R = 29·529
for h = 13·50 R = 28·009

h = Instanteneous Height
R = Instanteneous Flange Radius

Fig. 4.13 Progressive stages for the component in Example Part 2

EXAMPLE PART 3

For Example Part 3, we have considered a brass cup of flange radius 34.95 mm with a punch radius of 26.95 mm. the cup has a height 13.5 mm and the original thickness is 0.86 mm. Table 4.13 lists various geometrical data along with the material properties. Next, in the same table, the value of flat pattern radius, the obtained flange radius and the maximum and minimum thickness for each iteration is shown. The iteration was stopped when the flange radius was found to be within the accuracy of 0.01 mm. The radius flat pattern obtained for this example is 40.7053 mm giving a flange radius of 34.959 mm. The maximum and minimum thickness are found to be 0.9342 mm and 0.7486 mm respectively. These values are also presented in Table 4.13.

Fig. 4.14 shows the flat pattern along with a comparison between the desired and obtained part. Fig. 4.15 shows the instantaneous height and flange radius of the cup at different stages of drawing of the cup.

SUMMARY RESULT FOR DEEP DRAWING

EXAMPLE PART 3

****

INPUT DATA

Material Properties

Material	: Brass
Yield Stress (sigma_o)	: 200.26 MPa
Exponent (n)	: 0.2
Strength Coefficient (k)	: 500.65 MPa

Part Geometry

Punch Diameter (R_p)	: 26.95 mm
Die Corner Radius (r_d)	: 5.00 mm
Punch Corner Radius (r_p)	: 5.00 mm
Height (H_max)	: 13.50 mm
Clearance (epsn)	: 1.25 mm
Flange Diameter (r_f)	: 34.95 mm
Sheet Thickness (t_0)	: 0.86 mm
Coeff. of Friction	: 0.2
Blank Holding Force	: 500 kgf

OUTPUT DATA

Blank Size	: 40.7053 mm
Final Flange Size	: 34.959 mm
Maximum Thickness	: 0.9342 mm
Minimum Thickness	: 0.7486 mm

****

The blank size obtaine for the component is 40.7053 mm

Table 4.13 Result and convergence history for Example Part 3 of deep drawing (contd.)

Convergence history of flat pattern for example 3

Iteration Number	Blank Rad. (mm)	Flange Rad. (mm)	Cup Thickness (mm)	Periphery Thickness (mm)
1	44.0158	38.5849	0.7728	0.9278
2	42.3766	36.7966	0.7609	0.9308
3	41.5477	35.8848	0.7550	0.9324
4	41.1280	35.4437	0.7519	0.9332
5	40.9165	35.1897	0.7504	0.9337
6	40.8095	35.0714	0.7496	0.9339
7	40.7549	35.0129	0.7491	0.9340
8	40.7278	34.9822	0.7489	0.9341
9	40.7135	34.9660	0.7487	0.9342
10	40.7058	34.9591	0.7486	0.9342

Table 4.13 Result and convergence history for Example Part 3 of deep drawing

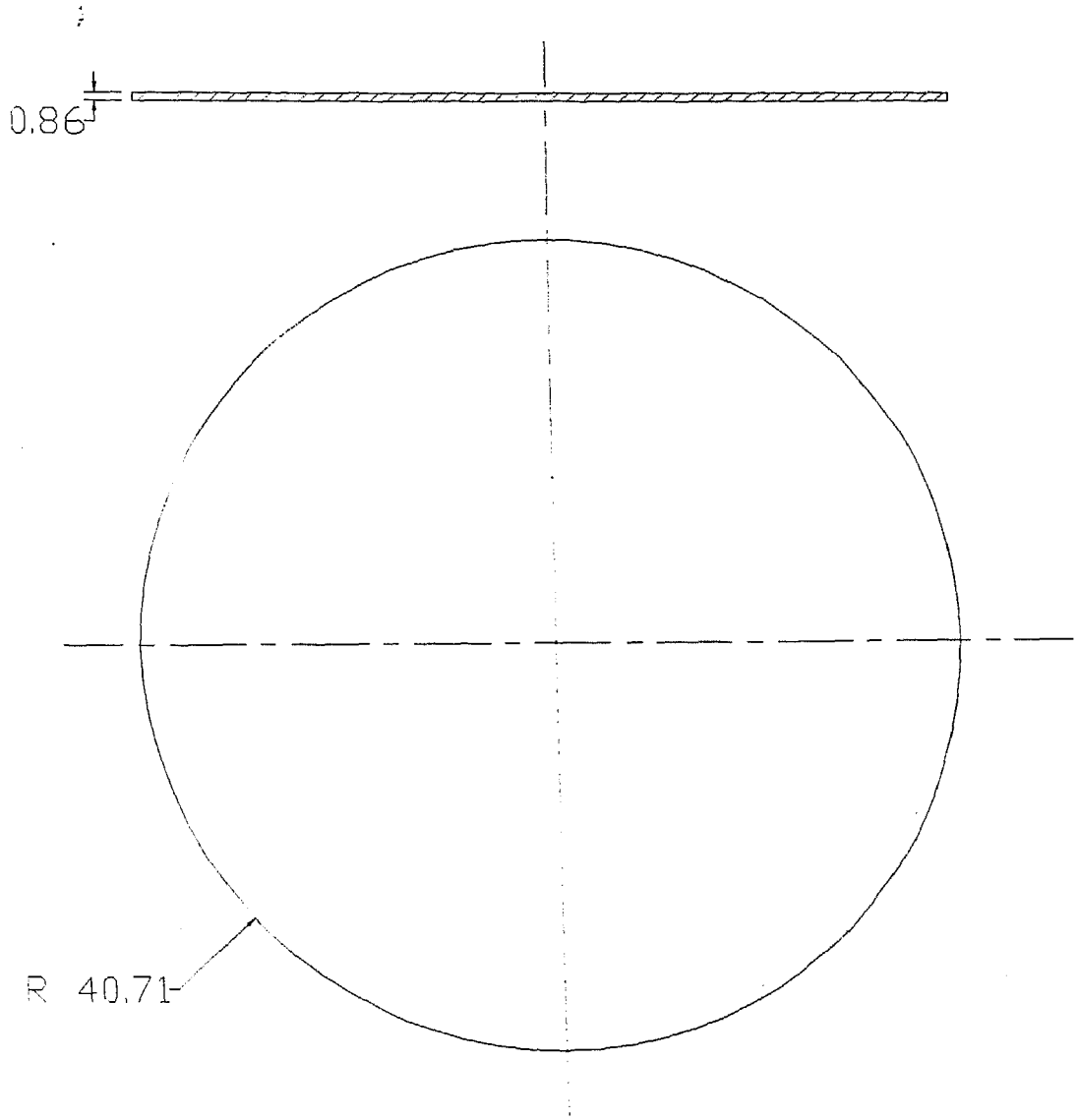

Fig. 4.14(a) Flat pattern obtained for Example Part 3

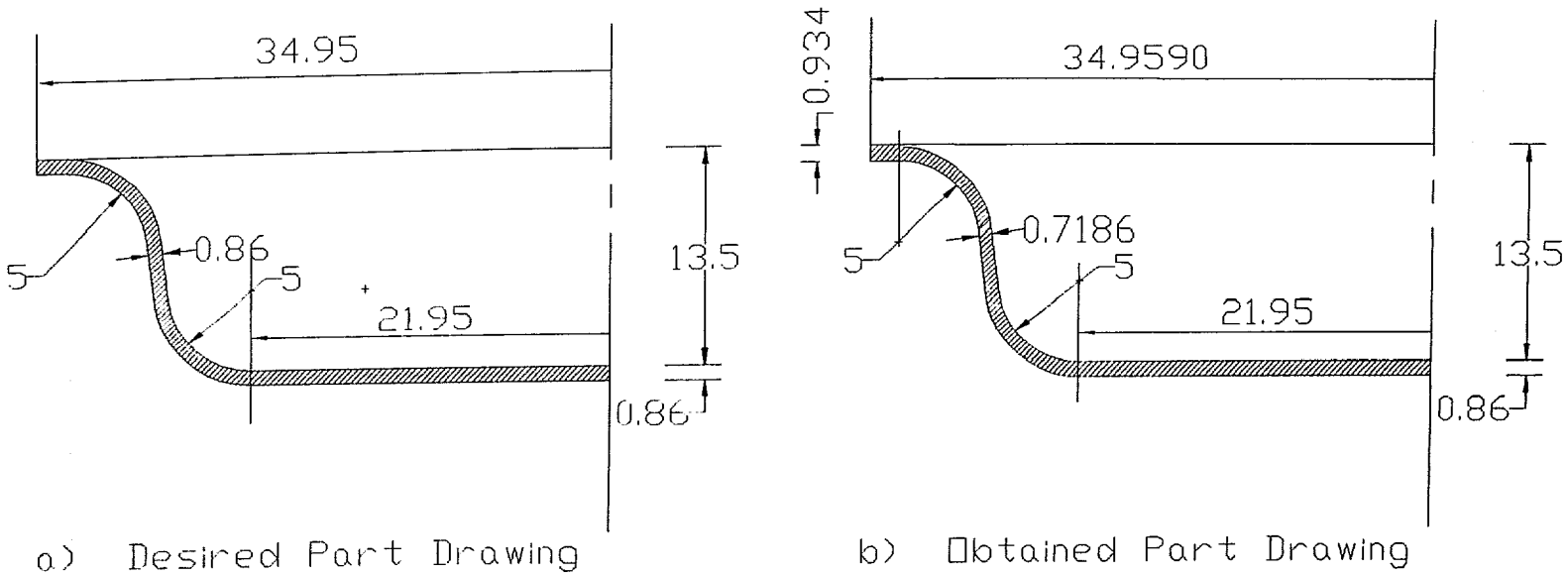

Fig. 4.14(b) Desired and obtained part drawings for the component in Example Part 3

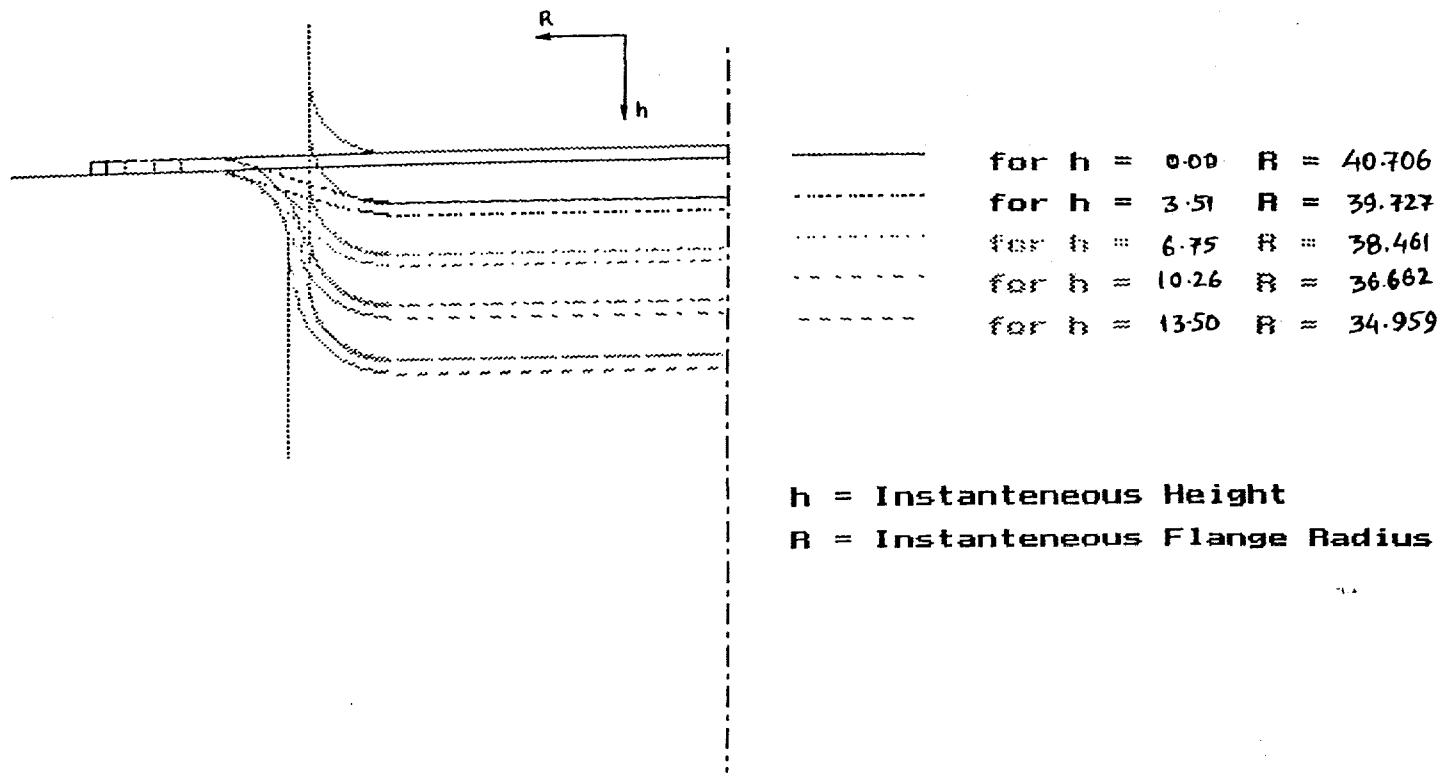

Fig. 4.15 Progressive stages for the component in Example Part 3

CHAPTER 5

CONCLUSIONS AND SCOPE FOR FUTURE WORK

5.1 CONCLUSIONS

Different approaches used for finding the flat pattern for bent and deep drawn components have been discussed. The literature survey has indicated that the presently used methods for finding the flat pattern for bent components are mainly based on experience and thumb rules, so they are inaccurate and unreliable. For flat pattern development for axisymmetric deep drawn cups, no methods were available in the literature. Though a few methods have been reported for non-axisymmetric cases. This has indicated the need for a fast, reliable and accurate method for finding the flat pattern for bent and axisymmetric deep drawn components.

In this work, a plane strain field is assumed and the thinning effect for the bending problem is considered. The deep drawing problems are analyzed considering a plane stress field in the flange as well as in the curved segments over the die and punch corners. The strain hardening effect of materials using Ludwik's strain hardening rule, is considered in both the cases. Required mathematical models are also developed for analyzing the deep drawing process to calculate the stress and strain in the sheet during the drawing operation. Algorithms are developed to find the flat patterns for bending and deep drawing. Based on these models and algorithms, prototype systems are developed for finding the required flat patterns. The results obtained by the present prototype systems are compared with the results available in the literature. Later, these systems were applied to a number of example cases varying in type of material and part geometry, and results obtained are satisfactory. A substantial variation in thickness, from the original sheet thickness, have been observed. The flange was found to be thickened by about 10% - 15% and the minimum thickness of the curved profile was also found to be 10% -

15% less than the original sheet thickness.

The flat pattern obtained can be used for generating the optimum nested layout for the sheet metal components. This can also be used for generating an automatic process plan and appropriate machine codes for an automated manufacturing system.

5.2 SCOPE FOR FUTURE WORK

Above discussed systems is based on certain simplifying assumptions. Hence, to make it more exhaustive and complete, further research on the following lines is suggested :

* A plane strain field is assumed for the bending and a plane stress field is assumed for deep drawing. These assumptions can be relaxed and the problem may be solved for three dimensional stress and strain fields to make it more realistic.
* Presently, the prototypes are developed for bending, however, similar features like curling can also be handled by the present prototype systems. To make it more exhaustive, other sheet metal features like louvering, shearing, hemming etc. should be included.
* The system does not work for sharp bends, i.e., bends having zero radius of curvature. This limitation can be removed for incorporating more practical cases.
* In case of deep drawing, we have assumed only circular cross-sections. Models can be developed to consider non-axisymmetric cross-sections.
* At present, the process of ironing is not considered in this work. In future research, it can be incorporated.
* Redrawing operation is not considered in present work. It can also be included in future.
* As a significant variation is thickness is observed during the operation, the process can be improved to produce a constant thickness product.
* A faster convergence method can be used to reduce the

number of iterations taken for finding the flat pattern.

* We have neglected the deformation of the unsupported annular zone between the die and the punch. This will also give some error in results because high tensile stresses will be acting on this part of the sheet and the magnitude of this stress may go beyond the yield stress of the sheet material causing further thinning of the this part. A detailed analysis of the stresses acting in this part of the sheet may be taken in future to predict the thickness of the sheet in this segment of the cup. This will give a more accurate result.

Extension of the present work on the suggested lines would increase its utility and help in achieving a higher degree of integration between CAD and CAM.

REFERENCES

Calladine, C. R., "Plasticity For Engineers", Ellis Horword Ltd., West Sussex, England, 1985, p 23.

Chen, X. and Sowerby, R, "The development of ideal blank shapes by the method of plane stress characteristics", Int. Jour. of Mechanical Sciences, V 34, n 2, 1992, pp 159 - 166.

Iseki, H. and Murota, T., "On determination of the optimum blank shapes of non-axisymmetric drawn cups by FEM", Bulletin of the JSME, V 29, n 249, Mar 1986, pp 1033 - 1040.

Jagirdar, R., "Set theoretic and graph based approach for automatic feature recognition of sheet metal components", PhD Thesis, 1995, IIT- Kanpur.

Jimma, T. and Kuwabara, T., "Analysis of deep drawing", Blazynski, T. Z., ed., Elsevier Science Publishers Ltd., UK, 1989, p 207.

Karima, M., "Blank development and tooling design for drawn parts using a modified slip line field based approach", Trans. ASME, Jour. of Engineering for Industry, V 111, Nov 1989, pp 345 - 350.

Nee, A. Y. C., Loh, H. T. and Chong, T. C., " Computer generated flat pattern development of heating, ventilation and air conditioning ductings", Jour. of Material Processing Technology, V 29, 1992, pp 173 - 189.

Nnaji, B. O., Kang, T. S., Yeh. S. and Chen, J. P., "Feature reasoning for sheet metal components",

Int. Jour. of Production Research, V 29, n 9, 1991, pp 1867 - 1896.

Prasad, Y. K. D. V. and Somasundaram, S., "A mathematical model for bend allowance calculation in automated sheet metal bending", Jour. of Material Processing Technology, V 39, n 3, 1993, pp 337 - 356.

Rogers, D. F. and Adams, J. A., "Mathematical elements of computer graphics", McGraw - Hill Publishing Co., NY, 1990, p 121.

Sachs, G., "Principles and methods of sheet metal fabrication", Reinhold Publishing Co., NY, 1966, p 95.

Szczepinski, W., "Introduction to the plastic forming of metals", Sijthoff & Noordhoff Int. Publishers, Warsazawa, Netherland, 1987.

Toh, C. H., and Kobayashi, S., "Deformation analysis and blank design in square cup drawing", Int, Jour of Machine Tool Design and Research, V 25, n 1, 1985, pp 15 - 32.

Zharkov, V. A., "Theory of the drawing of circular parts from sheet material", Jour. of Material Processing Technology, V 31, 1992, pp 379 - 392.

BIBLIOGRAPHY

Metals Hand Book, Vol. 4, Eighth edition, American Society of Metals, 1979.

Vogel, J. H. and Lee, D., "An analysis method for deep drawing process design", Int. Jour. of Mechanical Science, V 32, n 11, 1990, 891 - 907.

Woo, D. M., " On complete solution of deep drawing problem", Int. Jour. of Mechanical Science., V 10, 1968, pp 83 - 94.